# Nuclear Cross Sections and Technology
## Volume I



+Special publication, no. 425.

Proceedings of a Conference
Washington, D.C.
March 3-7, 1975

Edited by

R. A. Schrack and C. D. Bowman

Center for Radiation Research
National Bureau of Standards
Washington, D.C. 20234

U.S. DEPARTMENT OF COMMERCE, Rogers C. B. Morton, *Secretary*

U.S. NATIONAL BUREAU OF STANDARDS, Ernest Ambler, *Acting Director*

Issued October 1975

# MEASUREMENT, ANALYSIS, AND IMPLICATIONS OF THE FISSION CROSS SECTION OF THE IMPORTANT FISSIONABLE ISOTOPES*

M. S. Moore
Los Alamos Scientific Laboratory
Los Alamos, NM 87544

Recent measurements on the resonance cross sections of isotopes of uranium and plutonium are reviewed, with the objective of determining average parameters suitable for calculations at higher energies. The average parameters obtained are useful in two ways: they provide the necessary input for statistical calculations of resonance cross sections in the unresolved region, and they provide a normalization point for the calculation of smooth cross sections above the unresolved region. The particular problem we address is the systematic trend of average fission cross sections from 3-5 MeV, which have been found to follow the equation $\sigma_f = -39.031 + 17.231\ Z^2/A^{3/2}$. We find that a very simple statistical model calculation, based on R-matrix parameters which adequately describe the total cross section from 20 keV to 20 MeV, can provide a qualitative understanding of this systematic behavior.

[NUCLEAR REACTIONS, FISSION, U, Pu isotopes, calculated $\langle\sigma_f\rangle$, E = 3-5 MeV.
$^{235}$U(n,f), deduced channel spectrum.]

## Introduction

It is often said that one of the justifications for making detailed measurements of cross sections of fissionable isotopes in the resonance region is that these data can be used in extrapolating to the unresolved resonance region and above. As one of the most promising techniques for providing cross sections in the unresolved resonance region, we recommend following the pioneering work of Brissenden and Dursten[1] with resonance ladders, and using the probability table method of Levitt.[2] While much remains to be done in this area, the technique is well known and will not be reviewed here. Instead, we should like to review significant new results at low energies with the objective of using these data as an evaluation guide in the region of smooth cross sections.

W. G. Davey[3] has suggested that a program to provide significantly improved cross section data for fissionable isotopes should be based on an interactive approach involving microscopic measurements, integral experiments, and model calculations. In such a program, it is the interactive feedback which is most important. The integral experiments and model calculations suggest areas where new measurements are needed; discrepancies in microscopic measurements and between measurement and calculation might be resolvable by carefully designed integral experiments; and both the integral and microscopic data can lead to refinements in the model. Ultimately, one might hope to be able to calculate, in a reasonable way, data sets for isotopes which are difficult or impossible to measure (e.g., the heavier actinides which may be important as radioactive wastes, heavy element production with underground nuclear explosions, and neutron production by medium energy charged particle beams).

It is this last area, in particular, which prompted the present study. We are involved in planning the experimental program for the Weapons Neutron Research (WNR) facility at the Los Alamos Scientific Laboratory. In this facility, neutrons are produced by short bursts of 800 MeV protons incident on a $^{238}$U target. Below neutron energies of 20 MeV, calculations are based on a Monte Carlo treatment using ENDF/B cross sections. Above 20 MeV, we have been using the Nucleon-Meson Transport Code NMTC[4] which ignores fission. The results of the calculations, carried out by Russell and reported at this conference, show a discontinuity at 20 MeV and suggest that an improved treatment is needed.

Following Davey's suggestion that model calculations can play an important part in the refinement of nuclear data, we shall explore two questions: (1) how can the systematics derived from low energy microscopic measurements be used in nuclear model calculations, and (2) what can one hope to learn from such calculations?

To make a model calculation for fissionable isotopes, we find that we need the following input: (1) neutron transmission coefficients for elastic and inelastic scattering, (2) the low-lying level structure of the target nucleus with spins and parities, (3) a description of the variation of the nuclear level density with energy for saddle point and ground state deformation, (4) the variation of the radiation width with energy, (5) the fission channel spectrum at the saddle point with spins and parities, (6) the pairing gap for ground-state and saddle-point configurations, (7) the neutron binding energies and fission thresholds, and (8) the barrier curvature parameters for the formulation chosen to represent barrier penetration. Many of these are not very well known, and for the studies we have done, the keyword is simplicity: we shall try to use constant values for many of the parameters as possible over the limited range of target nuclides considered.

## Neutron Transmission Coefficients

The measured neutron widths for resolved resonances provide the s- and p- wave strength functions, as taken from the recent compilation of recommended parameters by Mughabghab and Garber.[6] The weighted averages for the uranium and plutonium isotopes are $1.03 \times 10^{-4}$ for the s-wave strength function, and $1.85 \times 10^{-4}$ for the p-wave strength function. The usual approach to obtaining neutron transmission coefficients for model calculations is with the optical model. The optical model fits recently reported by Lagrange[7] represent the current state of the art. Lagrange used the coupled-channel model of Tamura[8] (the JUPITOR-I code), and fitted in decreasing order of importance the total cross sections, the s- and p- wave strength functions at low energies, and the elastic plus low-lying inelastic angular distributions. While calculations[9] using the Lagrange parameters give good agreement for $^{238}$U, the description is less satisfactory for $^{239}$Pu, suggesting that the optical model parameterization is not only energy dependent, but is different for each nuclide to be considered. For this reason, we have chosen a simpler representation for this study, which follows the R-matrix approach used by Uttley et al[10] in the analysis of total cross sections. We use the generalized one-level formula of Lane and Thomas[11] which leads to the following expressions for the average total, shape-elastic, and compound-nucleus reaction cross sections:

$$\langle\sigma_T\rangle = \frac{2\pi}{k^2}\sum_\ell\left(2\ell+1\right)\cdot$$

$$\cdot\left[\left(1-\cos 2\phi_\ell\right)\left(1-\frac{\pi\Gamma_n^{(\ell)}}{D}\right)+\frac{\pi\Gamma_n^{(\ell)}}{D}\right], \quad (1a)$$

$$\langle\sigma_{se}\rangle = \frac{2\pi}{k^2}\sum_\ell\left(2\ell+1\right)\left(1-\cos 2\phi_\ell\right)\left(1-\frac{\pi\Gamma_n^{(\ell)}}{D}\right), \quad (1b)$$

$$\langle\sigma_x\rangle = \frac{2\pi}{k^2}\sum_\ell\left(2\ell+1\right)\frac{\pi\Gamma_n^{(\ell)}}{D}\cdot\frac{\pi\Gamma_x^{(\ell)}}{D}\Big/\sum_x\frac{\pi\Gamma_x^{(\ell)}}{D}. \quad (1c)$$

In the above expressions, the wave number $k = \frac{1}{\lambda\!\!\!^{-}} = \frac{\mu v}{\hbar}$, where $\mu$ is the reduced mass and $v$ is the relative velocity, $\ell$ is the neutron orbital angular momentum, $\Gamma_n^{(\ell)}$ is the average neutron width, $\Gamma_x^{(\ell)}$ is the average reaction width, and D is the average level spacing. The quantity $2\pi\Gamma_n^{(\ell)}/D$ is the neutron transmission coefficient we are seeking. The average compound-nucleus reaction cross section was written in the above form to show the relationship $\langle\sigma_T\rangle = \langle\sigma_{se}\rangle + \sum_x\langle\sigma_x\rangle$; it is properly written as a compound-nucleus spin expansion

$$\langle\sigma_x\rangle = \frac{2\pi^2}{k^2}\sum_{J,\ell} g_J\,\frac{\Gamma_n^{(J,\ell)}}{D_J}\,\frac{\Gamma_x^{(J)}}{D_J}\Big/\frac{\Gamma^{(J)}}{D_J}, \quad (2)$$

where $g_J$ is the statistical factor $(2J+1)/2(2I+1)$, and where J is the spin of the compound nucleus and I is the spin of the target nucleus. The statistical factor $g_J$ obeys the sum rule $\sum_J g_J = 2\ell+1$, and the total width $\frac{\Gamma^{(J)}}{D_J} = \sum_x\frac{\Gamma_x^{(J)}}{D_J}$. In this study, we assume that $\Gamma_n^{(J,\ell)}/D_J$ depends only on $\ell$, and ignore width correlation corrections and multilevel interference, except for the diagonal $R^\infty$ term. In the absence of $R^\infty$, the transmission coefficients $2\pi\Gamma_n^{(\ell)}/D$ are related to the strength functions $\Gamma_n^{0(\ell)}/D$ by the expression

$$\frac{\Gamma_n^{(\ell)}}{D} = \frac{\Gamma_n^{0(\ell)}}{D}\cdot E\cdot P_\ell/\rho, \quad (3)$$

where $\rho = ka$, a is the nuclear radius, and $P_\ell$ and $\phi_\ell$ in Eq. (1) are given by the Lane and Thomas recursion relations

$$P_0 = \rho;\ P_\ell = \rho^2 P_{\ell-1}/[(\ell - S_{\ell-1})^2 + (P_{\ell-1})^2],$$
$$S_0 = 0;\ S_\ell = \rho^2(\ell - S_{\ell-1}),$$
$$\phi_0 = \rho;\ \phi_\ell = \phi_{\ell-1} - \tan^{-1}[P_{\ell-1}/(\ell - S_{\ell-1})], \quad (4)$$

If $R^\infty_\ell$ is non-zero and diagonal, the relations are modified as follows:

$$\frac{\Gamma_n^{(\ell)}}{D} = \frac{\Gamma_n^{0(\ell)}}{D}\cdot E\cdot P'_\ell/\rho,$$
$$P'_\ell = P_\ell/d_\ell,$$
$$S'_\ell = [S_\ell(1 - R^\infty_\ell S_\ell) - R^\infty_\ell P_\ell^2]/d_\ell,$$
$$\phi'_\ell = \phi_\ell - \tan^{-1}[R^\infty_\ell P_\ell/(1 - R^\infty_\ell S_\ell)],$$
$$d_\ell = (1 - R^\infty_\ell S_\ell)^2 + (R^\infty_\ell P_\ell)^2. \quad (5)$$

The purpose of this part of the exercise is to obtain the simplest possible parameterization of a set of neutron transmission coefficients which fairly well describe the total cross sections of the uranium and plutonium isotopes over a wide range of neutron energies. We note that recent measurements of Schwartz et al[12] of the total cross section of $^{235}U$, $^{238}U$, and $^{239}Pu$ between 10 keV and 15 MeV do not differ from one another by more than a few percent. The s- and p- wave average parameters provide a normalization point for obtaining these neutron transmission coefficients, but they give no information for higher partial waves. To obtain a reasonable set of parameters to use in the present formalism, we choose strength functions consistent with Lagrange's average transmission coefficients for $^{238}U$ in the energy regions where the partial cross sections are highest. Finally, we solve, by least-squares fitting the average of the measurements of Schwartz et al, for the $R^\infty$ matrix elements. The results are given in Table 1, and the fit is shown in Fig. 1. The neutron transmission coefficients calculated from the parameters in Table 1 agree with those of Lagrange to about 10% in the energy regions of importance.

Table 1. Parameters used in calculating neutron transmission coefficients.

| $\ell$ | Strength function | $R^\infty_\ell$ |
|---|---|---|
| 0 | $1.03\times10^{-4}$ | -0.111 |
| 1 | $1.85\times10^{-4}$ | +0.125 |
| 2 | $1.0\times10^{-4}$ | +0.043 |
| 3 | $2.25\times10^{-4}$ | -0.071 |
| 4 | $1.0\times10^{-4}$ | -0.058 |
| 5 | $1.2\times10^{-4}$ | +0.068 |
| 6 | $2.0\times10^{-4}$ | 0.0 |
| ≥7 | $1.0\times10^{-4}$ | 0.0 |

## Discrete Levels for Inelastic Scattering

For this study, we are interested primarily in treating the average behavior of inelastic scattering. For simplicity, we construct a standard spectrum of levels which is used for all nuclides. For rotational band structure, there are three standard spectra: the K = 0 spectrum, the K > 0 spectrum, and the spin 1/2 spectrum which takes into account Coriolis coupling. All these are generated as averages of the known rotational structure for the uranium and plutonium isotopes as evaluated by Ellis.[13] The energies of

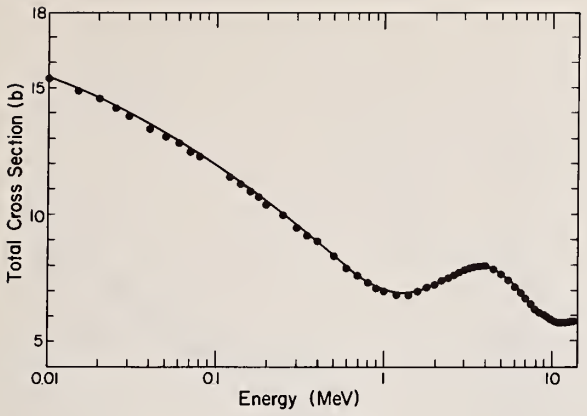


Fig. 1. Average total cross section of $^{235}U$, $^{238}U$, and $^{239}Pu$ from 0.01 to 15 MeV. Points show averaged data from measurements of Schwartz et al[11] and from ENDF/B-IV; the solid line shows the calculated curve using parameters of Table 1.

vibrational band heads again represent averages for the known low lying level structure of the even-even isotopes. Included as part of the vibrational spectrum are the negative parity octupole vibrations with K = 0, 1, 2, and 3, the positive parity beta and gamma vibrations with K = 0 and 2, and a second $K,J^{\pi} = 0,0^{+}$ band near 1 MeV. The spectra of intrinsic levels for the even-odd targets are constructed from average energy differences as tabulated by Ellis and Schmorak.[14] In some cases, it is necessary to extend the single-particle spectrum beyond the range of known levels. Additional levels (and the entire spectrum of single-particle fission channels) are taken from the level diagrams of Seeger and Howard[15] at the appropriate average deformation.

For the even-even nuclei, it is necessary to include certain of the two-quasiparticle states. From the $^{234}U$ spectrum evaluated by Ellis,[13] we conclude that these start to be important at ~1.5 MeV excitation. We construct a spectrum which looks reasonable by taking the appropriate energy differences for the single particle states and adding 1.5 times the pairing gap, for both neutrons and protons.

The calculation of inelastic scattering is done in the usual way,[16] using reciprocity. We find that the calculated inelastic scattering to the lowest rotational states in $^{238}U$ is low by 30-50%, probably because we ignore direct processes by using a diagonal representation for $R^{\infty}$. There is reasonably good agreement with inelastic scattering to the higher states in $^{238}U$, suggesting that this simplified approach may be adequate for describing compound nucleus processes, and in particular, competition between inelastic and fission.

## Level Densities and the Radiation Width

The next step in model calculations is to obtain a description of the level density for continuum inelastic scattering and of the variation of the radiation width with neutron energy. The usual prescription is to use the Gilbert and Cameron level density formula,[17] normalizing the radiation width to the correct value in the resonance region. We follow Gilbert and Cameron in the assumption that the important parameter in the level density formula is $E_B + E - E_p$, where $E_B$ is the binding energy, E is the neutron energy, and $E_p$ is the pairing gap. We obtain an estimate of the pairing gap by looking at neutron and proton separation energy differences, and find, as show in Figs. 2 and 3, that these appear to depend on the mass number. The reduced level spacing (taking out the expected 2J + 1 dependence and applying the Gilbert and Cameron spin-cutoff correction) is plotted as a function of $E_B - E_p$ for the uranium through americium isotopes in Fig. 4, where the data points are again from the compilation of parameters recommended by Mughabghab and Garber.[6] The Gilbert and Cameron formula with parameters set equal to the average for this region of A does not fit the data points, so we assume the Weisskopf description,[18] $\rho = A \exp a\sqrt{E}$, solving for the parameters A and a by the method of least squares.

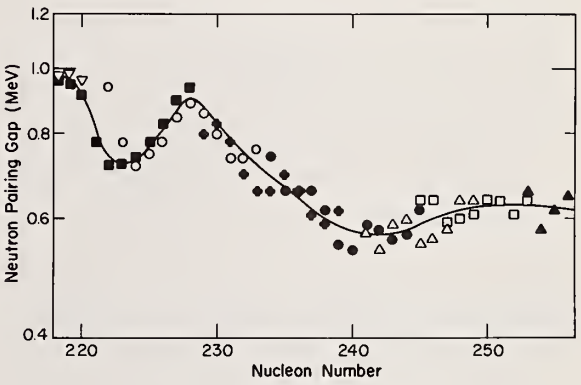


Fig. 2. Estimate of the pairing gap for neutrons, inferred from neutron separation energies for even-even and even-odd nuclei as a function of mass number.

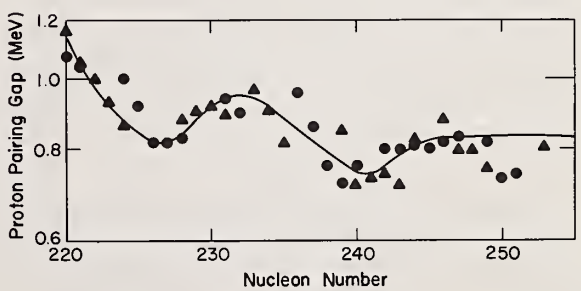


Fig. 3. Estimate of the pairing gap for protons, inferred from proton separation energies for even-even and odd-even nuclei as a function of mass number.

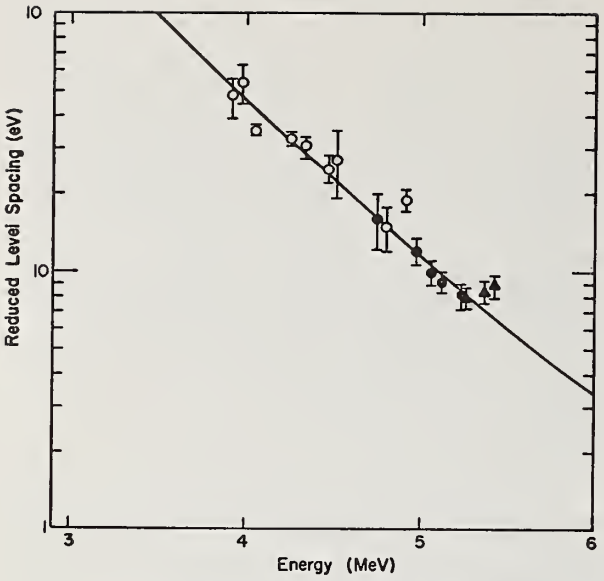


Fig. 4. Reduced level spacing for uranium through americium isotopes, as a function of $E_B - E_p$. The solid line shows the calculated curve used, given by $\rho = 0.145 \exp(5.88\sqrt{E})$.

The resonance parameters recommended by Mughabghab and Garber are also used in deriving a simple expression for the energy dependence of the radiation width. Figure 5 shows a plot of the radiation widths for the actinides of interest as a function of $E_B - E_p$. We follow the usual procedure of normalizing in the center of the range, calculating the energy dependence to be expected for $(\hbar\omega)^3$ and $(\hbar\omega)^5$, corresponding to El and E2 radiation. For purposes of this study, we conclude that the $(\hbar\omega)^3$ dependence is adequate. finally, as an internal consistency check, we calculate the radiative capture cross section of $^{238}U$, and find satisfactory agreement with the recommended curve of ENDF/B-IV below 1 MeV, as shown in Fig. 6. We find that the Gilbert and Cameron level density formula tends to overpredict radiative capture at 1 MeV by a substantial amount (~50%). This is because the Gilbert and Cameron formula gives a stronger increase in the number of levels as the energy increases in this region of A than does the Weisskopf representation we are using; hence $\Gamma_\gamma/D$ increases much faster.

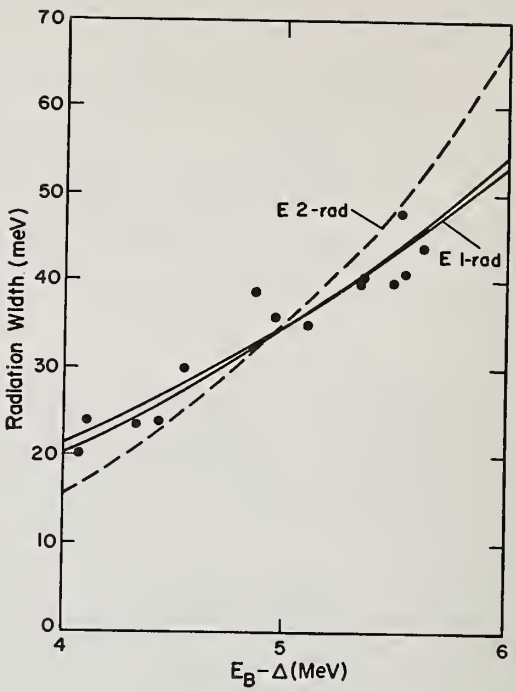


Fig. 5. Average recommended radiation widths[6] as a function of $E_B - E_p$. The dashed curve corresponds to an assumed $(\hbar\omega)^5$ dependence of the partial radiation width. The solid curves correspond to an assumed $(\hbar\omega)^3$ dependence, but the calculation is not sensitive to the expression used for the level density. The two solid curves correspond to the Gilbert and Cameron formula[17] and the one we use as described in the text.

## Fission and Inelastic Competition from 3-5 MeV

Our simplified approach to including the fission contribution is based on the definitive analysis by Back et al[19,20] of charged-particle induced fission measurements. We use the double-humped barrier with curvature constants set equal to the averages given by Back et al for even-even and for even-odd fissioning species. We are interested primarily in fission above both barriers, so we use the strong coupling approximation, setting the matrix elements connecting Class I and Class II states equal to unity. The difference in first and second barrier heights appears to be slightly N-dependent, but we ignore it. The Z-dependence is taken into account by a linear fit to the average given by Back et al, as shown in Fig. 7.

One of the first things one finds in trying to calculate fission cross sections below the second-chance threshold is that both the magnitude and the slope of the cross section in the plateau region (3-5 MeV) are determined by competition between continuum inelastic scattering and continuum fission. (By the word "continuum," we mean the region in which the level density formula is applicable.)

Several years ago, Smith et al[21] measured fission cross sections for a number of the actinides, and found that the average cross sections between 3 and 5 MeV could be described within 5-10% by the empirical relationship $\sigma_f = -39.031 + 17.231\ Z^2/A^{3/2}$. If we plot the most recent evaluations, as given in ENDF/B-IV, for the average fission cross sections for uranium and plutonium from 3-5 MeV, we find that the relationship is still remarkably good, as shown in Fig. 8.

We know that the Smith et al empirical formula cannot be pushed to extremes; for example for $^{250}U$, the fission cross section would be far negative and for $^{220}U$ it would greatly exceed the total. However, it would seem that any model calculation, even one as simplified as the one we are using for these studies,

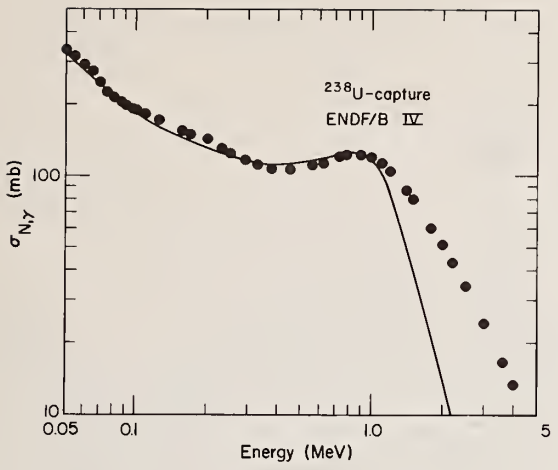


Fig. 6. The radiative capture cross section of $^{238}$U. Data points are from ENDF/B-IV; the solid line represents the calculated curve.

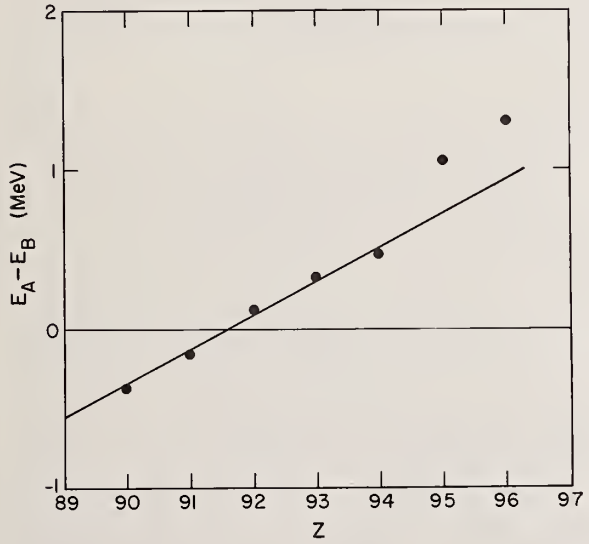


Fig. 7. Average energy difference between first and second barrier heights as a function of proton number, calculated from barrier heights derived by Back et al.[19,20]

should be able to explain physically this systematic behavior.

Before we can do a meaningful calculation, however, we still need two pieces of information: the level of density formula for continuum fission, and the pairing gap at the barrier. While it is reasonable to assume that the form of the level density formula is the same for continuum fission and continuum inelastic, we do not expect to be able to use exactly the same constants. If one carried out a Strutinsky calculation[22] of single-particle levels to find the barrier height as a function of deformation, he would find that the single-particle level density at the Fermi surface for barrier deformations is lower than for ground state deformations. At energies well above the barrier, the densities must eventually be the same on the average, although one still expects local fluctuations. In other words, the existence of the barrier is attributable to a lower level density in its vicinity, but at some energy above the barrier we should expect that the same level density formula would be applicable at both deformations.

To account for this effect we use the same level density formula for continuum inelastic and for continuum fission, but change the width of the interval over which the levels are counted in fission by a constant factor. For low energies, (i.e., 3-5 MeV) the value of this constant factor will be treated as a free parameter in fitting the data; at higher energies (i.e., where the level density for continuum fission becomes equal to that for first-well levels) it will be set equal to unity.

The best guesses for the pairing gap at the barrier are from Britt and Huizenga,[23] who suggest that it is roughly equal to the pairing gap at the ground state, or from Seeger and Howard,[15] whose results indicate that it is somewhat larger than the ground state gap. This is not good enough, and we are forced to introduce another free parameter, which we shall call the continuum fission barrier, $E_c$. This parameter is defined by the relation $E_c = E_{A,B} + E_p(\text{bar.}) - E_p(\text{g.s.})$, where $E_{A,B}$, the usual barrier parameter, is the height of either the first or second hump (whichever is greater) measured from the ground state, and $E_p(\text{bar.})$ and $E_p(\text{g.s.})$ are the pairing gaps at deformations corresponding to the barrier and to the ground state, respectively. (The introduction of $E_c$ as a free parameter simply allows us to defer the problem of the pairing gap at the barrier; we can carry out the calculations without knowing what it is.)

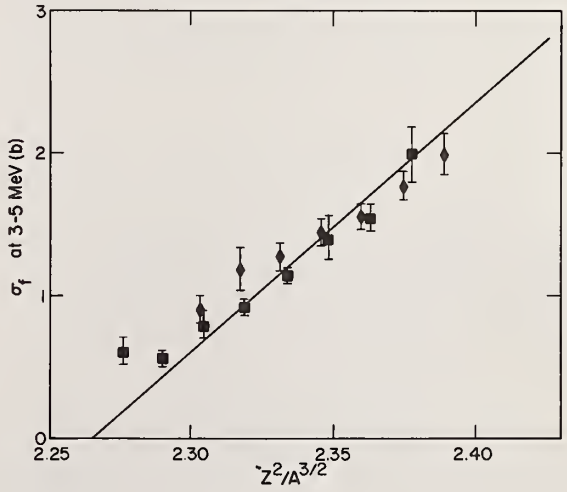


Fig. 8. Average fission cross sections of uranium and plutonium from 3-5 MeV, plotted against $Z^2/A^{3/2}$. The solid curve is the empirical relationship of Smith et al.[21]

The continuum barrier $E_c$ lies above the usual barrier by the pairing gap at that deformation. If we assume that the pairing gap is only slightly dependent on Z and N (cf. Figs. 2 and 3), then it follows that $E_c$ will show properties similar to $E_{A,B}$. In particular, we expect that the continuum barrier will have a slight N-dependence, which we neglect, and a fairly strong Z-dependence. We assume that the Z-dependence of the continuum barrier in going from uranium to plutonium is equal to the average given by Back et al[19] for the measured barriers for the even-even uranium and plutonium nuclei, which are presumably $0^+$ at both deformations. This gives a difference of 0.24 MeV in the barriers for uranium and plutonium.

With this assumption, we need to fit only one target nucleus (value and slope) from 3 to 5 MeV in order to fix both the parameters we have left free. We choose to normalize to $^{235}U$, and in particular, to the recent measurements of Hansen et al[24] which are the basis for ENDF/B-IV in this region. We find that the values which best describe the $^{235}U$ data give a continuum barrier of 6.02 MeV, and a continuum level density 6.5% higher at an energy of 1.5 MeV above the barrier than at the ground state deformation. For the plutonium isotopes, we use a continuum barrier which is 0.24 MeV lower, or 5.78 MeV.

The results of a calculation of the 3-5 MeV fission cross sections for all the uranium and plutonium isotopes, using these constants, are shown in Figs. 9 and 10. The calculated averages are plotted against the empirical curve of Smith et al in Fig. 11.

In the calculations, we find that the key parameter is the energy difference between the onset of continuum inelastic and continuum fission, as shown in Fig. 12. We have assumed that continuum inelastic occurs when the neutron energy exceeds the pairing gap of the target nucleus, and that continuum fission occurs when the neutron energy plus the binding energy exceeds the continuum fission barrier plus the pairing gap of the compound nucleus. The variable responsible for this systematic behavior is thus the binding energy plus or minus the ground-state pairing gap for the last neutron. It is the binding energy plus the pairing gap if the target nucleus is even-even, and minus if even-odd. The above results also suggest that the pairing gap at the barrier is roughly 10% larger than at the ground-state, in agreement with recent estimates.[15,23]

The most puzzling discrepancy in Figs. 9 and 10 is for $^{241}Pu$. The calculations for $^{239}Pu$ and $^{242}Pu$ agree fairly well, and $^{240}Pu$ gives about the right average even though the slope is much too large. But $^{241}Pu$, which should fit best, is underpredicted by 10-20%. Even though existing measurements on $^{241}Pu$ appear to agree to ~5%, we are tempted to suggest that a remeasurement may be in order. It should be noted that there is a small continuing effort at the Los Alamos Scientific Laboratory in the measurement of neutron cross sections with nuclear explosions. Forman et al,[26] who recently completed a measurement of the gamma-ray prodution cross section of $^{241}Am$ below 6 MeV by this technique, are planning to remeasure the fission cross section of $^{241}Pu$ to 6 MeV in the near future.

Using the results of these calculations, it is possible to predict the magnitude and slope of the plateau cross sections for second, third, fourth-chance fission, etc., which arise by the mechanism of inelastic scattering to continuum levels which lie above the fission threshold in the residual nucleus. The decay of these levels is again dominated by competition between neutron emission and fission.

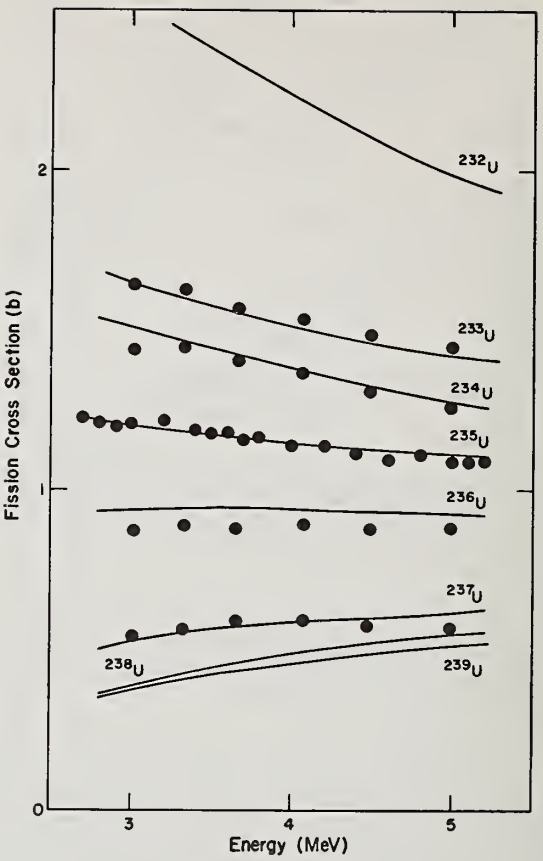


Fig. 9. Fission cross sections of the uranium isotopes from 3-5 MeV. The points are evaluated data; the curves represent the results of calculations as described in the text.

The results of such a calculation for $^{235}U$ below 25 MeV, compared to evaluated data from ENDF/B-IV, are shown in Fig. 13. These results are similar to those obtained by Jary,[27] who concluded that it is possible to calculate multiple-chance fission with a statistical model with no free parameters, using the magnitude of the observed plateau for first-chance fission.

Our results may also be compared to those of Gavron et al,[28] who use a microscopic calculation of level densities and a spherical optical model for neutron transmission coefficients. They find that they are able to fit fission probabilities for a wide range of fissioning species, primarily induced by charged particle reactions, again with no free parameters. From the fission probabilities, they expect to be able to obtain neutron cross sections for targets which would be unmeasurable by usual techniques, following methods similar to those of Cramer and Britt.[29]

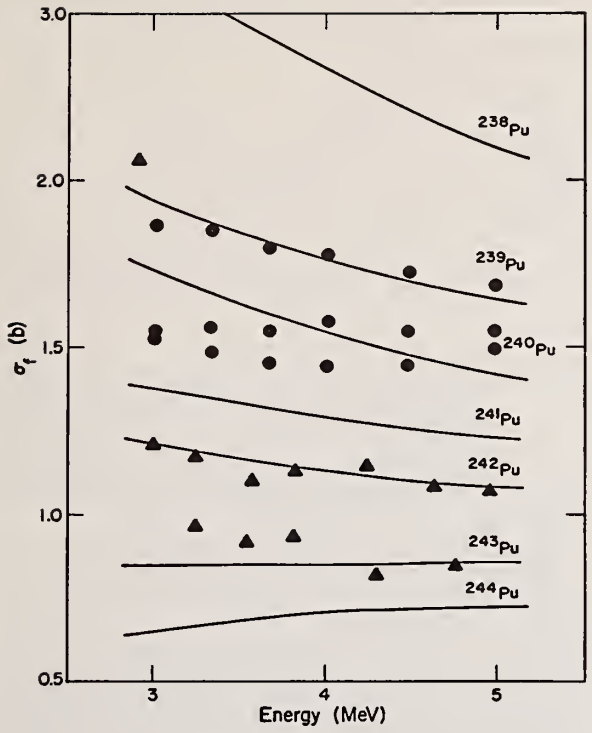


Fig. 10. Fission cross sections of the plutonium isotopes from 3-5 MeV. The points, except for $^{242}$Pu and $^{244}$Pu, are evaluated data, the curves represent the results of calculations as described in the text. For $^{242}$Pu and $^{244}$Pu, the points are taken from measurements reported by Auchampaugh and Bergen.[25]

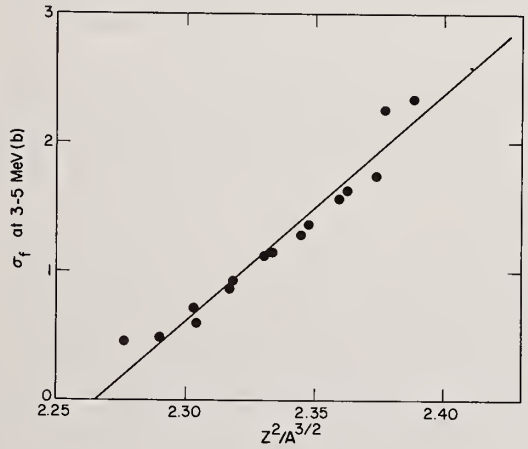


Fig. 11. Calculated average fission cross sections of the uranium and plutonium isotopes from 3-5 MeV, plotted against $Z^2/A^{3/2}$. The solid curve is the empirical relationship of Smith et al.[21]

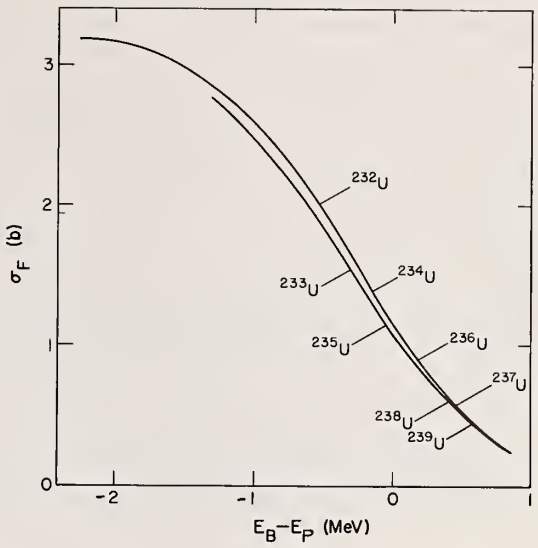


Fig. 12. Calculated average fission cross sections of the uranium isotopes as a function of the energy difference between the continuum fission threshold and the pairing gap governing continuum inelastic scattering.

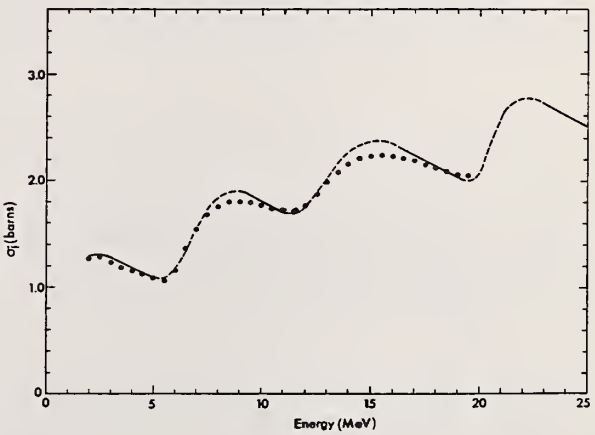


Fig. 13. Fission cross section of ($^{235}$U+n) from 2 to 25 MeV. Data points are taken from ENDF/B-IV; calculations were carried out only for the plateau regions corresponding to first-, second-, third-, and fourth-chance fission.

## Discrete Fission Channels

The last question we should like to address is that of the discrete fission channel spectrum, and what we can expect to learn from the resonance region. The situation is best for $^{235}$U; we have the definitive spin assignments from measurements by Keyworth et al[30] using polarized neutrons incident upon polarized targets. We also have effective anisotropies, leading to K-assignments, from the work of Pattenden and Postma[31] with aligned targets. These results suggest $\langle A_2 \rangle = -1.54$ for

J=3 and $\langle A_2 \rangle$ = -2.05 for J=4. For the fission widths, we have the results of a multilevel analysis carried out by Smith and Young[32] for ENDF/B-IV, which give average fission widths of 0.074 eV for J=4 and 0.186 eV for J=3. The purpose of this part of the excercise is to deduce, from the average resonance parameters and the assumed fission barrier description from Back et al,[19,20] the spectrum of the low-lying fission channels. We shall then test these in a statistical model calculation in the region of a few hundred keV.

If the resonances had pure K, Pattenden and Postma note that we should expect $A_2$ = -2.92, -2.19, 0, and +3.65 for (K,J) = (0,3), (1,3), (2,3), and (3,3), respectively. We expect $A_2$ = -2.48, -1.17, +1.02, and +4.08 for (K,J) = (1,4), (2,4), (3,4), and (4,4), respectively. From the average parameters, we set up the following equations:

For J=3,

$$(-2.92\langle\Gamma_{f_0}\rangle - 2.19\langle\Gamma_{f_1}\rangle + 0.0\langle\Gamma_{f_2}\rangle + 3.65\langle\Gamma_{f_3}\rangle)/\langle\Gamma_f\rangle = -1.54, \quad (6)$$

and

$$\langle\Gamma_f\rangle = \langle\Gamma_{f_0}\rangle + \langle\Gamma_{f_1}\rangle + \langle\Gamma_{f_2}\rangle + \langle\Gamma_{f_3}\rangle = 0.186 \text{ eV}, \quad (7)$$

where $\langle\Gamma_{fK}\rangle$ is the average width for the fission channel of the appropriate K.

For J=4, we have a similar expression,

$$(-2.48\langle\Gamma_{f_1}\rangle - 1.17\langle\Gamma_{f_2}\rangle + 1.02\langle\Gamma_{f_3}\rangle + 4.08\langle\Gamma_{f_4}\rangle)/\langle\Gamma_f\rangle = -2.05, \quad (8)$$

and

$$\langle\Gamma_f\rangle = \langle\Gamma_{f_1}\rangle + \langle\Gamma_{f_2}\rangle + \langle\Gamma_{f_3}\rangle + \langle\Gamma_{f_4}\rangle = 0.074 \text{ eV}. \quad (9)$$

In order to solve these equations, we use the conclusion reached by Pattenden and Postma, that channels with K=3 and 4 are effectively closed and that their contributions can be neglected. The equations for J=4 can be solved immediately, giving $\langle\Gamma_{f_1}\rangle$ = 0.049 eV and $\langle\Gamma_{f_2}\rangle$ = 0.025 eV.

We assume that these partially open channels for J=4 are rotational members of bands which also have J=3 members. In this case, knowledge of the energy difference between the $4^-$ members of these two bands can be used to give the energy difference between the $3^-$ members of the same two bands.

In order to solve Eqs. (6) and (7) for J=3, we calculate the fission penetrabilities, $2\pi\Gamma_f/D$, as a function of excitation energy, as shown in Fig. 14. Using D=1.65 eV and 1.41 eV for J=3 and 4, respectively (implying a 6% correction for missed levels below 30 eV), we find that the $4^-$ members of the K=1 and K=2 bands are separated by 0.065 MeV. We assume that this same number applies for the J=3 members. This permits the solution of the equations for J=3, for which we find $\langle\Gamma_{f_0}\rangle$ = 0.023 eV, $\langle\Gamma_{f_1}\rangle$ = 0.101 eV, and $\langle\Gamma_{f_2}\rangle$ = 0.062 eV. If we then assume that the lowest threshold for $^{236}$U is at 5.70 MeV, as given by Back et al, we estimate the transition state band heads at 0.87, 0.72, and 0.85 MeV for $K=0^-$, $1^-$, and $2^-$, respectively. These are quite different from the transition state energies suggested by Back et al for $^{236}$U, 0.15 and 0.45 MeV for $K=0^-$ and $1^-$, respectively. Our transition state energies are similar to the energies of negative parity bands observed near the ground state; 688 keV for the lowest (K = 0?),[33,34] and 970 keV for $K^\pi = 1^-$.[35] Using the channel sequence inferred from the low energy resonances, the calculated fission cross section agrees quite well with the measurements below 300 keV; we find, in particular, that the lowest $3^+$ channel, presumably corresponding to gamma vibrations with K=2, cannot have a transition-state energy much below 1 MeV. This again is quite different from the transition-state energy of 0.18 MeV suggested by Back et al, but is quite close to the first well energy of 0.95 MeV. It may be noted that if the gamma-band transition state lies well below 1 MeV, the p-wave contribution to fission in ($^{235}$U + n) is much too large. We could, however, include the beta vibrational band with K=0 without changing the results. This occurs for the following reason: after the fission penetrability approaches unity for a given spin, fission dominates in compound nucleus decay. Increasing the fission width for this spin by a factor of two, by doubling the number of open channels, has no appreciable affect on the average decay probability.

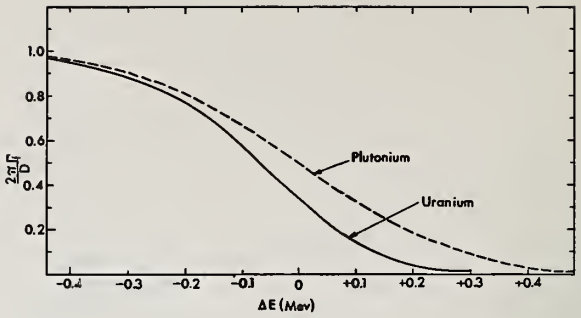


Fig. 14. Calculated fission penetrability, $2\pi\Gamma_f/D$, for uranium and plutonium, as a function of the difference between the barrier height and the excitation energy. The curve for uranium is different from that for plutonium because of the difference in height of the second hump.

It may also be noted, from Fig. 14, that $2\pi\Gamma_f/D$ changes quite rapidly with excitation energy. The surprising success we have had in describing the fission cross section below 300 keV, simply by pegging the channel structure at the neutron binding energy, gives us some confidence in the barrier parameterization we have used.

In order to fit the data above 400 keV, several additional channels are required, but their quantum numbers and exact locations are not critical. We construct these using the procedures described above for inelastic levels, and modify the energies slightly as required. Figure 15 shows the kind of fit one can achieve below the second-chance fission threshold. We divide the energy range into four regions of interest: (1) At the lowest energies, $\lesssim$ 50 keV, we find that fission through the s-wave channels is dominant, and the average cross section is determined primarily by competition between fission and radiative capture. (2) Between 50 and 400 keV, p-wave fission becomes important, and discrete inelastic channels need to be considered as well. (3) Between 400 keV and roughly 2 MeV, we find higher partial waves becoming important, and we see that competition between many discrete fission channels and inelastic channels is the dominant consideration. This

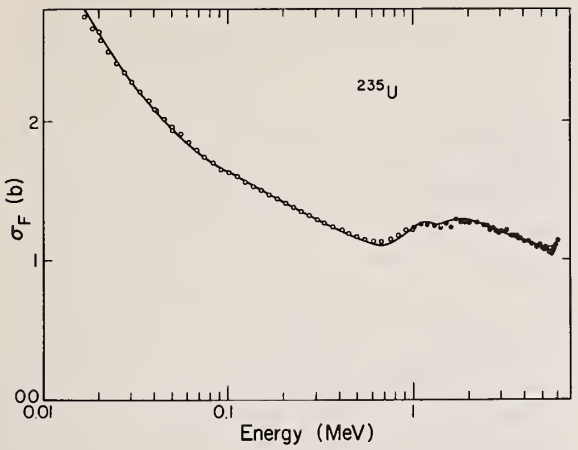


Fig. 15. The fission cross section of ($^{235}$U + n) below 6 MeV. The solid line represents the calculated curve, and shows the broad structure one expects to be able to reproduce by model calculations in the region of smooth cross sections.

is the region which gives the most difficulty, because we have very little knowledge of either spectrum. (4) Finally, above 2 MeV, we reach what we have called the continuum region, where the very rapidly increasing level density both for fission channels and inelastic levels gives the familiar plateau and quickly drives all other compound-nucleus cross sections to zero.

When we first began this study, we had hoped to find that the same approach, perhaps even the same parameters, would provide an adquate representation for all the isotopes of uranium and plutonium. We find that this is not the case. For ($^{239}$Pu + n), the resonance parameters suggest that there is one $0^+$ channel fully open at the neutron binding energy, and a second is partially open; the $1^+$ channel should correspond to an average fission width of 0.04 eV. In fitting the smooth cross sections below 400 keV, however, we find that this gives too much s-wave-neutron-induced fission. To achieve a fit, we must reduce the average width for $1^+$ levels at the neutron binding energy by a factor of two. For both ($^{233}$U + n) and ($^{241}$Pu + n), placing the excitation energy of the transition state which produces $3^+$ fission near the energy of the observed gamma vibrational band in $^{234}$U and $^{242}$Pu is not satisfactory; it must be nearly 300 keV lower if it is to provide enough $3^+$ fission to describe the resonance fission widths and the fission cross sections below 400 keV. For fissile targets other than $^{235}$U, we find that this simplified calculation tends to underpredict the fission cross section below 1.5 MeV and to overpredict significantly near 2 MeV. For the even-even targets, we have not seriously attempted to fit the data from threshold to 3 MeV. The fission channel spectrum is not well known, and the low energy resonances give no information. While this is an important region, it is not within the scope of the present study.

## Discussion

The primary purpose of this review is to show how one might go about using average parameters obtained from neutron cross section measurements in the resonance region to extrapolate to substantially higher energies in describing the fission cross sections for actinide nuclei. For illustration purposes, we have chosen a greatly simplified nuclear model, holding as many parameters fixed as possible. We find that average resonance spacings provide a level density formula which seems to be adequate. Average s- and p-wave neutron widths provide input for a least-squares adjustment giving neutron transmission coefficients. Average radiation widths provide an expression for the energy dependence which is adequate for extrapolation over a limited range. Finally, we suggest a way in which average partial fission widths might be used to give some indication of the appropriate fission channel spectrum.

We feel that model calculations can be an extremly useful tool in both measurement and evaluation of nuclear data. We have shown how even a very simple calculation can provide qualitative understanding of certain systematic behavior. One can expect that a state-of-the-art programmatic effort in nuclear modeling can provide suggestions for important new areas where measurements are needed, either as input to the calculations or to resolve serious discrepancies. Finally, there is the problem of non-existent and unmeasurable data for which modeling is the only solution.

## Acknowledgements

The author would like to express his appreciation to Philip A. Seeger of the Los Alamos Scientific Laboratory for countless helpful discussions and for a critical reading of the manuscript, to Augustus Prince of the Brookhaven National Laboratory for communicating his results of JUPITOR-1 calculations for $^{238}$U and $^{239}$Pu, and to William G. Davey of the Los Alamos Scientific Laboratory, who, in pointing out the connection between low energy measurements and nuclear modeling, suggested the outline for this study.

---

*Work performed under the auspices of the USERDA.

[1] R. J. Brissenden and C. Dursten, U.K.A.E.A., Winfrith, in Proceedings of the Conference on the Application of Computing Methods to Reactor Problems," May 17-19, 1965, Argonne National Laboratory, Illinois, USAEC Report ANL-7050, p. 51, August 1965.

[2] L. B. Levitt, Nuc. Sci, Eng. 49, 450 (1972).

[3] W. G. Davey, Private communication (1975).

[4] W. A. Coleman and T. W. Armstrong, USAEC Report ORNL-4606, October 1970.

[5] L. R. Veeser, G. J. Russell, E. D. Arthur, P. A. Seeger, W. F. Sommer, D. M. Drake, and R. G. Fluharty, in "Proceedings of the Conference on Nuclear Cross Sections and Technology," Washington, D.C., March 1975, paper FB3.

[6] S. F. Mughabghab and D. I. Garber, USAEC Report BNL-325, 3rd Ed., Vol. 1 (1973).

[7] Ch. Lagrange, in "Critique of Nuclear Models and their Validity in the Evaluation of Nuclear Data," EANDC Topical Discussion, Tokyo, March 1974 (to be published.)

[8] T. Tamura, Revs. Mod. Phys. 37, 679 (1965), and USAEC Report ORNL-4152 (1967).

[9] A. Prince, Private communication (1974). We are greatly indebted to Dr. Prince for communicating the results of these calculations.

[10] C. A. Uttley, C. M. Newstead, and K. M. Diment, in "Nuclear Data for Reactors," IAEA, Vienna, Vol. I, p. 165 (1967).

[11] A. M. Lane and R. G. Thomas, Revs. Mod. Phys. 30, 257 (1958).

[12] R. B. Schwartz, R. A. Schrack, and H. T. Heaton II, Nuc. Sci. Eng. 54, 322 (1974).

[13] Y. Ellis, Nuclear Data Sheets B4, 581, 623, 635, 661, 683 (1970).

[14]Y. A. Ellis and M. R. Schmorak, Nuclear Data Sheets B8, 345 (1972).
[15]P. A. Seeger and W. M. Howard, Nuc. Phys. A238, 491 (1975).
[16]W. Hauser and H. Feshbach, Phys. Rev. 87, 366 (1952).
[17]A. Gilbert and A. G. W. Cameron, Can. J. Phys. 43, 1446 (1965).
[18]J. M. Blatt and V. F. Weisskopf, Theoretical Nuclear Physics, John Wiley and Sons, New York (1952), p. 371.
[19]B. B. Back, O. Hansen, H. C. Britt, and J. D. Garrett, Phys. Rev. C9, 1924 (1974).
[20]B. B. Back, H. C. Britt, O. Hansen, B. Leroux, and J. D. Garrett, Phys. Rev. C10, 1948 (1974).
[21]H. L. Smith, R. K. Smith, and R. L. Henkel, Phys. Rev. 125, 1329 (1962).
[22]V. M. Strutinsky, Nuc. Phys. A95, 420 (1967).
[23]H. C. Britt and J. R. Huizenga, Phys. Rev. C9, 435 (1974).
[24]G. E. Hansen, D. M. Barton, G. A. Jarvis, P. G. Koontz, and R. K. Smith, Private communication (1973).
[25]G. F. Auchampaugh, J. A. Farrell, and D. W. Bergen, Nuc. Phys. A171, 31 (1971).
[26]L. Forman, M. G. Silbert, and A. D. Schelberg, to be published (1975).
[27]J. Jary, in "Critique of Nuclear Models and their Validity in the Evaluation of Nuclear Data," EANDC Topical Discussion, Tokyo, March 1974 (to be published).
[28]A. Gavron, H. C. Britt, E. Konecny, J. Weber, and J. B. Wilhelmy, Phys. Rev. Letters, to be published (1975).
[29]J. D. Cramer and H. C. Britt, Nuc. Sci. Eng. 41, 177 (1970).
[30]G. A. Keyworth, C. E. Olsen, F. T. Seibel, J. W. T. Dabbs, and N. W. Hill, Phys. Rev. Letters 31, 1077 (1973).
[31]N. J. Pattenden and H. Postma, Nuc. Phys. A167, 225 (1971).
[32]J. R. Smith and R. C. Young, USAEC Report ANCR-1044, ENDF-161 (1971)
[33]C. M. Lederer, J. M. Jaklevic, and S. G. Prussin, Nuc. Phys. A135, 36 (1969).
[34]F. K. McGowan, C. E. Bemis, Jr., W. T. Milner, J. L. C. Ford, Jr., R. L. Robinson, and P. H. Stelson, Phys. Rev. C10, 1146 (1974).
[35]K. Katori, A. M. Friedman, and J. R. Ershine, Phys. Rev. C8, 2336 (1973).

# SAFEGUARDS AGAINST THEFT OR DIVERSION OF NUCLEAR MATERIALS

T.B. Taylor
International Research and Technology Corporation
1501 Wilson Boulevard
Arlington, Virginia 22209

An overview of the risks and safeguards relevant to the possible theft or national diversion of special nuclear materials from peaceful nuclear enterprises is presented.

This paper is a brief overview of the risks of theft or diversion of nuclear materials from components of non-military nuclear technology and present and possible future safeguards designed to reduce those risks. Various technical and non technical aspects of this subject are covered in much greater detail in a number of recent publications. (1-7)

The information and non-nuclear materials needed to make fission explosives are now widely distributed and available to the general public. Dozens of nations have or could acquire the skills and facilities required to design and build reliable, lightweight, and efficient fission explosives. Crude, inefficient, and statistically variable yield, but nonetheless highly destructive fission explosives that could be transported by automobile could be designed and built by small groups of people, conceivably by individuals working alone, if they somehow managed to acquire the needed quantities of special nuclear materials. Under some conditions this could be done in an ordinary home workshop, using equipment and materials that are commercially easily available worldwide.

Plutonium, highly enriched uranium, or U-233 of the isotopic compositions used or produced in all types of power reactors could be used as core materials for fission explosives. Metallic, oxide, and some other chemical forms of these could all be used. The required amounts and the resulting explosion efficiencies, however, would depend on the chemical forms, as well as the specific type of supercriticality assembly system used.

The presence of Pu-240 and Pu-242, and the associated neutrons released by their spontaneous fission does not preclude the use of reactor grade plutonium in fission explosives. Under some conditions the minimum yield of such explosives might be comparatively low, of the order of the equivalent of 100 tons of high explosive, and the actual yield of a specific device could only be predicted to be within a rather wide range; i.e., a probability distribution of a yield, rather than a specific yield, is all that could be predicted.

It is well known that imposion-type fission explosives achieve supercriticality by compressing the special nuclear material core. Thus fission explosives can be made with amounts of special nuclear material that are initially subcritical at normal densities. The normal density critical masses of metallic spheres of uranium enriched to 93% in U-235, plutonium containing a volume fraction of 30% of Pu-240 plus Pu-242, and 95% of U-233, each in a thick natural uranium reflector, are, respectively, about 17 kilograms, 8 kilograms, and 6 kilograms. In the form of oxides at crystal density, the corresponding critical masses are 20% to 30% greater.

Plutonium, if dispersed in micron-size or smaller particles suspended in air, could also be used as a means for causing large numbers of human casualties and considerable property damage in a densely populated area. As little as a few grams of plutonium more or less uniformly distributed in the air inside an office or residential building area of several thousand square feet for fifteen minutes could deliver an inhalation dose to the occupants that would be likely to cause death from cancer some years later. Dispersal of somewhat larger quantities of plutonium in outside air could cause the evacuation from and decontamination of significant fractions of a large metropolitan area, the actually affected areas depending on weather conditions, the characteristics of buildings in the area, and a number of other factors.

Thus the presence of special nuclear materials within components of the world's nuclear energy system carries with it the risks of their diversion by nations from peaceful to military purposes, or of their theft by criminals for extortionist, terrorist, or other criminal purposes. The extent of these risks depends not only the motives of national governments and non-national groups of people, but also on the numbers and geographical distribution of places where these materials exist, the quantities of special nuclear materials at such places, and the types of safeguards against national diversion or criminal theft to which the materials are subjected.

The total amount of plutonium that has already been produced in the world's nuclear power plants (excluding the reactors in the United States, the Soviet Union, and the Peoples' Republic of China that have been used only for production of nuclear materials for weapons) is roughly 60,000 kilograms, a majority of which is still contained in irradiated reactor fuel assemblies that have not been reprocessed. Of this, about 12,000 kilograms are accounted for in 15 countries that have operating power reactors, but that have not publicly announced nuclear weapons systems: Argentina, Belgium, Bulgaria, Canada, Czechoslovakia, Western Germany, Eastern Germany, India, Italy, Japan, the Netherlands, Pakistan, Spain, Sweden, and Switzerland. (8) In addition, the following 30 countries have announced intentions to acquire large nuclear power plants within the next ten years: Australia, Austria, Bangladesh (perhaps recently cancelled), Brazil, Chile, Egypt, Finland, Greece, Hong Kong, Hungary, Iran, Ireland, Israel, Jamaica, South Korea, Luxembourg, Mexico, New Zealand, Norway, Pakistan, the Phillipines, Poland, Portugal, Romania, Singapore, South Africa, Taiwan, Thailand, Turkey, and Yugoslavia. (9) This brings to at least 50 the total number of countries that can be expected to have sufficient quantities of plutonium for at least dozens of fission explosives by 1985. By 1980 the world's total rate of production of plutonium in power reactors in about 30 countries is expected to be more than 40,000 kilograms per year, and the cumulative total produced by then will be more than 200,000 kilograms.

At least ten countries--the United States, the Soviet Union, the United Kingdom, france, the Peoples' Republic of China, Belgium, Western Germany, Italy, Japan, and India--have or are constructing nuclear fuel reprocessing plants capable of separating several hundred kilograms or more of plutonium per year. No

commercial reprocessing plant has been in operation in the United States since early 1972, and none will be until mid 1976, at the earliest. In Western Europe, on the other hand, substantial reprocessing facilities now exist in several countries.

The International Atomic Energy Agency (IAEA) in Vienna has the responsibility for safeguards to detect diversion of nuclear materials from peaceful purposes to destructive purposes by nations that are parties to the Treaty on Non-Proliferation of Nuclear Weapons (NPT) or that have otherwise agreed to place their civilian nuclear materials under international safeguards. It is not responsible, however, for applying physical security safeguards to prevent overt theft or clandestine diversion by non-national groups, such as terrorists or other criminals. This is left to individual countries to take care of.

Although the IAEA has served an international safeguarding function for more than 15 years, its present safeguards system requires additional strengthening to assure that national diversion of significant quantities of nuclear weapons materials will be promptly detected. The present IAEA annual budget for this purpose is roughly $5 million. Somewhere around 50 IAEA inspectors have the job of performing audits of nuclear material balances and periodically inspecting nuclear facilities in several dozen countries, a huge task for such a small group.

Present U.S. physical security applied to special nuclear materials for civilian purposes, though strengthened substantially during the last two years, is still inadequate to prevent theft by determined groups having resources and skills similar to these that have been used for successful bank robberies or hijacking of valuable shipments in the past.(10) Serious consideration is now being given by the Nuclear Regulatory Commission to possible new regulatory actions designed to protect special nuclear materials in the United States against overt theft or clandestine diversion considerably more effectively than is implied by current regulations and regulatory guides. There are also indications that other countries are planning to do the same. The remainder of the paper is concerned with possible new safeguards measures that might be adopted in the United States and other countries to provide much better physical security for special nuclear materials than at present.

A guiding principle, called the "principle of containment" has been proposed for the design and assessment of security systems for the protection of special nuclear materials. (11) According to this principle, all materials that could be used to make fission explosives and that are used, produced, or processed in the nuclear power industry would be contained in areas circumscribed by a well defined set of barriers. These barriers would exclude unauthorized persons. A minimum number of authorized channels for the flow of such materials through the barriers would be established. All other channels would be continuously monitored, by means of the best available technology, to detect any unauthorized flow of materials. In addition to the physical barriers, and other deterrents to theft, a network of alarms, communications, and security forces would be set up in such a way that no credible attempt to remove nuclear materials from authorized channels, whether by employees, outsiders, or a combination, would be successful.

Some of the specific security measures that might effectively be used in applying this principle and that are under study are the following:

- Co-location of fuel reprocessing and fuel fabrication plants at the same site, to remove the particularly vulnerable transportation link for recycled plutonium in concentrated form. This is not current practice.

- Dilution of separated plutonium by slightly enriched or natural uranium at the output stages of reprocessing plants, to produce the mixed oxide fuel materials before transfer to a fuel fabrication plant. (12) In equilibrium, the concentration of plutonium in mixed oxide fuel would be about 0.6% if all refabricated fuel for a light water reactor power system consisted of mixed oxides. This would not only lead to a requirement for chemical separation of the plutonium from stolen fuel material before it could be used for making fission explosives, but also, and perhaps more importantly, increase by more than a factor of 100 the total weight of fuel material that would have to be stolen to provide a given weight of contained plutonium.

- "Spiking" of plutonium, or, where applicable, highly enriched uranium or U-233 with intensive gamma ray emitters in sufficient quantities to require massive shielding to prevent lethal doses of gamma radiation from being delivered, in an hour or less, to people handling kilogram quantities of these special nuclear materials. The "spiking" materials could be retained fission products with relatively low thermal neutron cross sections, or added isotopes, such as Co-60. "Spiking" at such high levels (in the range of hundreds of REM's per hour per kilogram of plutonium at one meter, for example) would require use of massive shielding at all subsequent steps in a fuel cycle, to keep radiation exposures to workers at acceptable levels. Although some preliminary studies of this possibility are underway, it is not yet clear whether it will be cost effective.

- "Spiking" of special nuclear materials with gamma ray or neutron emitters in order to make them easier to detect with passive monitoring equipment. Routine use of this technique could lower the threshold for detection of unshielded special nuclear materials at doorway monitors, for example, to less than one gram, without requiring anywhere near as much shielding to keep worker exposures at acceptable limits as if "spiking" were used to make the materials "self-protecting."

- Use of specially designed motor vehicles and shipment vans designed to protect shipments of special nuclear materials from rather massive and sophisticated attempts to penetrate the van or commandeer the vehicle for sufficiently long times to allow large law enforcement, or even military forces to arrive at the scene of an attempted hijacking before it can be completed.

- As an alternative to the above measure, the use of rail transport of all special nuclear materials inside shipping containers similar to the roughly 100 ton containers contemplated for use in shipping irradiated fuel from reactors to reprocessing plants.

- The establishment of a Federal protective service for the explicit purpose of safeguarding nuclear materials in transit and also at fixed sites. This possibility is currently being assessed by the Nuclear Regulatory Commission.

A common reaction to these and other proposed major new safeguards measures is that, taken together, their costs are likely to make nuclear power economically uncompetitive with alternative sources of energy. Preliminary studies of the capital and operating costs of considerably more effective safeguards than those called for by present regulations, however, strongly suggest that this is not the case. One such set of estimates, for example, leads to the conclusion that the operating costs of a rather massive security system applied to light water reactor fuel cycles, with routine recycle of plutonium, would correspond to less than 1% of the cost of nuclear electric power produced by the system. (13) The total number of physical security personnel employed for the safeguarding of an 80,000 MW(e) light water reactor fuel cycle, with 20 separately sited power plants, was taken to be about 800, of whom approximately 150 would be on duty at any particular time.

Thus, from technical and economic standpoints, it appears to be possible to design physical security systems that would require skills and resources greater than those used for major thefts of valuables in the past for successful theft of potentially dangerous quantities of special nuclear materials. Whether or not the institutional and political obstacles confronting efforts to implement such effective safeguards against theft, and also against national diversion of special nuclear materials, can be overcome within the next few years, however, remains to be seen.

References


1. Leachman, R.B., Althoff, P., ed., *Preventing Nuclear Theft: Guidelines for Industry and Government.* New York: Praeger, 1972.
2. Willrich, M., ed., *International Safeguards and Nuclear Industry.* Baltimore, Md: Johns Hopkins University Press, 1973.
3. Comptroller General of the United States, *Improvements Needed in the Program for the Protection of Special Nuclear Materials.* Report to the Congress by the General Accounting Office, Washington, 1974, and *Protecting Special Nuclear Material in Transit: Improvements Made and Existing Problems (B-184105),* GAO, 1974.
4. McPhee, J., *The Curve of Binding Energy.* New York: Farrar, Straus, and Giroux, 1974.
5. Willrich, M., Taylor, T.B., *Nuclear Theft: Risks and Safeguards.* Cambridge, Mass: Ballinger, 1974.
6. Rosenbaum, D.M., et al., *Special Safeguards Study.* Prepared for the AEC's Director of Licensing in the spring of 1974.
7. U.S. Atomic Energy Commission. Tech. Rep. WASH-1535 *Proposed Final Environmental Statement, Liquid Metal Fast Breeder Reactor Program,* 1974.
8. U.S. Atomic Energy Commission, *Nuclear Power Growth, 1974-2000,* WASH-1139, 1974.
9. Ibid.
10. See References 1-7.
11. See Reference 5.
12. Private communication: Puechl, Karl, 1975.
13. See Reference 7.

# FISSION THEORY AND ACTINIDE FISSION DATA

A. Michaudon
Service de Physique Nucléaire - Centre d'Etudes de Bruyères-le-Châtel
B.P n° 61 - 92120 Montrouge , France

Abstract

The understanding of the fission process has made great progress recently, as a result of the calculation of fission barriers, using the Strutinsky prescription . Double-humped shapes were obtained for nuclei in the actinide region . Such shapes could explain, in a coherent manner, many different phenomena : fission isomers, structure in near-threshold fission cross sections, intermediate structure in subthreshold fission cross sections and anisotropy in the emission of the fission fragments . A brief review of fission barrier calculations and relevant experimental data is presented. Calculations of fission cross sections, using double-humped barrier shapes and fission channel properties, as obtained from the data discussed previously, are given for some U and Pu isotopes .

The fission channel theory of A. Bohr has greatly influenced the study of low-energy fission .However, recent investigation of the yields of prompt neutrons and $\gamma$ rays emitted in the resonances of $^{235}U$ and $^{239}Pu$, together with the spin determination for many resonances of these two nuclei cannot be explained purely in terms of the Bohr theory . Variation in the prompt neutron and $\gamma$-ray yields from resonance to resonance does not seem to be due to such fission channels, as was thought previously, but to the effect of the (n, $\gamma$ f) reaction .

The number of prompt fission neutrons and the kinetic energy of the fission fragments are affected by the energy balance and damping or viscosity effects in the last stage of the fission process, from saddle point to scission . These effects are discussed for some nuclei, especially for $^{240}Pu$ .

## 1 - Introduction

The design of nuclear reactors, especially for the fast breeders, requires the knowledge of a great variety of accurate fission data ; among them are i) the neutron-induced reactions for the fuel elements and for the transuranic nuclei formed during the operation of the reactor ii) the average number $\bar{\nu}_p$ and the spectrum of the prompt neutrons which are emitted per fission . These data are often needed over a wide range of incident neutron energies (for example from thermal energy to 20 MeV) and sometimes with an accuracy equal to or better than 1 % . It is obvious that such data cannot be obtained from the nuclear theory of a very complex phenomenon which is not very well known yet, despite extensive studies carried out for more than 35 years . Therefore, most of the accurate fission data come from measurements supplemented by evaluation . But fission theory plays an important role . It is essential, indeed, to have a good understanding of the fission process in order to know what the available fission data actually mean and to treat them adequately . For example, the intermediate structure effect in some subthreshold fission cross sections has changed completely the picture previously accepted of statistical properties of fission resonance parameters . This effect had not been understood until double-humped fission barrier shapes were obtained in Strutinsky's calculations and a new fission mechanism was proposed .Also, calculations based on reliable fission models, hence on fission theory, are needed to provide good evaluated fission data not only by fitting the experimental data but also and mainly by interpolating and extrapolating the known data to energy regions and/or to nuclei where no experimental results are available yet . This type of "model calculations" is more and more used by the evaluators and must be based on good fission theory .

An extensive and detailed assessment of the contribution of fission theory to fission data is largely beyond the scope of this paper . Rather, we shall focus our attention on some aspects of the fission process which may be useful for obtaining or understanding various fission data . This explains the following organization of the talk :

- Fission barriers (static and dynamical aspects) .
- Fission channel theory of Bohr .Application to the $^{239}Pu$ resonances . The (n, $\gamma$ f) reaction .
- Damping effects . Application to the fission of $^{240}Pu$ at low energy .

## 2 - Fission barriers

2.A - The fission barrier of a nucleus is determined from the knowledge of the multidimensional potential energy surface over a wide range of deformations, from the ground state to scission through the saddle point . This potential energy cannot yet be calculated accurately by fundamental methods . Though Hartree-Fock methods are making rapid progress for the treatment of largely deformed nuclear systems[1] , they cannot be used at present to calculate fission barriers with a good precision . The most reliable method consists in using the phenomenological prescription of Strutinsky[2] in which the total energy $E_{\{s\}}$ of the nuclear system at a given deformation $\{s\}$ is obtained by adding to the liquid drop energy $E_{LD}$ ( $\{s\}$ ) a shell energy correction $\Delta E_{sh}$ ($\{s\}$) which takes into account the bunching of the single-particle levels near the Fermi surface :

$$E_{(\{s\})} = E_{LD}(\{s\}) + \Delta E_{sh}(\{s\}) \qquad (1)$$

Several groups are actively engaged in such macroscopic-microscopic calculations in which the correction $\Delta E_{sh}$ ( $\{s\}$ ) is obtained by using different types of shell-model potentials : Harmonic oscillator[2,3] , Woods-Saxon[4] , folded Yukawa[5] , two-centre potentials[6,7,8] . These calculations give fission barrier shapes with two humps for nuclei in the actinide region, as is illustrated in Fig.1 . Such barrier shapes can explain in a coherent manner many different aspects of the fission phenomenon which were discovered independently one from another, for example : fission isomers, intermediate structure in subthreshold fission cross sections, structure in near-threshold fission cross sections, angular distribution of the fission fragments . This subject has been treated already in several review papers[9,10,11,12] .

2.B - Let us sum up the main aspects of the situation. About 45 fission isomers have been identified in nuclei from U through Cf isotopes with half-lives between $5.10^{-11}$ s. ($^{242}Cm$) and $1.4.10^{-2}$ s. ( $^{241}Am$)
The subnanosecond time region has been explored for even-even U and Cm fission isomers using a geometrical magnifying effect in the fission-in-flight method[13] . No doubt that other fission isomers having shorter life-times and formed with lower isomeric ratios could be observed using improved techniques . Strong odd-even effects in the life-time values, sometimes as large as $10^3$ in ratio, are observed for most of the

fission isomers . It is not clear at present whether these effects are due to a change in barrier height (as modified by pairing and/or specialization energies) or in barrier penetration (caused by a different curvature and/or mass inertia parameters) or both . Delayed fission deexcitation of the fission isomers seems to come not only from the ground state but also from excited states in the second well of the fission barrier . Prompt $\gamma$-ray transition between excited states of the ground state rotational band in the second well, preceding delayed fission deexcitation, has been detected through conversion electrons for the 4 ns $^{240}Pu$ fission isomer[14]. The low value of their measured energy gives the first piece of evidence that the fission isomers have a large moment of inertia, hence a large deformation, in agreement with the double-humped barrier representation[14]. The $\gamma$-ray decay of a shape isomer by tunneling through the inner barrier (the $\gamma$-branch) has been observed for $^{238}U$ (ref.15). Information on the spin and parity $I^{\pi}$ of the fission isomers is extremely scarce . Indication on the $I^{\pi}$ values for some of them is obtained from the angular distributions or the anisotropy of the fission fragments[16,17] .Unambiguous $I^{\pi}$ values are very difficult to determine since i) several combinations of I and K quantum numbers can fit the data iii) it is not sure that value of K for the nuclear system is conserved when crossing the outer barrier and ii) the initial alignment of the compound nucleus formed by the reaction can be modified by neutrons and $\gamma$ rays emitted before the formation of the shape isomer and also by the perturbation brought about by extra nuclear fields .

The intermediate structure in subthreshold fission cross sections has been observed for several non-fissile isotopes (a review of the subject is given in[9]) This phenomenon has been interpreted as being due to the existence of compound nucleus states in the second well of the double-humped fission barrier (class-II states)[18] as is illustrated in Fig.2 . The fine structure of the narrow resonances due to the compound nucleus states in the first well (class-I states) is then modulated by the coupling of these states to the fission exit channels through the class-II states acting as intermediate states . According to this proposed mechanism, all the large fission resonances belonging to a given cluster should have the same spin, that of the class-II state responsible for their enhanced fission width . This has been verified experimentally for $^{237}Np$ where the intermediate structure effect is quite pronounced[19] and where the "s" wave resonances can have two J values (J=2 and 3) . An unambiguous experiment using polarized neutrons and a polarized $^{237}Np$ target, clearly demonstrates that the fission contribution in the first cluster at 40 eV comes essentially from one spin state (J=3) (See Fig. 3)[20] . This mechanism also predicts that, in a given cluster, the large fission resonances should have their fission widths distributed, on the average, along a lorentzian, as a function of incident neutron energy . In addition to this smooth behavior these fission widths should exhibit-Porter-Thomas fluctuations . Such a distribution is actually observed in presently available data[9,21] .

Analysis of available fission data relevant to an interpretation in terms of the double-humped barrier can yield information on barrier parameters such as the heights of the two maxima and of the second minimum relative to the energy of the ground state . Comparison of such "experimental" fission barrier parameters with calculated values shows in general, good overall agreement but with a few areas of discrepancies ; for instance, in the Th region , the measured inner barrier is definitely higher than all values obtained from calculations[9] .

Another interesting aspect to investigate in the potential energy landscape of the fissioning nucleus is the behavior of the surface as a function of odd deformation parameters . It is a well-known fact that low-energy fission is an asymmetric fragmentation for most actinides except for the lighter ones where a mixture of symmetric and asymmetric yields can appear (see $^{227}Ac$, for example) and also for $^{258}Fm$ which seems to prefer symmetric fragmentation only . Compilation of fragment mass distributions for the actinides shows also that, for increasing mass of the fissioning nucleus, the leading side of the heavy fragment peak seems very stable (around Z=50 and N=82) whereas the light fragment peak moves toward higher masses . These features seem connected to shell effects but no satisfactory explanation could be provided before extensive calculations for odd and even deformation parameters, using the Strutinsky prescription, could be available . An illustration of calculations of this type is shown for $^{236}U$ in Fig.4[8] , where it can be seen that asymmetry in the fission fragment yields is apparent in the potential energy surface at scission . A closer examination of the picture indicates that asymmetry in the nuclear system already appears at the second saddle point, between the shape isomer and scission, where a double valley starts to develop and deepens for increasing deformation as the shell structure of the nascent fragments plays a more important role due to a more pronounced necking-in . Comparison of experimental mass distributions with those obtained from such calculations shows qualitative agreement . In particular, it is of interest to note that, for light actinides ($^{226}Ac$), the threshold for symmetric fission appears a few MeV higher than that for asymmetric fission[22] . Nevertheless, a quantitative account of the experimental results cannot be obtained from the theory yet[12],especially since these potential energy calculations should be supplemented by a satisfactory theory of the fission dynamics which is started being studied .

2.C - The calculation of fission cross sections or fission life-times (for example for the ground state), requires the knowledge of the equation of motion for the fissioning system all the way to scission . This cannot be achieved without some theory of fission dynamics which, on the other hand, is poorly understood at present. One does not even know what type of fission dynamics is to be applied since it seems to depend strongly on the excitation energy (See Section 4). In the absence of an appropriate theory, one is led to make very crude assumptions in actual calculations .

- At low energy, in the sub-barrier region, it is generally assumed that the phase corresponding to the crossing of the barrier (i.e. where $E(\{s\})$ is greater than the energy E of the system) is adiabatic. This hypothesis means that the fission mode does not induce real intrinsic excitations in the system. After the crossing of the barrier, when the nucleus moves, in an irreversible manner, from the point of exit (where $E = E(\{s\})$) to scission, the fastness of the process is such that the adiabatic approximation is questionable. Viscosity effects may then appear in which real intrinsic excitations can be produced due to their coupling to the fission mode . These effects can affect the properties of the fragments (kinetic and excitation energies) but do not modify the fission probability since they appear in the last stage of the process only.

- At higher excitation energy, above the barrier, the situation is more complicated since viscosity (or damping) effects can appear at a much earlier stage of the process and therefore modify the value of the fission probability . In this energy range, general use is made of the Bohr-Wheeler formula :

$$2\pi \frac{\langle \Gamma_f \rangle}{\langle D \rangle} = N_f \qquad (2)$$

where :

- $\langle \Gamma_f \rangle$ and $\langle D \rangle$ are respectively the average fission width and spacing of the compound nucleus states taken into account .

and - $N_f$ is the number of states available at the saddle point .

This formula, which will be discussed in more detail in Section 3, is derived by assuming statistical equilibrium and is generally verified experimentally . It has been pointed out, nevertheless, that this relation requires finite viscosity for the collective motion .

Let us now comment on these two hypotheses and illustrate how they can be used for the calculation of some fission data .

- The adiabatic approximation is certainly justified for the calculation of life-times $\tau_{g.s}$ for spontaneous fission of nuclei in their ground state . In that case, the fission probability $\lambda$ per unit time ( $\lambda = (\tau_{g.s})^{-1}$ ) is equal to the frequency $2\pi\omega_f$ for the zero-point motion mode, multiplied by the barrier penetrability P .

$$\lambda = 2\pi\omega_f \times P \qquad (3)$$

In actual calculations, it is generally assumed that $1/2\hbar\omega_f = 0.5$ MeV and the value of P can be obtained by standard WKB techniques[25] . The calculations of P are greatly simplified for one dimensional fission barriers and constant mass parameters B . One then obtains :

$$P \cong \exp\left(-2\frac{S}{\hbar}\right) \text{ if } S \gg \hbar \qquad (4)$$

with $$S = \int_{s'}^{s''} \sqrt{2\,|\,E - E(s)\,|\,.\,B}\;.\;ds \qquad (5)$$

In this last expression :

- s is the deformation parameter along the fission path .
- s' and s" (with s" > s') are the values of s, respectively at the entrance and exit of the barrier for which the total energy E of the system is equal to that of the barrier (E = E(s') = E(s")).

Improvements to life-time calculations have been brought about recently by a more sophisticated approach [4,26], that we shall summarize below .

It is first considered that the potential energy is known in a multidimensional space with a set $\{s\} = (s_1, s_2, \ldots s_i \ldots s_j \ldots)$ of deformation coordinates, using the Strutinsky procedure . But the major step forward is to consider that the mass inertia parameter B is no longer constant but can vary with $\{s\}$ . This is justified by noting that the shell structure, which is so important in the calculation of the potential energy also plays a major role in the value of the mass tensor $B_{ij}$ (the indices i and j refer to the deformation coordinates $s_i$ and $s_j$ respectively) . Actual calculations of $B_{ij}$, using the "cranking" formula show oscillations in these values with deformation quite similar to those of $\Delta E_{Sh}$ discussed previously . In this multidimensional representation, with possible variations in $B_{ij}$ with $\{s\}$ taken into account explicitly, the expression for S now reads :

$$S = \int_{\sigma'}^{\sigma''} \sqrt{2\,|\,E - E(\{s\})\,|\;B(\sigma)}\,d\sigma \qquad (6)$$

where :

- the deformation parameters $s_i$, $s_j$, are supposed to be functions of some arbitrary parameter $\sigma$ .
- $\sigma'$ and $\sigma''$ are the end-point values of the parameter $\sigma$, similar to s' and s" defined in (5), for which $E = E(\sigma') = E(\sigma'')$ .
- $B(\sigma)$ is the effective mass defined by the following relation :

$$B(\sigma) = \sum_{i,j} B_{ij}\left(s_1(\sigma), s_2(\sigma) \cdots s_i(\sigma)\, s_j(\sigma) \cdots\right) \frac{\partial s_i}{\partial \sigma} \cdot \frac{\partial s_j}{\partial \sigma} \qquad (7)$$

In the adiabatic approximation, the collective motion in the fission mode is supposed to be slow enough so that, for each deformation $\{s\}$ ,(or a given $\sigma$ value) the nucleons have enough time to rearrange themselves . It is then justified to consider the state of the system (including the single-particle states $|m\rangle$) at any deformation $\{s\}$ in the sub-barrier region . In these conditions, it is possible to derive an expression for $B_{ij}$ , in terms of the single-particle states $|m\rangle$ ,having eigenvalue $E_m$, using the cranking formula :

$$B_{ij}(\sigma) = 2\hbar^2 \sum_{m \geq 1} \frac{\langle o|\partial/\partial s_i|m\rangle\langle m|\partial/\partial s_j|o\rangle}{E_m - E_o} \qquad (8)$$

The calculation of S, with equation (6), can be carried out provided that a trajectory, the fission path, is defined between the two end points $\sigma'$ and $\sigma''$ . If B had a constant value, the fission path would follow the extremal values of the potential energy surface . This condition defines what is called the "static barrier" . The fission path is no longer the static barrier if B varies with deformation . For example, the fission trajectory may reach higher potential energy if the mass parameter takes there a smaller value . The fission path is then determined by the least-action principle ,which leads to the smallest possible value for S and, consequently, for $\tau_{g.s}$ . Such a path gives the so-called "dynamical barrier" which is illustrated in Fig.5 for $^{240}$Pu. It is interesting to note that the least-action trajectory does not pass through the "static" saddle points, but prefers a path at a somewhat higher energy . This seems to apply to most of the cases studied so far and appears to be a consequance of a large mass parameter at the saddle point . This effect itself is due to the shell structure which gives a large positive shell-energy correction at that deformation .

The validity of this method can be checked by comparing the fission life-time values obtained from such calculations with the experimental ones . This comparison must be carried out with great care since, according to the authors themselves[4,26] the calculations seem to be extremely sensitive to both microscopic and macroscopic properties of the nucleus . Some of these properties are not well known and the uncertainty associated with their values can drastically change the results of the calculations .For example,the variation of the pairing strength with deformation is practically unknown but plays a crucial role in the derivation of the mass tensor $B_{ij}$ from expression (8) . In the absence of more detailed information, it is generally assumed that the pairing strength is either constant or proportional to the surface area of the nucleus. But switching from one to the other of these two assumptions changes the $\tau_{g.s.}$ values by an enormous factor, from 8 to 10 orders of magnitude for Uranium isotopes . A change as small as 10 % in the pairing strength can bring about as large as about five orders of magnitude in the life-time determination . Such variations can be expected in the deformation dependence of the pairing strength . For example, self-consistent calculations of the properties of Sm isotopes for various deformations, using the Hartree-Fock-Bogolyubov method with external constraint, show oscillations in the pairing strength as high as 20 % over a limited range of deformations, much smaller than that met in fission[28]. Also, the liquid drop parameters need to be correctly adjusted to reproduce the experimental data. For example, in Fig.6, where a good overall agreement is achieved between experimental and calculated values of $\tau_{g.s}$, not only a simple assumption was made on pairing but also the reduced fissility parameter $\zeta$,as defined in[5], had to be adjusted separately for the various series of isotopes

Therefore, it would seem that this very interesting method needs to be supplemented by a more accurate knowledge of both microscopic (pairing strength) and macroscopic (LD parameters) properties of the fissioning nucleus as a function of deformation .

- The difficulty in calculating, from basic theory, such a simple quantity as the fission life-time for the ground state is still more pronounced for the calculation of fission cross sections. For example, the theory cannot predict as yet the detailed sequence and the exact energies of the available transition states above the two saddle points of the double-humped barrier. All practical calculations make very crude assumptions about the physical quantities which are needed. In fact, most of the calculations still assume a single-humped barrier with a constant mass parameter B .

A more sophisticated approach, though far from being completely satisfactory, has been developed recently in terms of the double-humped shape, including damping in the two wells of the barrier, and in which the physical quantities needed in the calculations are adjusted by fitting as many relevant fission data as possible[29]. We summarize below this method which makes use of the statistical model for the calculation of the neutron cross sections (including that for fission) of heavy nuclei between 3 keV and 1 MeV .

The main difficulty of the calculations lies in the determination of the fission probability at a given energy and for a well-defined set $\{c\}$ of quantum numbers (generally J,π,M and K). For all sets $\{c\}$ , one-dimensional fission barriers are considered, all of them having the same shape, as sketched in Fig.7 . This shape is obtained by smoothly joining three parabolas having parameters extracted from fits to relevant fission data such as those discussed in Section 2[9,30]. For each set $\{c\}$ ,the barrier is shifted as a whole of an energy $\Delta E$ ($\{c\}$) determined by the fitting procedure. Damping is introduced through the form of an imaginary part in the potential in order to simulate the coupling of the fission mode to the intrinsic degrees of freedom .

The transmission of the barrier is calculated by solving the Schrödinger equation in the complex potential thus obtained .

The experimental data Di, used in this procedure when they are available, are the followings :

$D_1$ - the total fission cross section $\sigma_f$ ($E_n$) at incident neutron energy $E_n$ .

$D_2$ - the angular distribution $\sigma_f$ ($\theta$,$E_n$) of the fission fragments emitted at angle $\theta$ relative to the direction of the incident neutron beam .

$D_3$ - the coefficients $G_L$ ($E_n$) of the Legendre polynomial expansion $\sigma_f(\theta,E_n)=\sum_L G_L(E_n)\cdot P_L(\cos\theta)$ used to fit the $\sigma_f$ ($\theta$,$E_n$) data .

$D_4$ - The anisotropy $a_s(E_n)=\sigma_{f(0°,En)}/\sigma_{f(90°,En)}$

The fission parameters $P_i$ , determined by fitting the above data are :

$P_1$ - the energy shift $\Delta E$ ($\{c\}$) for the lowest fission channel having quantum numbers $\{c\}$ .

$P_2$ - the effective number N ($\{c\}$) of fission channels having quantum numbers $\{c\}$ . This takes into account the possible opening of more fission channels for increasing $E_n$ .

$P_3$ - the coefficients $\alpha_n$ of an analytical expression $N(\{c\}) = f(E_n, \alpha_n)$ describing the variation of N ($\{c\}$) with $E_n$ .

$P_4$ - the maximum depth $W_m$ of the imaginary part of the potential supposed to have a parabolic shape, in the 2nd well.(Full damping is assumed in the first well)

These parameters Pi are determined by a least-square fit to the data Dj . In order to simplify the fitting procedure, only the most important of the 16 combinations Pi x Dj are taken into account, those which connect the available data Dj with the most sensitive parameters Pi .

Illustration of the results obtained in such calculations is given in Fig. 8 and 9 where the calculated fission and capture cross sections for $^{236}U$, $^{238}Pu$ and $^{240}Pu$ are plotted as a function of $E_n$ . Other cross sections such as those for elastic and inelastic scattering are also obtained with this procedure . All the cross sections are calculated by using a coupled-channel optical model potential with the parameters obtained by fitting $^{238}U$ data (ref. 31) .

It is interesting to note that not only the calculated results are in agreement with the experimental data (in fact most of the data have been used in the fitting procedure) but also that this method can give calculated cross sections where no experimental data are available (for example $\sigma(n,\gamma)$ for $^{232}U$, $^{236}U$ and $^{238}Pu$).

In summary, despite the lack of a good fission theory to calculate fission data such as life-times or cross sections, it is nevertheless possible to make use of the fairly good knowledge of the fission barriers and of simple fission models provided that their parameters can be adjusted to accurate and relevant experimental data .

We shall now discuss the fission theory of A.Bohr which is commonly used in the interpretation and the calculation of fission data .

### 3 - Fission Channel Theory of A. Bohr : Application to $^{239}Pu$ resonances . The (n, γf) reaction .

As we have seen in Section 2, it is far beyond the present capabilities of fission theory to predict the fission properties of a specific fissioning state having spin and parity $J^\pi$ and at an excitation energy above the neutron emission threshold and, a fortiori, to predict how these properties vary with $J^\pi$ . Nevertheless, a simplification in this very complex problem appeared when A. Bohr showed that many properties of the fission process through these individual excited states could be discussed in terms of a small set of reaction alternatives or channels, even though the number of different fragment pairs is very large in binary fission of a heavy nucleus[32]. In this approach, A. Bohr proposed the concept of fission exit channels by considering that the passage from saddle point to scission is so rapid that the properties of fission, though strongly dependent on several factors, are nevertheless influenced by those of the transition states at the saddle point. In this picture, the fission exit channels are therefore these transition states whose spectrum, according to A. Bohr, is very similar to that of the first excited states of the nucleus at ground-state deformation .

This channel theory of fission provides also another interpretation of the number $N_f$ of fission exit channels[23]. This concept of "open" fission channels was expressed in terms of fission saddle-point configurations which were energetically available . Their number $N_f$ is given by expression (2) . This expression simply comes from the fact that the ensemble of nucleons finds itself in all allowed configurations (including the N saddle-point configurations) once every period $\tau \sim 2\pi\hbar/\langle D\rangle$ . The life time $\tau_f$ for fission is thus $\tau_f \sim 2\pi\hbar/N\langle D\rangle$ from which the average fission width and Eq.(2) are then deduced .

Within the framework of the channel theory of Bohr, an effective number of fission channels, called $(N_{eff})_{J^\pi}$ , is now defined for each spin and parity $J^\pi$ . This number $(N_{eff})_{J^\pi}$ is also expressed in terms of the average fission width and spacing as in (2) , but, in addition, is equal to the sum of the penetrabilities $P_i$

for each fission channel i having spin and parity $J^\pi$. Each $P_i$ is calculated for the fission barrier associated with the transition state i . Thus :

$$(N_{eff})_{J^\pi} = 2\pi \frac{\langle \Gamma_f \rangle_{J^\pi}}{\langle D \rangle_{J^\pi}} = \sum_i P_i \qquad (9)$$

Let us now examine how the predictions of the Bohr theory are verified in the case of $^{239}Pu$ resonances which are fairly well known (including their spin J) and for which the fission channel properties are very different for the two possible $J^\pi$ values ($J^\pi = 0^+$ and $1^+$) obtained in the capture of "s"-wave neutrons by $^{239}Pu$ . Whereas the lowest $J^\pi = 0^+$ transition state is symmetric and below the neutron separation energy $S_n$ in $^{240}Pu$ (this is in fact the ground state of the system), the lowest $J^\pi = 1^+$ transition state seems to be asymmetric, since it has been postulated to be a combination of the two $K^\pi = 0^-$ and $K^\pi = 1^-$ octupole vibrations, and at an excitation energy above $S_n$ .

The discussion of this subject , as already published in a previous paper[9], is summarized below and supplemented by new results obtained for prompt neutron and $\gamma$-ray emission in the $^{239}Pu$ resonances .

The fission width distribution for the $^{239}Pu$ resonances shows, as for the other fissile nuclei, large fluctuations due to the small number of available fission exit channels defined in terms of the Bohr theory . But, in contrast to all similar distributions, the one for $^{239}Pu$ shows clearly a break, explained by the existence of two families of resonances having widely different average fission width values . This interpretation is supported by the spin determination for a large number of resonances, as obtained by both direct and indirect methods . The values of $N_{eff}$, for $J^\pi = 0^+$ and $1^+$ from the average widths and spacings of the resonances are respectively $(N_{eff})_{0^+} = 1.48$ and $(N_{eff})_{1^+} = 0.07$ . This is in agreement with the Bohr theory if the existence of a $1^+$ transition state of collective character is postulated below the 2-quasiparticle excitations.

The different symmetry properties of the transition states should be reflected in the fission properties of the $0^+$ and $1^+$ resonances .

The mass distribution of the fission products was measured by the "wheel technique" using a nuclear explosion as a pulsed-neutron source[33]. By radiochemical analysis, the valley-to-peak ratio of the mass distribution, or more exactly the $^{115}Cd/^{99}Mo$ ratio R was obtained for more than twenty resonances with energies ranging from 15 to 82 eV. The R-values seem to fall into two categories having average values of R in ratio 3.5 . High and low values of R are associated respectively with $0^+$ and $1^+$ spin states, in agreement with the theory. Moreover , there is also a correlation between the R values and the fission widths, as expected : the fission widths are larger, on the average for the group of resonances having high values of R (Fig. 10).

Variations of the total kinetic energy of the fission fragments were observed and they can also be correlated with the spin states and the variations of R in the way predicted by theory of Bohr[34] .

The behavior of $\bar{\nu}$ , the average number of prompt neutrons per fission, from resonance to resonance, has been more difficult to understand for quite a long time. The situation was very puzzling several years ago when the most complete set of data available at that time showed definite variations in $\bar{\nu}$ , but in opposite directions[35,36] . Moreover, these variations could be correlated with J, but in a different manner ; the high values of $\bar{\nu}$ were associated with $J^\pi = 1^+$ for one set of data[35] but with $J^\pi = 0^+$ for the other one[36]. Nevertheless, both results could find an interpretation in terms of the Bohr theory . For one case[35] it is possible to justify the observed correlation between $\bar{\nu}$ and $J^\pi$ by postulating that, neglecting viscosity effects, the fission barrier associated with the $1^+$ transition state remains higher than for $J^\pi = 0^+$ all the way to scission. This energy difference can them be found in an increase in the excitation energy of the fission fragments, hence in a larger $\bar{\nu}$ value. A different argument can be invoked to explain the other set of results[36] ; since the $1^+$ transition state is asymmetric, a more asymmetric mass division is expected and is actually found for the $1^+$ resonances, as we discussed above. This effect should be accompanied by a lower value due to the well-known saw-tooth behavior of $\bar{\nu}(A_f)$ as a function of the fragment mass $A_f$ (ref.37) .

This confusion was not dissipated by other experiments, carried out a little later, since they concluded to the existence of fluctuations, but not correlated with $J^\pi$ [38,39]. The situation has been clarified by more recent measurements of $\bar{\nu}$ and $\bar{E}_\gamma$ ,the mean $\gamma$-ray energy emitted per fission[40,41].The Saclay results[40] were obtained by using a big (520 l) Gd-loaded liquid scintillator for the detection of the prompt neutrons and $\gamma$ rays emitted per fission. Large fluctuations are observed both in $\bar{\nu}$ and $\bar{E}_\gamma$ measured values which appear to be strongly anticorrelated . This means that high values are generally associated with low $\bar{E}_\gamma$ values . These data can be better understood if they are plotted separately for the $0^+$ and $1^+$ resonances which have been analysed below 200 eV. The fluctuations in $\bar{\nu}$ and $\bar{E}_\gamma$ values together with the anticorrelation between these two quantities clearly appear for the $1^+$ resonances (see Fig.11) but are much less significant for the $0^+$ resonances. Statistical tests applied to these data confirm this effect. The probability that the fluctuations in $\bar{\nu}$ and $\bar{E}_\gamma$ are of purely statistical nature is below $5.10^{-5}$ for the $1^+$ resonances but as large as 0.1 and 0.63 respectively for the $\bar{\nu}$ and $\bar{E}_\gamma$ values of the $0^+$ resonances. Also the correlation coefficient between $\bar{\nu}_i$ and $\bar{E}_{\gamma i}$ , for a set of resonances i, is -0.84 and 0.07 respectively for the two sets of $1^+$ and $0^+$ resonances. There is respectively 7 % and 77 % probability that these two coefficients can be caused by statistical fluctuations only .

A closer examination of the data shows that the fluctuations in $\bar{\nu}$ and $\bar{E}_\gamma$ are larger for the $1^+$ resonances having smaller fission widths. This effect appears more clearly in Fig.12 where both $\bar{\nu}$ and $\bar{E}_\gamma$ are consistent with a linear dependence with $1/\Gamma_f$.

An interpretation of this phenomenon has been put forward[42] in terms of the $(n,\gamma f)$ reaction already considered in a more general context[43] . The width $\Gamma_{\gamma f}$ for the reaction $(n,\gamma f)$ is expected to be fairly small (a few meV according to calculations[43]) and constant from resonance to resonance since it corresponds to a many-exit-channel process. It may occur that, due to the large fluctuations of $\Gamma_f$ discussed previously, $\Gamma_{\gamma f}$ becomes comparable to $\Gamma_f$ for some resonances, more likely to have $J^\pi = 1^+$ rather than $J^\pi = 0^+$ since $\langle \Gamma_f \rangle_{0^+} \gg \langle \Gamma_f \rangle_{1^+}$.For these resonances, the $(n,\gamma f)$ process competes with comparable probability with "direct fission", called (n,fd) in which the initial compound nucleus deexcites directly by fission. This competition explains the properties observed in $\bar{\nu}$ and $\bar{E}_\gamma$ . In the $(n,\gamma f)$ reaction, more $\gamma$ rays and therefore less neutrons are emitted because i) $\gamma$ rays are emitted before scission by the compound nucleus which is thus less excited and ii) the final $\gamma$-ray emission by the fragments below their neutron emission threshold is common to both $(n,\gamma f)$ and $(n, f\, d)$ processes .

These considerations lead to the following relations :

$$\Gamma_f = \Gamma_{\gamma f} + \Gamma_{fd} \quad (10)$$

$$\overline{E}_{\gamma f} = \overline{E}_{\gamma fd} + \overline{e}_{\gamma} \quad (11)$$

$$\overline{\nu}_{\gamma f} = \overline{\nu}_{fd} - \overline{e}_{\gamma} \frac{\partial \overline{\nu}}{\partial E^*} \quad (12)$$

where - the subscripts f, $\gamma$f and fd refer to the total fission, (n,$\gamma$f) and (n,f d) processes

- $-\frac{\partial \overline{\nu}}{\partial E^*}$ is the variation of $\overline{\nu}$ with excitation energy E in "direct fission"

- $\overline{e}_{\gamma}$ is the mean energy of the pre-scission $\gamma$rays emitted in the (n, $\gamma$f) reaction

In the resonances where the (n, $\gamma$f) and (n,f d) reactions compete, the neutron and $\gamma$-ray yields are as follows :

$$\overline{E_{\gamma}} = \overline{E_{\gamma fd}} + \overline{e_{\gamma}} \; \Gamma_{\gamma f}/\Gamma_f \quad (13)$$

$$\overline{\nu} = \overline{\nu_{fd}} - \overline{e_{\gamma}} \frac{\partial \overline{\nu}}{\partial E^*} \cdot \Gamma_{\gamma f}/\Gamma_f \quad (14)$$

These calculated yields show a linear variation with $1/\Gamma_f$ which is actually found in the experimental results for the $1^+$ resonances. The phenomenon is certainly present in the $J^\pi = 0^+$ resonances but is masked by their large fission width .

This seems to be the first piece of evidence for the existence of the (n, $\gamma$f) reaction which is also confirmed by the fact that the average multiplicity $\overline{n_\gamma}$ of the fission $\gamma$ rays emitted in the $^{239}$Pu resonances shows a linear dependence with $1/\Gamma_f$ in the same manner as $\overline{\nu}$ and $\overline{E_\gamma}$ [42] .

Analysis of the $\overline{\nu}$ and $\overline{E_\gamma}$ data, by a least-square fit to the experimental values, is consistent with the conservation of the energy for the sum of the prompt neutron and $\gamma$-ray yields. This analysis gives the following value :

$$\Gamma_{\gamma f} \cdot \overline{e}_{\gamma} = (4.6 \pm 0.4) \times 10^3 \text{ eV}^2 \quad (J^\pi = 1^+) \quad (15)$$

For the $0^+$ resonances, a similar expression can be derived though the phenomenon is much less pronounced :

$$\Gamma_{\gamma f} \cdot \overline{e}_{\gamma} = (8.0 \pm 1.9) \times 10^3 \text{ eV}^2 \quad (J^\pi = 0^+) \quad (16)$$

These values are in agreement with recent calculations making conventional assumptions about the fission and $\gamma$-ray decay of compound nucleus states[40] .

The existence and the influence of the (n, $\gamma$f) reaction for the $^{239}$Pu resonances seems to be clearly established and explains most of the variations observed in $\overline{\nu}$ and $\overline{E_\gamma}$ . It explains also the fact that no resonances have been observed with a fission width smaller than 4 meV, which is very close to the expected value for $\Gamma_{\gamma f}$ .

After removal of the effect of the (n, $\gamma$f) reaction in the $^{239}$Pu resonances, one obtains for the neutron and $\gamma$-ray yields and for the two spin states :

$$(\overline{\nu}_{fd})_{0^+} - (\overline{\nu}_{fd})_{1^+} = 0.0130 \pm 0.0055 \text{ neutrons} \quad (17)$$

$$(\overline{E}_{\gamma fd})_{0^+} - (\overline{E}_{\gamma fd})_{1^+} = 10 \pm 10 \text{ keV} \quad (18)$$

This results in the following difference in the excitation energy $E_f^x$ for the fission fragments and for the two spin states :

$$(E_f^x)_{0^+} - (E_f^x)_{1^+} = 109 \pm 43 \text{ keV} \quad (19)$$

It seems therefore that there is a weak effect of the fission exit channels on the prompt neutron and possibly on the $\gamma$-ray yields and also on the excitation energy of the fission fragments .

Similar studies have been carried out on $^{235}$U (ref. 40) and $^{241}$Pu (ref. 44) but show much smaller effects in the first case and practically none in the second case.

In summary, the fission channel theory of A. Bohr seems generally verified in the fission data, in particular for the case of the $^{239}$Pu resonances which are fairly well known . A careful study of the prompt fission neutron yields supplemented by that of the prompt fission $\gamma$ rays, in the $^{239}$Pu resonances, has clarified a situation which was previously rather confusing . The fluctuations in $\overline{\nu}$ from resonance to resonance seem to be caused by the (n, $\gamma$f) reaction rather than by the effect of fission channels .

4 - Damping effects in fission. (Application to the fission of $^{240}$Pu at low energy)

A complete theory of fission must take into account not only the static aspects, essentially the potential energy surface as a function of deformation coordinates but also the dynamical aspects which include inertial and damping effects . In Section 2, we described the present status of the potential energy surface which is now known with a relatively good accuracy, in contrast to the dynamics of the process . A discussion of a derivation of mass inertia parameter for spontaneous fission, supposed to be adiabatic during the crossing of the barrier, has shown the limitations of the calculational method. But even less is known about damping or viscosity effects which describe the coupling of the fission mode to other degrees of freedom . It seems that damping is quite large in the first well, moderate in the second well, but very little is known about the damping in the last phase, i.e in the descent from the second saddle point to scission. This information is nevertheless very important for predicting the energy share between the kinetic and excitation energies of the fission fragments and therefore the prompt neutron emission . Many contradictory assumptions have been made between the two following extremes : i) full damping in which all the available energy at scission is dissipated into excitation energy with no pre-scission kinetic energy ii) weak damping in which this available energy appears almost completely in the form of pre-scission kinetic energy without intrinsic excitation of the fissioning system .[45,46,47] It is very difficult to find out from the experimental results, what type of damping actually occurs in the descent to scission and how this damping varies with excitation energy . The fragment total kinetic energy $\overline{TKE}$ for the low energy fission of actinides shows a linear dependence with $Z^2 A^{-1/3}$ over a wide range of mass numbers[49] . Under simple assumptions, the Coulomb energy $V_c$ of the two fragments at scission can also show a linear dependence with $Z^2 A^{-1/3}$ :

$$V_c = \frac{Z_{f1} \times Z_{f2}}{d} e^2 \quad (20)$$

where :

- $Z_{f1}$ and $Z_{f2}$ are the atomic numbers of the two fragments

and - d is the distance of the two charge centers at scission .

The $Z^2 A^{-1/3}$ dependence, for a given fragment mass ratio, can be derived by assuming that the distance d is proportional to $A^{1/3}$ . One then obtains :

$$V_c \propto \frac{Z^2}{A^{1/3}} \quad (21)$$

This linear dependence of $V_c$ with $Z^2 A^{-1/3}$ could suggest that, at scission, there is no appreciable kinetic energy and that the total kinetic energy $\overline{TKE}$ comes from Coulomb repulsion only . This would tend to favor the strong damping hypothesis. Nevertheless, this simple picture is unrealistic as has been pointed out already[47]. In fact, at scission, the distance d depends not only on A but also on Z . For higher Z values,

the scission configuration is relatively more elongated, therefore with lower Coulomb energy . Liquid drop calculations[45] show that the variation of $V_c$ with $Z^2/A$ actually flatens and even decreases for increasing $Z^2/A$ for large $Z^2/A$ values . But, assuming this time the zero-damping hypothesis to apply, the pre-scission kinetic energy added to $V_c$ gives $\overline{TKE}$ values which are also in fairly good agreement with the experimental results[45] .

Ternary-fission data cannot help much in clarifying this complex situation since they can be explained equally well in terms of either weak damping[50] or full damping[46] .

In spite of our poor knowledge of damping effects in the last phase of fission, let us examine how they can play a role by comparing TKE and $\overline{\nu}$ data for spontaneous and neutron-induced fission of some even-even nuclei . Special attention is given to the $^{240}Pu$ case for which (d,p f) data are also considered[48] .

It can be seen in Fig.13 that, for a given even-even nucleus, $\overline{TKE}$ is systematically higher for thermal-neutron-induced fission that for spontaneous fission . Therefore, the full damping condition is not met for the cases plotted in Fig.13 since the excess $S_n$ of excitation energy for neutron-induced fission is found, at least partially, in the form of kinetic energy . But the difference $\Delta\overline{TKE}$ in $\overline{TKE}$ is less than 6 MeV (the approximate value of $S_n$ for such nuclei), implying that some damping can nevertheless occur which causes the rest ($S_n - \Delta\overline{TKE}$) of the excitation energy to appear in the form of dissipation . This is actually reflected in prompt-neutron emission since the $\overline{\nu}$-values, as plotted in Fig.14, are systematically higher for thermal-neutron-induced fission than for spontaneous fission, in agreement with $\overline{TKE}$ data . From these results, it would seem that moderate damping could apply to the low-energy fission of even-even actinides .

A closer examination of neutron-induced-fission for a wide range of neutron energies $E_n$ (below the threshold for second-chance fission) can help to know better what fraction of the increase in excitation energy $E^*$ of the fissioning nucleus goes into fragment excitation and how this fraction varies with $E^*$ . Many studies have been made on the variation of $\overline{\nu}$ with $E_n$ for a great variety of actinides[51] . An illustration of this $\overline{\nu}$ energy dependence for $^{240}Pu$ is given in Fig.15 where it can be seen that $\overline{\nu}$ increases linearly with $E_n$ . No attention is paid here to the details of the energy dependence, in particular to the fine structure which may exist at low energy, but rather the gross behavior of $\overline{\nu}$ versus $E_n$ is considered . These results show that the excitation energy of the fission fragments increases at a fast rate as a function of the excitation energy $E^*$ . If this effect, probably due to damping , is supposed to be present in the same manner for all excitation energies below $S_n$, the linear variation of $\overline{\nu}$ with $E_n$ can be extended down to zero-excitation energy to obtain the extrapolated value of $\overline{\nu}_{ext}$ (called $\overline{\nu}_{ext}$) for spontaneous fission. Comparison of extrapolated and measured values of $\overline{\nu}$ for $^{240}Pu$ spontaneous fission shows that the first one is lower than the second one (Fig.15). This effect is found for all even-even actinides for which relevant $\overline{\nu}$ data are available (Fig.14) . Therefore, it seems that the amount of damping would decrease for excitation energies somewhat below $S_n$ .

Ir is possible to pursue further this type of investigation for the low-energy fission of $^{240}Pu$ since a fairly large amount of experimental results are available on the properties of the fission fragments and their variation with excitation energy[48,52]. The variation of the total kinetic energy $\overline{TKE}$ for the fragments emitted in the low-energy fission of $^{240}Pu$ is plotted in Fig.15 which includes data for the spontaneous fission of the ground state (G.S), the 4 ns isomeric state (I.S), to the $^{239}Pu$ thermal-neutron induced fission and for the $^{239}Pu$ (d,p f) reaction. Also, the variation $d\overline{E_K}/dE^*$ of the kinetic energy $\overline{E_K}$ of the fission fragments as a function of excitation energy $E^*$ is plotted in Fig.16 for several groups of fragment mass ratios. Moreover the average mass $\langle m_H^* \rangle$ of the heavy primary fission fragments is plotted as a function of $E^*$ in Fig. 17 .

Examination of these data seems to demonstrate the existence of two types of fission . The first one (called type I) includes the G.S and I.S spontaneous fission and $^{239}Pu$ (d,p f) reaction at $E^* = 4.65$ MeV and for the fragments emitted at an angle $\Theta = 0°$ relative to the recoil axis of the $^{240}Pu$ compound nucleus . A 200 keV wide resonance appears at $E^* = 4.65$ MeV in the anisotropy data and is interpreted as being due to a vibrational level in the 2nd well of the $^{240}Pu$ double-humped fission barrier. The second one (called type II) refers to all other $^{239}Pu$ (d, p f) results and to the $^{239}Pu$ (n,f) reaction induced by thermal neutrons .

In the fission of type I, the kinetic energy $\overline{TKE}$ increases linearly as a function of $E^*$ with a slope of about + 1 . This means that practically all the excitation energy $E^*$ is found as an increase of the kinetic energy of the fission fragments and this holds for all types of fragmentations (Fig.16) . The average mass $\langle m_H^* \rangle$ is the same for the three fission reactions of this type . This strongly suggests that damping, if present, must be very small and the fission of type I may very well be an illustration of superfluid motion already envisaged[47] in which the nucleons remain coupled by the pairing force all the way to scission. In this hypothesis, no intrinsic excitation occurs in the descent to scission and the available energy at that point then appears as pre-scission kinetic energy . All increase in $E^*$ is then found entirely as an increase in pre-scission kinetic energy and therefore in $\overline{TKE}$ since the Coulomb energy does not change with $E^*$ in this picture. This applies to all types of fragmentation since all fission properties but the kinetic energy do not vary $E^*$ . The experimental results obtained for fission of the type I are consistent with this superfluid motion of the fissioning system .

In the fission of type II, on the contrary, the kinetic energy $\overline{TKE}$ decreases linearly as a function of $E^*$ with a slope of about $-0.43$ . This is consistent with the increase of $\overline{\nu}$ with $E^*$ observed above $S_n$ .Nevertheless the energy balance in fission calculated with these data leads to a fairly large value $\langle S_n^f \rangle$ of the average neutron separation energy in the fission fragments ($S_n^f \simeq 8.3$ MeV) . The type of fragmentation is different from that of type I since $\langle m_H^* \rangle$ takes a different value (Fig.17) . There does not seem to be a satisfactory interpretation of such a behavior of $\overline{TKE}$ and $\overline{\nu}$ with $E^*$. Several explanations have been proposed in terms either of damping or variation in stiffness of the fission fragments with $E^*$.[48] In the first case, the coupling of the fission mode to the other degrees of freedom reduces the pre-scission kinetic energy and induces intrinsic excitations which lead to a greater excitation of the fission fragments, hence to an increase in $\overline{\nu}$ .[47] In the second case, the greater excitation energy reduces the stiffness of the nascent fragments which then become softer to deform. At scission they are more elongated and the increase in the distance d between their charge centers decreases the Coulomb energy[52,53]. In these interpretations, shell effects seem to play an important role in agreement with the experimental results since the rate of decrease $d\overline{E_K}/dE^*$ of the kinetic energy $\overline{E_K}$ with increasing $E^*$ strongly depends on the fragment mass ratio (Fig.16) .

The existence of these two types of fission having different variations of $\overline{TKE}$ and $\overline{\nu}$ with excitation energy seems justified from these experimental data and has to be taken into account for the prediction of some fission properties such as the prompt neutron emission. From the discussion presented above, it does not seem correct to assume the same amount of damping in fission for all excitation energies, starting from the ground state. In particular, it is certainly erroneous to extrapolate at higher energy the $\overline{\nu}$ or $\overline{TKE}$ data obtained for spontaneous and thermal-neutron-induced fission.

## 5 - Conclusion

In summary, though our understanding of the fission process has recently greatly improved, a reliable fission theory does not yet exist ; we are far from completely understanding this very complex phenomenon and from calculating accurately all its properties .

Fission barriers can be calculated with a good accuracy by using the Strutinsky macroscopic-microscopic approach . More fundamental Hartree-Fock approaches are also making rapid progress. The double-humped barrier shapes which are obtained for the actinides can explain many aspects of fission, among them are fission isomers and intermediate structure in fission cross sections .

In contrast to the statics, the fission dynamics which includes inertial and damping effects is very poorly known . Attempts to calculate life-time for ground state spontaneous fission with a microscopic approach have shown the limitations of the method . Fission cross sections are still more difficult to obtain on a fundamental basis . Nevertheless, approximate values can be obtained, not from pure theory, but from simple models having parameters adjusted to selected available fission data . The fission channel theory of A. Bohr, generally verified experimentally, is widely used in such calculations. A similar situation seems to apply also for other fission properties such as prompt neutron emission. Correct treatment of the subject requires the knowledge of damping effects in the descent from the second saddle point to scission. At present one cannot but speculate on such effects though new data on fission fragment kinetic energy and prompt neutron emission start to throw some light on this difficult aspect of fission . Again, in this case, simple models can be used to predict $\overline{\nu}$-values when they are not measured, provided that the model parameters employed in the calculations are adjusted on reliable fission data . But, it has been shown that these data must be used with great care before being introduced in the calculations .

It is worth noting at this point, that damping effects are studied not only in fission but also in heavy-ion induced reactions and a lot of information on such matters is expected in the few years to come when the new heavy-ion accelerators, now under construction, will be put into operation .

## References


[1] H. Flocard, P. Quentin, D. Vautherin, A.K. Kerman P.C.F.+ (IAEA, Vienna 1974) Vol I, p. 231 .

[2] V.M. Strutinsky, Nucl. Phys. A 95 (1967), 420 . Nucl. Phys. A 122 (1968), 1 .

[3] S.G. Nilsson, Chin Fu Tsang, A. Sobiczewski, Z. Szymanski, S. Wycech, C. Gustafson, I.L. Lamm, P. Möller and B. Nilsson, Nucl. Phys. A 131, (1969),1

[4] M. Brack, J. Damgaard, A.S. Jensen, H.C. Pauli, V.M. Strutinsky and C.Y. Wong, Rev. Mod. Phys. 44, (1972), 320 .

[5] J.R. Nix, Ann. Rev. of Nucl. Sc. 22, (1972), 65 .

[6] B.L. Andersen, F. Dickman and K. Dietrich, Nucl. Phys A 159, (1970), 337 .

[7] P. Holzer, U. Mosel and W. Greiner, Nucl. Phys.A 138 (1969), 241 .

[8] M.G. Mustafa, U. Mosel and H.W. Schmitt, Phys. Rev. C 7 (1973), 1519 .

[9] A. Michaudon, Advances in Nuclear Physics - Ed. by M. Baranger and E. Vogt ; Vol 6, p.1 (Plenum Press, 1973) .

[10] a) V.M. Strutinsky and H.C. Pauli,P.C.F.++(IAEA,Vienna 1969) p. 155 .
b) J.E. Lynn, P.C.F.++(IAEA, Vienna 1969) p.249 .

[11] J.R. Nix, Ann. Rev. of Nucl. Sc. 22, (1972), 65 .

[12] a) H.J. Specht, Rev. Mod. Phys. 46 ,Nb 4 (1974) 773 .
b) V. Metag, E. Liukkonen, O. Glomset and A. Bergman P.C.F.+(IAEA, Vienna 1974) Vol I, p. 317 .

[13] P. Limkilde and G. Sletten, Nucl. Phys. A 199 (1973), 504 .

[14] H.J. Specht, J. Weber, E. Konecny and D. Heunemann, Phys. Let. B 41, (1972), 43 .

[15] P.A. Russo, J. Pedersen and R. Vandenbosch, P.C.F.+ (IAEA, Vienna 1974) Vol 1, p. 271 .

[16] R. Vandenbosch, P.C.F+ (IAEA, Vienna 1974) Vol I, p. 251 .

[17] H.J. Specht, E. Konecny, J. Weber and C. Kozhuharov, P.C.F + (IAEA, Vienna 1974) Vol I, p. 285 .

[18] a) J.E. Lynn, Nuclear Structure (IAEA, Vienna 1969) p. 249 .
b) J.E. Lynn, Report A.E.R.E Harwell R 5891 (1968) .
c) H. Weigmann, Z. Phys. 214 (1968), 7 .

[19] a) D. Paya, H. Derrien, A. Fubini, A. Michaudon and P. Ribon, Nuclear Data for Reactors (IAEA, Vienna 1967) Vol III, p. 128 .
b) A. Michaudon, Nuclear Structure (IAEA, Vienna 1968) p. 427 .
c) A. Fubini, J. Blons, A. Michaudon and D. Paya, Phys. Rev. Let. 20 (24) (1968) 1373 (C) .

[20] G.A. Keyworth, J.R. Lemley, C.E. Olsen, F.T. Seibel, J.W.T. Dabbs, P.C.F.+ (IAEA, Vienna 1974) Vol I, p.85.

[21] a) A. Michaudon, New Developments in reactor physics and Shielding Calculations, Kiamesha Lake 12-15 Sept 1972, Vol II, p. 1087 - CONF 720-901 .
b) A. Michaudon, Statistical Properties of Nuclei (Albany 23-27 August 1971) (Plenum Press) 1972, p.149

[22] E. Konecny, H.J. Specht and J. Weber, P.C.F.+ (IAEA, Vienna 1974) Vol II, p. 3 .

+ Physics and Chemistry of Fission (Proceedings of a IAEA Symposium, Rochester (N.Y) 13-17 August 1973) .

++ Physics and Chemistry of Fission (Proceedings of the second IAEA Symposium, Vienna 28 July-1 August 1969)

[23] N. Bohr and J.A. Wheeler, Phys. Rev. 56 (1939) 426 .

[24] H.A. Kramers, Physica 7 , (1940), 284 .

[25] P.O. Fröman and N. Fröman, J.W.K.B. Approximation, Contribution to the Theory, North-Holland, Amsterdam (1965) .

[26] H.C. Pauli and T. Ledergerber, P.C.F.+ (IAEA,Vienna 1974) Vol I, p. 463 .

[27] D. Inglis, Phys. Rev. 96 , (1954), 1059 .

[28] D. Gogny, private communication (1974) .

[29] a) P. Thomet, EANDC Topical Discussion (Tokyo, March 27, 1974) CEA-CONF 2855 .
b) P. Thomet, CEA-Report R-4631 (1974) .

[30] H. Weigmann and J.P. Theobald, Nucl. Phys. A 187 , (1972) , 305 .

[31] C. Lagrange, EANDC Topical Discussion (Tokyo, March 27, 1974) CEA-CONF 2852 - 2853

[32] A. Bohr, Proc. Int. Conf. Peaceful Uses of Atomic Energy (Geneva 1955) Vol II, United Nations, New York (1956) p. 220 .

[33] G.A. Cowan, B.P. Bayhurst, R.J. Prestwood,J.S. Gilmore and G.W. Knobeloch, Phys. Rev. 144 (3), (1966), 979 .

[34] E. Melkonian and G.K. Mehta, P.C.F.+++ (IAEA, Vienna 1965) Vol II, p. 355 .

[35] F.L. Shapiro, Nuclear Structure (IAEA, Vienna 1968) p. 283 .

[36] S. Weinstein, R. Reed and R.C. Block, P.C.F.++ (IAEA, Vienna 1969) p. 477 .

[37] J. Terrell, Phys. Rev. 127 , (1962), 880 .

[38] L. Weston and J. Todd, Conf. Neutron Cross Sections and Technology (U. of Tennessee, 1971) Vol II, p.961.

[39] J. Trochon, B. Lucas, A. Michaudon, D. Paya and Y. Ryabov, J. Physique 34 , (1973), 131 .

[40] a) D. Shackleton, J. Trochon, J. Fréhaut and M. Le Bars, Phys. Let. 42 B , (1972), p.344 .
b) J. Fréhaut and D. Shackleton, P.C.F.+ (IAEA, Vienna 1974) Vol II, p. 201 .
c) D. Shackleton, D. Sc. Thesis (Paris 1974) .

[41] L.W. Weston and J. Todd, Phys. Rev. 10 (4),(1974), 1402 .

[42] a)J. Trochon, Private Communication (1972) .
b)Y. Ryabov, J. Trochon, D. Shackleton and J.Fréhaut Nucl. Phys. A 216 , (1973), 395 .

[43] J.E. Lynn, The Theory of Neutron Resonance Reactions (Clarendon, Oxford, 1968) .

[44] J. Fréhaut, G. Simon, J. Trochon, Private Communication (1974) .

[45] J.R. Nix,Nucl. Phys. A 130 (1969), 241 .

[46] P.Fong P.C.F.++ (IAEA, Vienna 1969) p. 133 .

[47] W.J. Swiatecki and S. Bjørnholm, Physics Reports 4, (6) (1972), 325 .

[48] a) J. Lachkar, Y. Patin and J. Sigaud, J. de Physique Lettre (to be published)
b) Journées d'Etudes de la Fission (Cadarache, France 1974) (unpublished) .

[49] R. Vandenbosch and J.R. Huizenga "Nuclear Fission" Academic Press (1973) .

[50] J. Halpern and E.M. Henley, Comments on Nuclear and Particle Physics 3 , (1969), 52 .

[51] F. Manero and V.A. Konshin "Atomic Energy Review" (IAEA, Vienna 1972) Vol 10, (4), p.637 .

[52] E. Konecny, H.J. Specht and J. Weber Phys. Let. 45 B, (1973), 329 .

[53] W. Nöremberg, P.C.F.++(IAEA, Vienna 1969) p. 51 .

[54] R. Vandenbosch, Comments on Nuclear and Particle Physics , Vol V, (6), (1972), p. 161 .

[55] J.P. Unik, J.E. Gindler, L.E. Glendenin, K.F. Flynn, A. Gorski and R.K. Sjoblom, P.C.F.+ (IAEA, Vienna 1974) Vol II, p. 19 .

[56] A.J. Deruytter and G. Wegener-Penning P.C.F.+ (IAEA, Vienna 1974) Vol II, p. 51 .

+++ Physics and Chemistry of Fission (Proceedings of a IAEA Symposium, Salzburg 22-26 March 1965) .

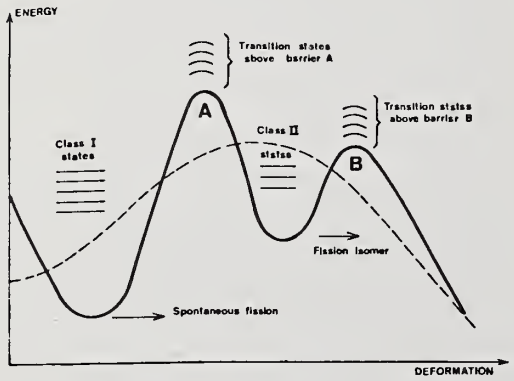


Fig. 1
Double-humped fission barrier (solid line) resulting from shell-energy corrections to the LD barrier (dashed line)

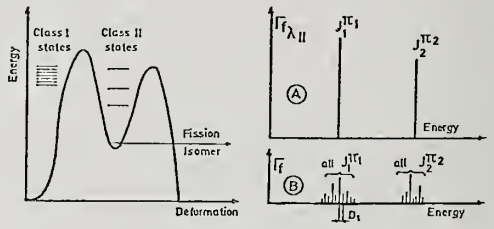


Fig. 2

Mechanism of intermediate structure in subthreshold fission cross sections . Clusters appear in the fission cross section when energy, spin and parity of a class-II state match those of the class-I resonances (at most two $J^{\pi}$ values are possible for "s" wave neutrons) . The fission widths are drawn at the energy of the respective levels for class-II states (diagram A) and for the observed resonances (diagram B) .

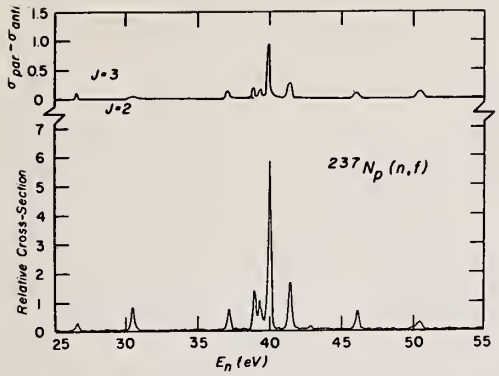


Fig. 3
Fission data obtained in the neighborhood of the first cluster at 40 eV in the $^{237}Np$ subthreshold fission cross section using a polarized neutron beam and a polarized $^{237}Np$ target[20]. The upper curve represents the difference between the cross sections measured with beam and target polarizations parallel and antiparallel These data demonstrate that most of the cross section in this cluster is due to J = 3 resonances[20].

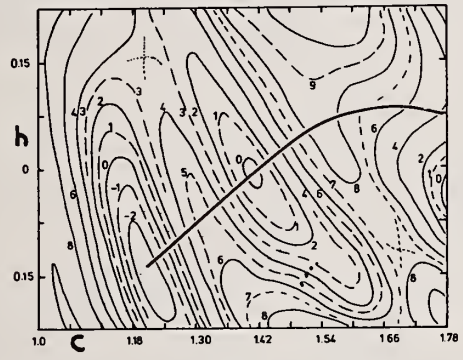


Fig. 5
The calculated deformation energy of $^{240}Pu$ versus the two symmetric deformations c(elongation) and h (constriction) is shown as a contour plot. Contour intervals are 1 MeV. The projection of the least action trajectory into the symmetric subspace (c,h) is shown by the thick solid line. Note the discrepancy between the static and dynamical barriers[26].

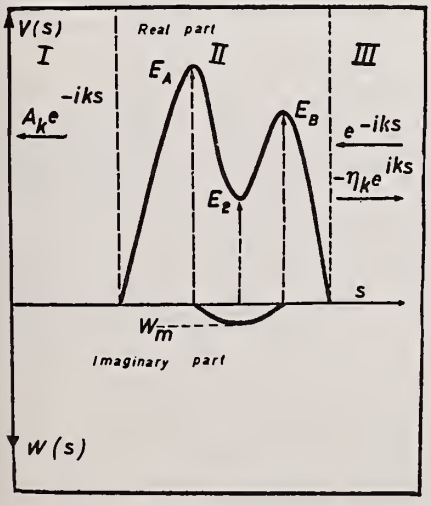


Fig. 7

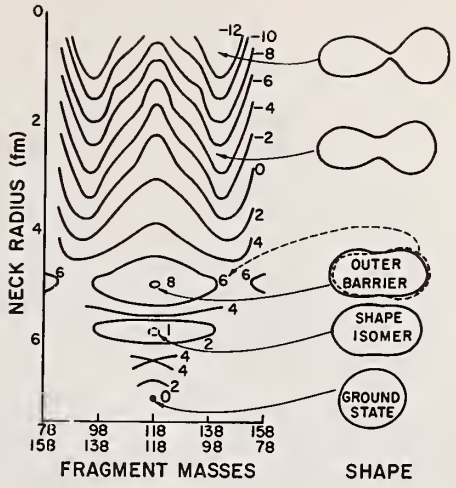


Fig. 4
Potential energy surface for $^{236}U$ as obtained from calculations using the Strutinsky procedure. Contour intervals are 2 MeV except for the shape isomer [8,54].

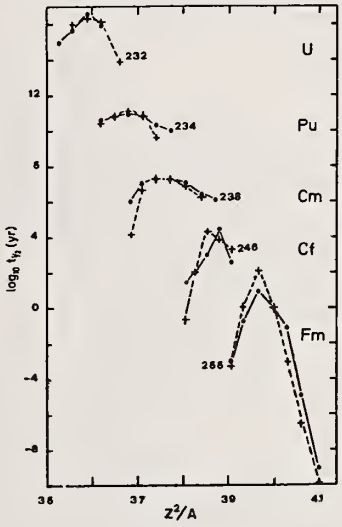


Fig. 6
Theoretical (•) and experimental (+) half-lives (in years) for ground-state spontaneous fission plotted versus $Z^2/A$ (ref.[26]). The parameterization of the fissionability parameter for each set of isotopes is given in [26]. A pairing strength proportional to the surface area of the deformed nucleus is assumed in the calculations.

Fig. 7
Real and imaginary parts of the potential, as a function of deformation s, used in the cross section calculations described in the text and in [29]. The real part V(s) represents the double-humped fission barrier obtained by smoothly joining three paraboles. The imaginary part is supposed to be parabolic with maximum $W_m$ in the second well. Full absorption is assumed in the first well.

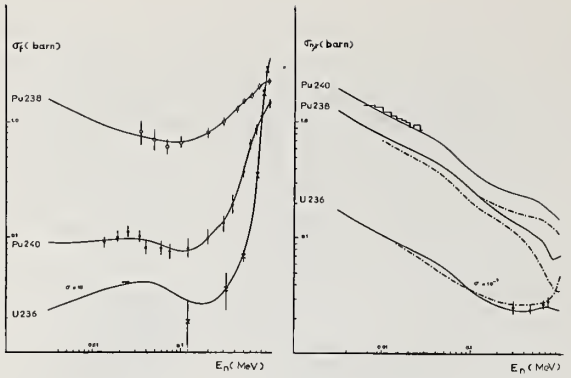


Fig. 8 Fig. 9

Fig. 8 - Fission cross sections of $^{236}U$, $^{238}Pu$ and $^{240}Pu$ as a function of neutron energy $E_n$ calculated with the method described in [29] (solid lines). The references for the experimental data are given in [29].

Fig. 9 - Capture cross sections of $^{236}U$, $^{238}Pu$ and $^{240}Pu$ as a function of neutron energy $E_n$ calculated with the method described in [29] (solid lines). The references for the experimental data are given in [29]. The lines come from ENDFB/III.

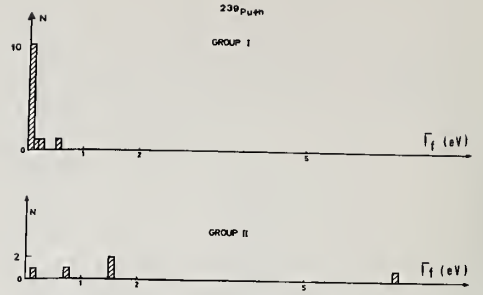


Fig. 10

Frequency distribution of the $\Gamma_f$ values for the two groups of $^{239}Pu$ resonances separated according to their R-values, as discussed in the text [9,33].

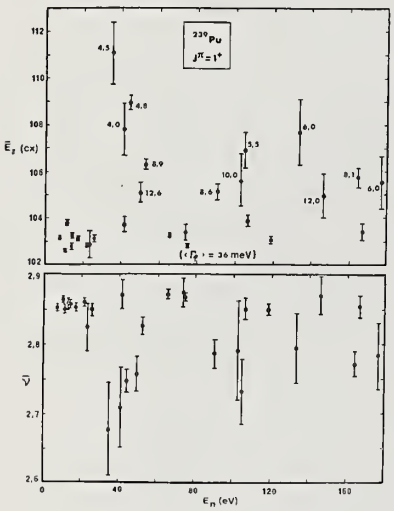

Fig. 11

The fission prompt neutron and $\gamma$-ray yields (respectively $\bar{\nu}$ and $\bar{E}_\gamma$) are plotted as a function of resonance energy for the $^{239}Pu$ resonances having $J = 1^+$ and analysed below 180 eV neutron energy [40]. The value of $\Gamma_f$ is indicate in meV near the $\bar{E}_\gamma$ point for the resonances having a small fission width.

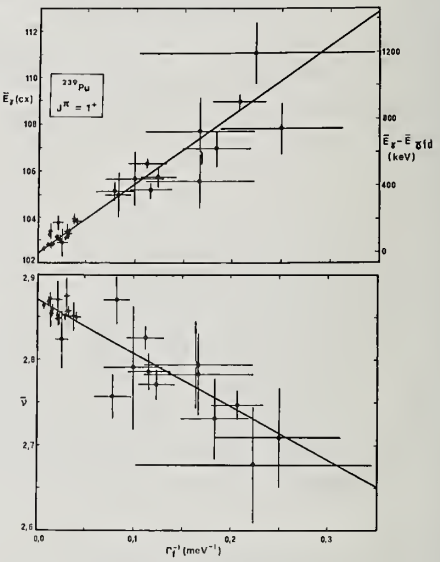

Fig. 12

The prompt-neutron and $\gamma$-ray yields (respectively $\bar{\nu}$ and $\bar{E}_\gamma$) are plotted as a function of $1/\Gamma_f$ for the $^{239}Pu$ resonances having $J^\pi = 1^+$ and analysed below 200 eV neutron energy, to demonstrate the effect of the $(n,\gamma f)$ reaction (ref.40). The solid lines are least-squares fits to the data.

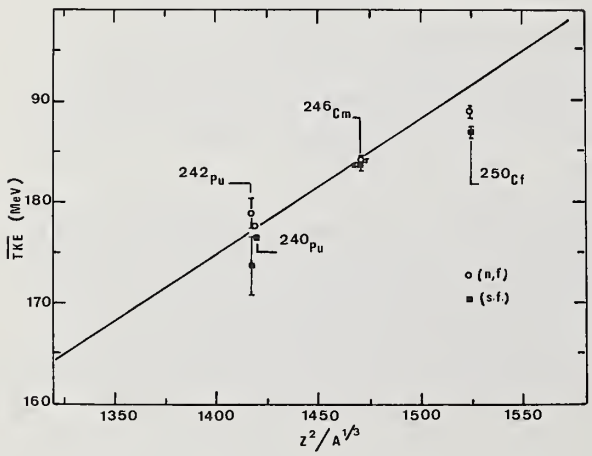


Fig. 13

Comparison of the total kinetic energy $\overline{TKE}$ of the fragments for the ground state spontaneous fission (■) the thermal-neutron-induced fission (o) of some even-even nuclei. The references for these data can be found in [55,56]. The solid line is a fit to the available data [55].

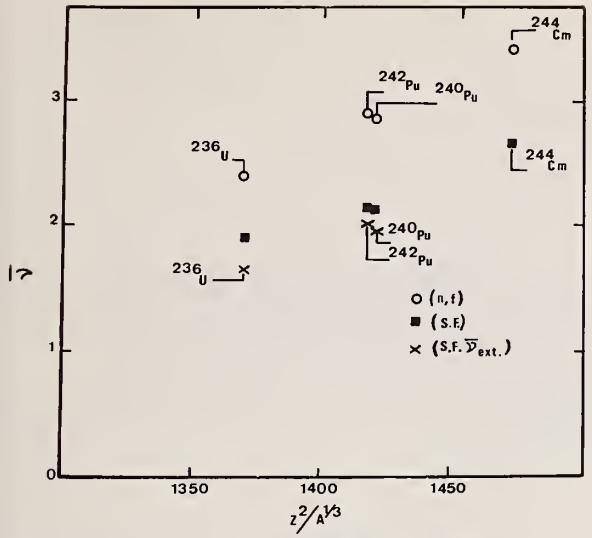


Fig. 14

Comparison of the average fission neutron multiplicity $\bar{\nu}$ for the ground state spontaneous fission (■) and the thermal-neutron induced fission (o) of some even-even nuclei. The value $\bar{\nu}_{ext}$ is obtained by extrapolating to zero excitation energy the $\bar{\nu}$ energy dependence observed for the neutron-induced fission .

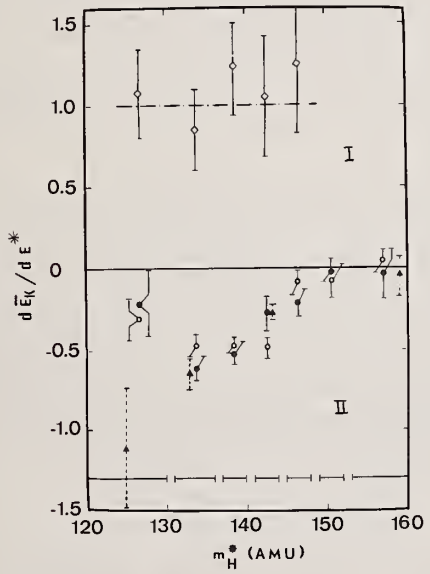


Fig. 16

Variation $\frac{d\bar{E}_K}{dE^*}$ of the fragment kinetic energy $\bar{E}_K$ with excitation energy $E^*$ of the fissioning nucleus $^{240}Pu$ for various groups of the mass $^*m_H$ of the heavy fission fragment (ref.48) . This variation $\frac{d\bar{E}_K}{dE^*}$ has been plotted for the two types of fission (I and II) discussed in the text. References for the data plotted in this figure can be found in[48] .

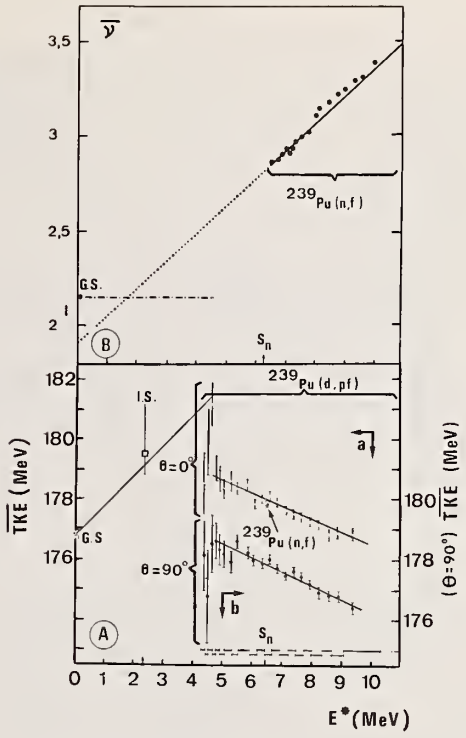


Fig. 15

Plots of the fragment total kinetic energy $\bar{TKE}$ (graph A) and prompt-neutron yield $\bar{\nu}$ (graph B) for the fission of $^{240}Pu$ as a function of excitation energy $E^*$ (ref.48) . References fot the various data plotted in this figure can be found in[48] .

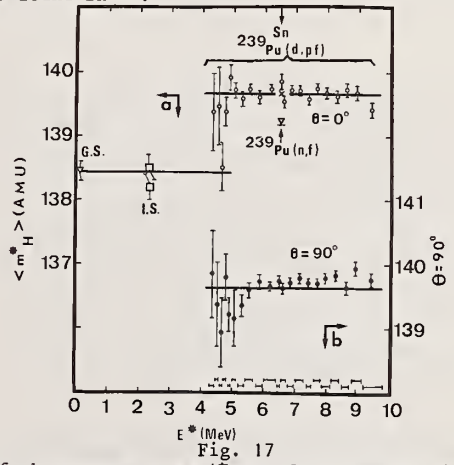


Fig. 17

Plot of the average mass $<^*m_H>$ of the heavy primary fragments emitted in the fission of $^{240}Pu$ as a function of excitation energy $E^*$ (ref. 48). Note the difference in $<^*m_H>$ for the two types of fission discussed in the text .

# A STUDY OF THE $^{233}U$-$^{232}Th$ REACTOR AS A BURNER FOR ACTINIDE WASTES*

S. Raman, C. W. Nestor, Jr., and J. W. T. Dabbs
*Oak Ridge National Laboratory, Oak Ridge, Tennessee 37830*

A plausible method for reducing the storage problems and hazards now associated with long-lived actinide wastes might be to recycle and convert these to fission products. Several reactor types can be envisaged for this purpose. We note that in a $^{233}U$-$^{232}Th$ reactor, the production of $^{237}Np$, Pu and transplutonium isotopes is greatly reduced compared to a $^{235}U$-$^{238}U$ reactor because several additional neutron captures are required to reach the same mass. Hence, the $^{233}U$-$^{232}Th$ reactor can be employed to effectively reduce Np, Pu, Am and Cm wastes to fission-product wastes which entail shorter (≈1000 yr) storage times.

(Actinide fuel, fertile material, and wastes; recycle concept; transuranium element production; waste recycling in a $^{233}U$-$^{232}Th$ reactor)

## Introduction

A major problem in connection with the development of large-scale nuclear energy is the potential hazard associated with the fuel, fertile material and wastes. These products must be processed, transported, stored and safeguarded with extreme care. Reactor fuel elements need to be processed in order to recover reusable fuel and fertile material. The unrecovered portions are usually termed "wastes", which can be broadly divided into fission products and actinides (Ac and higher Z elements). Most fission products decay to harmless natural elements in a relatively short span of ≈ 1000 years. It is generally believed that adequate storage means, either underground or above ground, can be found to handle fission product wastes safely. The fuel, fertile material and actinide wastes pose a different type of problem because several isotopes among them possess very long half-lives. For example, the main new fuel produced in a light-water $^{235}U$-$^{238}U$ reactor is $^{239}Pu$ which has $T_{1/2}$ = 24390 yr. The half-life of $^{243}Am$, a waste material, is 7370 yr. The hazards associated with the fissionable isotopes of the fuel are, however, of secondary concern because these isotopes can be depleted through their use in a reactor. Since the fertile materials *ab initio* came from the earth, whether or not they should be viewed as hazards newly created by reactor operations is debatable.

## The Actinide Recycle Concept

A plausible method which has been suggested for reducing the hazards associated with the remaining actinides might be to recycle these also in a suitable reactor. Among Pu, Am, and Cm isotopes, alternate ones ($^{239}Pu$, $^{241}Pu$; $^{242}Am$, $^{244}Am$; $^{243}Cm$, $^{245}Cm$) possess appreciable fission cross-sections and the remaining isotopes for the above elements can be transmuted to these by neutron capture. Therefore, in principle, the actinides can be partly converted into more manageable fission products.

Recycling requires a neutron source which might be the same reactor producing the wastes or a specially designed burner reactor or even a fusion reactor. Claiborne[1] has shown that a reduction by an order of magnitude in the hazard potential of the actinide wastes can be achieved through recycling in the same reactors (pressurized light-water reactors, operating on the 3.3% $^{235}U$-$^{238}U$ cycle) producing the bulk of the wastes. This reduction occurs because when recycled, the inventory of Am and Cm isotopes, for example, approaches a maximum value, an asymptote, rather than increasing linearly with time. Despite this reduction, the overall inventory of the actinides will be appreciable by the end of this century. There remains a problem of final disposal of reactor inventories if and when the nuclear fission power program draws to a close and is replaced by alternate energy sources.

## The $^{233}U$-$^{232}Th$ Reactor

The last-mentioned problem, among other things, led us to consider the reactor type operating on the $^{233}U$-$^{232}Th$ cycle. In this case, the capture of neutrons by the $^{232}Th$ fertile material leads to the replenishment of the original $^{233}U$ fuel. Successive neutron captures by $^{233}U$ result in higher U isotopes until $^{237}U$ is reached, when a higher Z isotope, $^{237}Np$, is produced. It is further obvious that Pu and transplutonium isotopes are generated to a far lesser extent in a $^{233}U$-$^{232}Th$ reactor when compared to a $^{235}U$-$^{238}U$ reactor. For nuclides above $^{238}Pu$, the typical reduction factor is > $10^6$ because in the $^{233}U$ case, five additional neutron captures are required to reach the same mass. Therefore, in the absence of substantial new production of these elements, the $^{233}U$-$^{232}Th$ reactor can be effectively employed to reduce the Np, Pu, Am and Cm inventories. By contrast, the best that can be contrived through recycling in a $^{235}U$-$^{238}U$ reactor is a situation in which these materials are transmuted at essentially the same rate as they are freshly produced.

To test these ideas, we have carried out some preliminary calculations with the ORIGEN (Oak Ridge Isotope Generation and Depletion Code) computer program originally written by Bell.[2] To keep the calculations as simple as possible we selected a 1000 MW(e) pressurized light-water reactor in which the fuel was 3.3% $^{235}U$-$^{238}U$ in the first instance and $^{233}U$-$^{232}Th$ in the other. The calculations are hypothetical in two senses--the fuel loadings are idealized and the $^{233}U$-$^{232}Th$ reactor of this type might not be practical. An operating cycle included a 3 yr power generation period followed by a 3 yr cooling off period. Table 1 shows the amounts of selected transuranium isotopes present at the end of 1 cycle. As expected, the production of these isotopes is greatly reduced in the case of the $^{233}U$-$^{232}Th$ reactor. This conclusion would remain valid notwithstanding the differences in the flux levels of the two reactors.

The recycle concept was tested next as follows. The Np, Am, Cm and higher isotopes together with 0.5% of U and Pu isotopes from a $^{235}U$-$^{238}U$ reactor were considered as wastes. Such wastes from a 1 cycle operation of 10 reactors were recycled repeatedly in a $^{233}U$-$^{232}Th$ reactor. The resulting growths and decays of several selected isotopes are shown in the figure. In 60 years (10 cycles), negative gradients have been established for all isotopes except $^{246}Cm$ and $^{252}Cf$. The negative gradients would have been steeper were it not for the presence of the $^{238}U$ material (200 gram atoms) which replenishes the transuranium isotopes. Further operation should establish negative gradients for $^{246}Cm$ and $^{252}Cf$ also. The rapid increase in the $^{252}Cf$ build-up, endemic to all recycling schemes, requires additional shielding for transportation and fuel reprocessing.

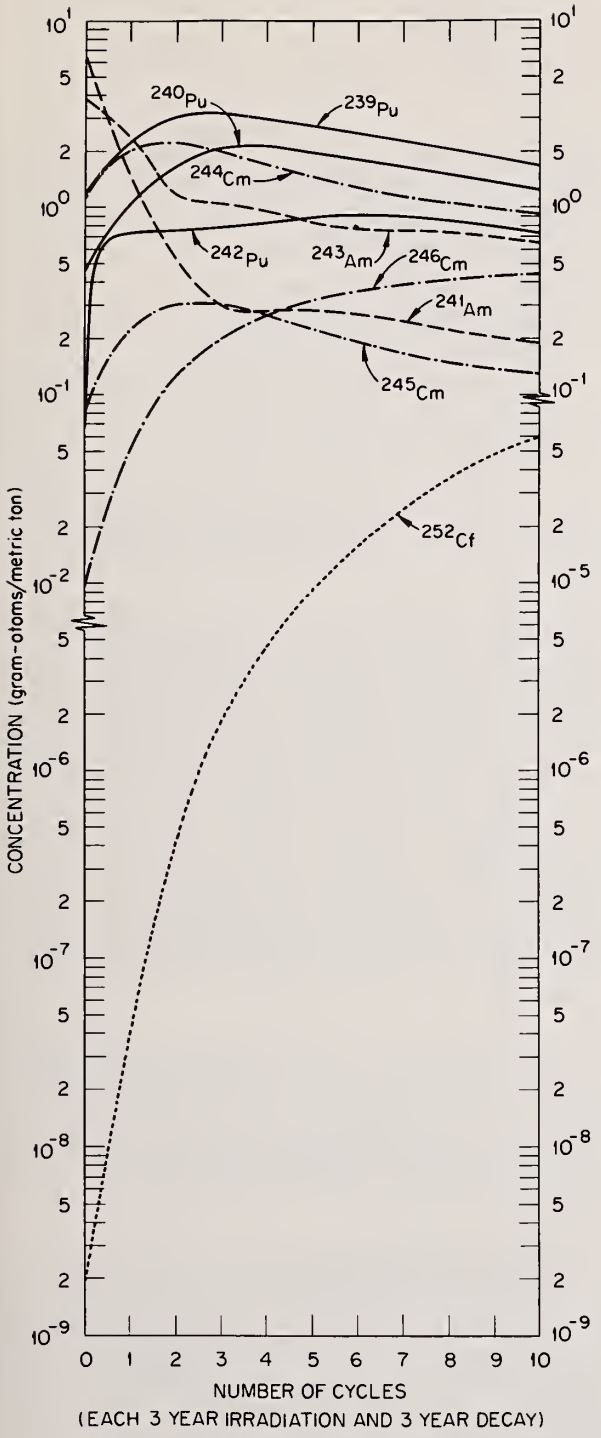


FIG. 1. Behavior of selected transuranium isotopes recycled in a $^{233}U$-$^{232}Th$ reactor. The $^{233}U$ and $^{232}Th$ concentrations were 240 and 4060 gram atoms, respectively, per metric ton of heavy elements charged to the reactor. To obtain the approximate quantities in kilograms in the actual reactor, multiply the ordinate numbers by 20. Note also the different scale for $^{252}Cf$.

Table I. Comparison between transuranium production in two 1000 MW(e) reactors with different fuels at the end of 1 cycle (3 yr power generation, 3 yr cooling).

| Fuel | | Fuel |
|---|---|---|
| $^{235}U$ - 2630 Kg<br>$^{234}U$ - 20 Kg<br>$^{238}U$ - 77350 Kg | | $^{233}U$ - 4500 Kg<br>$^{232}Th$ - 75500 Kg |
| Flux | | Flux |
| $2.9 \times 10^{13}$ n/cm$^2$ sec | | $1.2 \times 10^{13}$ n/cm$^2$ sec |
| Quantity (Kg) | Isotope | Quantity (Kg) |
| 39 | $^{237}Np$ | 0.04 |
| 14 | $^{238}Pu$ | 0.003 |
| 422 | $^{239}Pu$ | 0.0002 |
| 174 | $^{240}Pu$ | $< 2 \times 10^{-5}$ |
| 72 | $^{241}Pu$ | $< 2 \times 10^{-6}$ |
| 28 | $^{242}Pu$ | $< 8 \times 10^{-8}$ |
| 13 | $^{241}Am$ | $< 3 \times 10^{-7}$ |
| 0.07 | $^{242m}Am$ | $< 4 \times 10^{-10}$ |
| 8 | $^{243}Am$ | $< 4 \times 10^{-9}$ |
| 0.008 | $^{242}Cm$ | $< 2 \times 10^{-11}$ |
| 0.006 | $^{243}Cm$ | $< 3 \times 10^{-12}$ |
| 2.2 | $^{244}Cm$ | $< 3 \times 10^{-10}$ |
| 0.16 | $^{245}Cm$ | $< 5 \times 10^{-12}$ |

We find that it is possible to further reduce the inventories of several transuranium isotopes through sustained recycling in a $^{233}U$-$^{232}Th$ reactor. The operation of a $^{233}U$-$^{232}Th$ reactor, of course, results in a different set of actinides with attendant hazards. Therefore, an answer to the important question of whether or not recycling the wastes in a $^{233}U$-$^{232}Th$ reactor results in a significant net reduction in the hazard requires more detailed calculations than what have been attempted here. In particular, such calculations require a broader scheme in which the required nuclear power generating capacity is suitably apportioned among the different types of reactors. Several factors such as (i) the degree of chemical separation that can be achieved for different elements, (ii) which elements are discharged into the waste streams, (iii) the hazards associated with transportation, reprocessing and fuel fabrication, (iv) both the short and long-term hazards associated with the fuel, (v) conversion ratios, (vi) safety, etc., need to be considered. On a more fundamental level, there are significant gaps in the cross-section data needed for predicting in advance the amount and nature of actinide wastes that will be generated and for detailed testing of the several proposed recycle schemes. We note, for example, that $^{245}Cm$ is a doorway leading to Bk and Cf isotopes. Therefore, fission cross-section measurements on $^{245}Cm$ have been initiated, as described elsewhere in these Proceedings, at the Oak Ridge Electron Linear Accelerator (ORELA) as part of a comprehensive program aimed at providing basic data for the recycle concept.

* Research sponsored by the U. S. Atomic Energy Commission under contract with the Union Carbide Corp.

[1] H. C. Claiborne, Neutron-Induced Transmutation of High-Level Radioactive Wastes, ORNL-TM-3964 (Dec., 1972).

[2] M. J. Bell, Origen - The ORNL Isotope Generation and Depletion Code, ORNL-4628 (May, 1973). Program modified by C. W. Kee and by O. W. Hermann.

# MEASUREMENT OF THE NEUTRON CAPTURE CROSS SECTIONS OF THE ACTINIDES*

L. W. Weston and J. H. Todd

Oak Ridge National Laboratory
Oak Ridge, Tennessee 37830

The capture cross sections of the isotopes heavier than $^{239}Pu$ are of great importance for the core physics, fuel recycle, and waste management for power reactors. Since total cross sections are not sufficient, a program for the measurement of these needed capture cross sections is being carried out at ORNL. Measurements have been almost completed on $^{240}Pu$, $^{241}Pu$, and $^{241}Am$ and have been planned for $^{242}Pu$ and possible $^{237}Np$ and $^{243}Am$. The capture gamma-ray detector used is the "total energy detector" which is a modification of the Moxon-Rae detector. Fission, when present, is detected with fast neutron counters. Results obtained on $^{240}Pu$, $^{241}Pu$, and $^{241}Am$ will extend continuously from thermal neutron energies to 350 keV. The cross sections are normalized at thermal neutron energies and the neutron flux is measured relative to the $^{10}B(n,\alpha)$ cross section up to 2 keV and $^{6}Li(n,\alpha)$ at higher neutron energies. The accuracy of the techniques used varies with the sample but is about 8%. With such cross sections the long range management of the actinides produced in power reactors can be planned on a more systematic basis.

(Actinide management; neutron capture cross sections; Pu isotopes, $^{241}Am$)

## Introduction

The actinide nuclides of higher mass than $^{239}Pu$ are produced in reactors via successive neutron capture. In U fueled reactors they are produced with $^{238}U$ as the principal progenitor and in a Pu fueled reactor it is $^{239}Pu$. With the exception of $^{241}Pu$ these nuclides as a group are of little value as fuel for the reactor. In terms of fuel and waste management these actinide isotopes are important. The higher Pu isotopes, $^{240,241,242}Pu$, are about 26%, 12%, and 3% respectively of the total Pu discharged from a water reactor.[1] These isotopes must be considered in the core physics of a Pu-fueled reactor. Other actinide elements which are of importance to fuel and waste management are Np, Am, Cm, and Cf.

The isotopes of Np, Am, and Cm plus unrecovered U and Pu constitute the major long term (> 500 years) radiological hazard from reactor waste.[2] After the decay of fission products to innocuous levels as compared to naturally occurring minerals in about 500 years, the radiological hazard of these actinides will continue for a million years. Therefore, a knowledge of the neutron cross sections for the production (and transmutation) of these isotopes is essential. Because of the long term radiological hazard (> 500 years) of these nuclides, it has been proposed that they be recycled in reactors to be transmuted into fission products which are a shorter-term hazard.[2,3] Since the projected quantity of these nuclides to be produced by the year 2000 is 1,269 metric tons,[4] the conversion would be no minor undertaking. The burden on the neutron economy of the transmutation reactor may be acceptable since every other isotope of the actinides tends to have an appreciable fission cross section. If the actinide recycle concept is to be implemented or adequately assessed, the capture and fission cross sections of the nuclides involved need to be known over the whole neutron energy spectrum of potential waste-burning systems. The underground nuclear explosion technique[5] has provided a wealth of fission cross sections of these nuclides; however, the capture cross sections are not nearly as well known. Total cross sections and integral measurements[6] are of great value in deriving capture cross sections but are not sufficient in all cases, particularly above the resolved resonance region. One of the major problems in measuring the capture cross sections for the long-lived actinide isotopes is obtaining pure samples. Isotopes with appreciable spontaneous fission, even if present only as impurities, can cause prohibitive backgrounds.

Of particular importance to those involved in fuel recycle are the spontaneous fissioning isotopes of Pu, Cm, and Cf which make additional shielding necessary in the fabrication and shipping of fuel elements. The cross sections leading to the production of the spontaneous fissioning nuclides are needed for the various types of reactors. Additional shielding necessary for fission neutrons could be costly and needs advance consideration. If the long lived actinides are to be transmuted in reactors before disposal, there will be more of these spontaneously fissioning nuclides formed. Predictions of this additional neutron activity is dependent on the cross sections as well as the neutron energy spectrum of the type reactor used.

Since one of the major objectives of the Oak Ridge Electron Linear Accelerator (ORELA) is to produce the neutron cross sections needed by the power reactor program, there is a program to measure the needed capture and fission cross sections of the actinide nuclides of mass higher than $^{239}Pu$. The purpose of this paper is to discuss this measurement program and techniques involved.

## Experimental Procedure

The ORELA is used as a source of pulsed neutrons. Neutron energies are measured by time-of-flight along a flight path of 20 or 85 meters. Since ORELA has multiple flight paths which can be used simultaneously, the measurements can be carried out at the same time as other experiments.

In order to directly measure a capture cross section, means must be available to detect the capture gamma-ray cascade following a neutron capture event. The detection efficiency for the capture event must be independent of changes in the gamma-ray cascade. If a low-efficiency detector has an efficiency which is proportional to gamma-ray energy then its efficiency for detecting a capture event is proportional to the (constant) binding energy of the nucleus. Such detectors were first approximated by thick walled geiger counters, then Moxon-Rae detectors,[7] and finally the "total energy detector."[8] The "total energy detector" can be any gamma-ray detector whose pulse-height response to gamma-rays of different energies is known. Sets of weighting factors for different pulse height events have been developed to force the net efficiency to be proportional to gamma-ray energy. This method was suggested by Maier-Leibnitz[9] and developed by R. L. Macklin.[8] Fission events are also detected by such a detector because of the prompt fission gamma-rays.

The gamma-ray detectors used in these experiments are 2 by 10 cm diameter liquid scintillators of NE-226, a nonhydrogenous scintillator. Such a scintillator was desired to reduce the efficiency of response to fast

neutrons from fission events in the sample. The gamma-ray event weighting factors as a function of pulse-height derived by R. L. Macklin[8] were altered slightly to account for the 0.32 cm of Pb which was necessary between the sample and the detectors because of the high activity of low energy gamma-rays (< 100 keV) from most of the samples. No statistically significant differences were observed in the capture rate vs neutron energy when the capture events were not weighted according to their pulse-height. This infers that changes in the prompt gamma-ray spectrum following a capture event were not significant for the cases studied in these measurements. The efficiency for the detection of a capture or fission event by these detectors was about 1.5% per detector.

To detect fission events in the samples where there is a measurable fission cross section, fast neutron counters are used. These fast neutron detectors are liquid scintillators (NE-213) which are 10 cm in diameter and 5 cm thick. Pulse-shape discrimination is done on the pulses from the scintillators in order to discriminate between fast neutrons and gamma rays. These two fission neutron detectors are used in the same geometry as the gamma-ray detectors so that there is a total of four detectors facing the sample with their axis in the plane perpendicular to the neutron beam.

The shape of the neutron flux from thermal neutron energies to 2 keV is measured with a parallel-plate $^{10}BF_3$ chamber which intercepts the full neutron beam. Above 2 keV this chamber was calibrated vs a $^{6}Li$ glass detector of 0.5 mm thickness and 7.62 cm diameter. Thus the shape of the cross sections is based on the $^{6}Li$ cross section above 2 keV. The $^{6}Li$ cross section and corrections for scattering in the Li glass were these proposed by Macklin.[10] The $^{10}B(n,\alpha)$ cross section assumed is that proposed by Sowerby;[11] this evaluated cross section is nearly 1/v up to 2 keV.

The time-dependent background in the gamma-ray, neutron, and flux detectors is measured by means of the black resonance technique. Filters of S, Na, and Au were used to deplete all primary neutrons at their resonances at 105 keV, 2 keV, and 5 eV respectively and determine the background at these neutron energies. These backgrounds were used to normalize the shape of the time-dependent background as determined with a mock-up sample container. A relatively large background which is independent of time is usually caused by the radioactivity of the sample. The level of this background is determined at long times following the accelerator burst when essentially all neutrons have passed the sample position or have been depleted by a $^{10}B$ overlap filter.

The shape of the neutron cross sections vs neutron energy which is derived in these experiments is normalized to the absolute value of the cross section at 0.025 eV as listed in ENDF/B-IV. Resonance self-protection corrections were relatively small since 2-gram samples of 7.62 cm diameter have been used at eV neutron energies and 9-gram samples at keV neutron energies. The effects of multiple neutron scattering in the sample in most cases were negligible.

## Experimental Results

With the experimental techniques described, measurements have been carried out on $^{240}Pu$, $^{241}Pu$, and $^{241}Am$. The results of these experiments have not quite been finalized. In addition, measurements of $\alpha(\langle\sigma_c\rangle/\langle\sigma_F\rangle)$ have been done on $^{239}Pu$ in order to make a direct comparison of the present techniques with those using a fission chamber sample in a large liquid scintillator tank. The results of this comparison are discussed in another paper in these proceedings.[12] Preliminary results on $^{241}Pu$ have been described previously.[13]

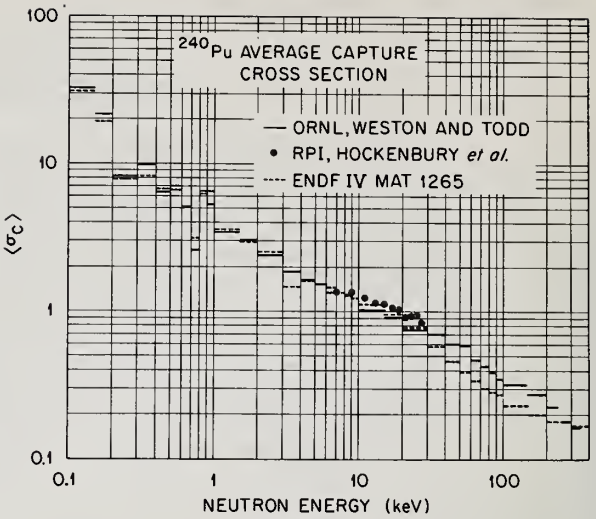


Figure 1

Figure 1 shows the results on the average capture cross section of $^{240}Pu$. These data were normalized at 0.025 eV to the ENDF/B-IV evaluation and the normalization was confirmed by using the black resonance technique of normalization with the large 1-eV resonance in $^{240}Pu$. Also shown for comparison are the results of Hockenbury et al.[14] and ENDF/B-IV MAT 1265 evaluation. The results of Hockenbury et al. are in agreement within experimental errors with the present results. The ENDF evaluation in the neutron energy range shown is based on the results of Hockenbury and preliminary results of these experiments. Measurements on the subthreshold fission of $^{240}Pu$ are discussed elsewhere in these proceedings.[15]

Figure 2 is the average absorption cross section of $^{241}Am$. The cross section is predominately capture since fission is small at these neutron energies. The ENDF/B-IV MAT 1056 evaluation is shown for comparison. The ENDF evaluation at keV neutron energies is based almost entirely on resonance parameters from total cross sections in the resolved resonance region so the agreement is considered satisfactory. The increase in the cross section above the ENDF/B-IV evaluation starting at 20 keV was indicated by measurements both at the 20 and 85 meter flight paths.

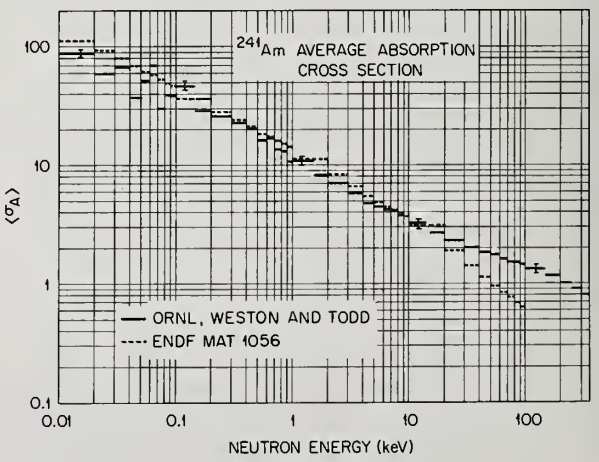


Figure 2

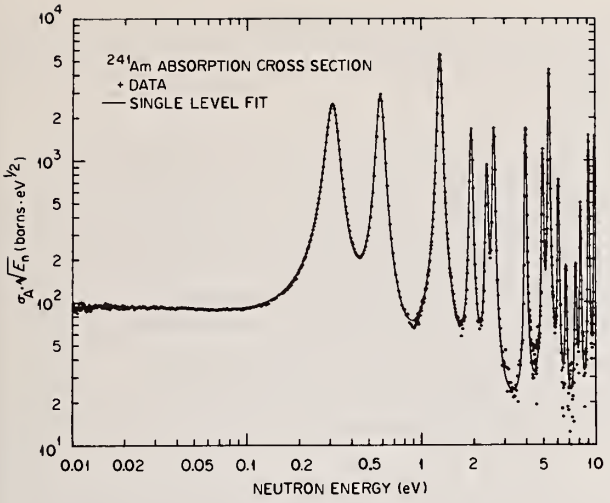


Figure 3

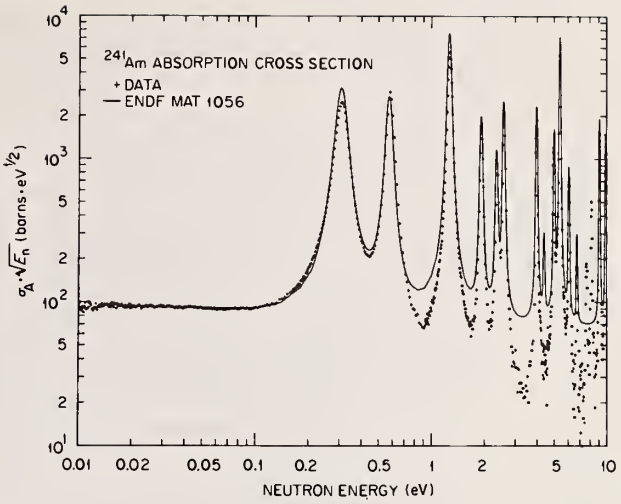


Figure 4

Figure 3 is the absorption cross section data in the eV region of neutron energies with the solid line being the single-level fit to the data. The fission cross section of $^{241}$Am was not measured in this experiment because of an inexplicably high spontaneous fission rate in the sample. Figure 4 is a comparison of ENDF/B-IV MAT 1056 with the present data. The ENDF evaluation in the resonance region of $^{241}$Am was based on total cross section measurements.[16] The agreement is not satisfactory, especially between the resonances where the ENDF evaluation is appreciably higher than the present data.

The neutron cross section data taken with this technique are of high neutron energy resolution as can be seen in Fig. 3. There is resonance structure which extends far above the nominal resolved resonance region. Average cross sections were used in the comparisons at keV neutron energies since the fine structure in the cross sections makes direct comparison difficult.

## Summary

Measurements have been made with the described techniques on the capture and fission cross sections of some of the nuclides of higher mass than $^{239}$Pu which are important to fast reactor core physics. Additional measurements are planned for $^{242}$Pu and perhaps $^{237}$Np and $^{243}$Am. If the actinide recycle concept is to be implemented or adequately assessed as an appropriate method of reducing the long term radiological hazard of the actinide waste, other similar measurements are possible and will be needed. Several of the long lived isotopes of Am and Cm are succeptable to cross section measurements with the present techniques. Sample preparation will be a major problem.

Total cross sections and integral measurements are of great value; however, measurement of the capture and fission cross sections are needed to produce the needed knowledge of the cross sections. With these cross sections the fuel and waste management for Pu fueled reactors can be planned on a systematic basis.

## References

*Research sponsored by the Energy Research and Development Administration under contract with the Union Carbide Corporation.

[1]P. Greebler, B. A. Hutchins, and C. L. Cowan, Proc. Conf. Nuclear Data for Reactors, vol. I, p. 19 (1972) Helsinki, IAEA.

[2]H. C. Claiborne, "Effect of Actinide Removal on the Long-term Hazard of High-level Waste," ORNL-TM-4724 (1975); also see ORNL-TM-3964 (1972).

[3]"High-level Radioactive Waste Management Alternatives," BNWL-1900, vols. 1-4, May 1974.

[4]J. O. Blomeke, C. W. Kee, and J. P. Nichols, "Projections of Radioactive Wastes to be Generated by the U. S. Nuclear Power Industry," ORNL-TM-3965, February 1974.

[5]B. C. Diven, Ann. Rev. Nucl. Sci. 20, 79 (1970); also A. Hemmendinger, Am. Scientist 58, 622 (1970).

[6]R. W. Benjamin, "Survey of Experimentally Determined Neutron Cross Sections of the Actinides," DP-1324 (1973).

[7]M. C. Moxon and E. R. Rae, in Neutron Time-of-Flight Methods, ed. J. Spaepen, European Atomic Energy Committee, Brussels, 1961.

[8]R. L. Macklin and J. H. Gibbons, Phys. Rev., vol. 159, No. 4, 1007 (1967).

[9]H. Maier-Leibnitz (private communication to R. L. Macklin).

[10]R. L. Macklin, J. Halperin, and R. R. Winters, "Gold Neutron Capture Cross Section from 3 to 550 keV," accepted for publication in Phys. Rev. C. See also B. J. Allen et al., Phys. Rev. C 8, 1504 (1973).

[11]M. G. Sowerby et al., Proc. Conf. Nuclear Data for Reactors, vol. I, p. 161 (1970) Helsinki, IAEA.

[12]R. Gwin et al., "A Direct Comparison of Different Experimental Techniques for Measuring Neutron Capture and Fission Cross Sections," Proc. Conf. Nuclear Cross Sections and Technology, March 3-7, Washington, D.C. (1975).

[13]L. W. Weston and J. H. Todd, "Neutron Fission and Absorption Cross Sections Measurements of $^{239}$Pu and $^{241}$Pu," Trans. Am. Nucl. Soc. 15, 480 (1972).

[14]R. W. Hockenbury, W. R. Moyer, and R. C. Block, Nucl. Sci. Eng. 49, 153 (1972).

[15]G. F. Auchampaugh and L. W. Weston, "Subthreshold Fission in $^{240}$Pu+n," Proc. Conf. Nuclear Cross Sections and Technology, March 3-7, Washington, D. C. (1975).

[16]For references on individual measurements see ref 6.

# MEASUREMENTS OF THE $^{6}Li$ and $^{10}B$ PARTIAL CROSS SECTIONS FROM 1 TO 1500 keV

S. J. Friesenhahn, V. J. Orphan, A. D. Carlson,
M. P. Fricke, and W. M. Lopez
IRT Corporation
San Diego, California 92138

The $^{10}B(n,\alpha_0+\alpha_1)^{7}Li$, $^{10}B(n,\alpha_1)^{7}Li^*$ and $^{6}Li(n,\alpha)T$ cross sections have been measured between 1- and 1500-keV neutron energy. The neutron spectrum was measured using proton scattering as observed in a methane-filled proportional counter. Gamma rays from the $^{10}B(n,\alpha_1)^{7}Li^*$ reaction were observed with a high-resolution Ge(Li) spectrometer, and the reaction products from the $^{10}B(n,\alpha_0+\alpha_1)^{7}Li$ and $^{6}Li(n,\alpha)T$ reactions were observed in a large ion chamber. In an auxiliary measurement, the ratio of the $^{10}B(n,\alpha_0+\alpha_1)^{7}Li$ cross section to the hydrogen scattering cross section was obtained between 200 and 1000 keV by observation of interactions in a specially constructed $^{10}BF_3$ proportional counter containing a methane additive.

(Neutron cross section; $^{10}B$; $^{6}Li$; standard)

## Introduction

The large, smoothly varying reaction cross sections of $^{10}B$ and $^{6}Li$, combined with the ease of their implementation in neutron detectors, has resulted in the use of these isotopes as standard cross sections for neutron flux determinations. The reaction energies are sufficiently large to make event detection relatively easy, and in the case of $^{10}B$, the interactions may be detected via both charged-particle and gamma-ray detectors. However, relatively few measurements of these cross sections have been made. Many of the direct measurements made previously may contain systematic errors from long-counter flux determinations, and are subject to a variety of uncertainties associated with background determinations. The indirect results [e.g., the $^{10}B(n,\alpha)$ cross sections deduced from the total and scattering cross sections] may contain substantial systematic errors inherent in such determinations. The present measurements were undertaken to remove or reduce these uncertainties, by making high-accuracy, direct measurements relative to the H(n,n) standard cross section.

## Measurements and Data Reduction

The measurements were made using a 226-meter evacuated flight path and the IRT Linac as a neutron source. The 70-MeV Linac electron beam of 0.1-μsec duration struck a tungsten alloy target located at the center of a 7-inch-diameter $^{238}U$ cylinder. The emergent neutron spectrum was partially moderated in a 1-inch-thick slab of polyethylene before entering the flight path. Thick aluminum, sodium, or polyethylene filters were inserted at the 45-meter position for determining the background. Data were acquired with an on-line CDC-1700 computer, which employed interfaces to three analog-to-digital converters and a time digitizer to store data in multiparameter form on magnetic tape. These four-parameter data were subsequently sorted on a Univac-1108 computer.

The neutron flux measurements were performed using a 24-inch-long, 2-inch-diameter ceramic end window methane counter. The filling pressure of 2 atmospheres is sufficient to produce high-quality proton-recoil response functions which are relatively free of wall and end effects up to 1 MeV. The response was improved further by use of a collimator just upstream from the counter, which confined the neutron beam to the central region of the counter, thus further reducing the wall-interaction effect.

Since the ionization/eV of recoiling proton energy is not constant, the energy dependence of this effect was measured in the course of the flux determination by sorting the multiparameter data into proton-recoil response functions at various neutron energies. The location of the leading edge of the distribution divided by the incident neutron energy was taken as a measure of the relative number of ion pairs/eV produced. This function, along with the calculated wall and resolution effects, was used to calculate the bias efficiency for the proton-recoil data, which had been sorted with an energy-dependent bias equal to 35% of the incident neutron energy.

One of the parameters stored on the magnetic tape is a rate-of-rise signal, which is derived by differentiating the pulse from the counter in a fast amplification system. This pulse rise-time information was used to discriminate between neutron and gamma-ray interactions in the counter. Gamma-ray background subtractions were quite small throughout the region of interest.

Since the only material with appreciable neutron cross section between the neutron source and the detection position was a $^{10}B$ filter used to avoid neutron burst overlap, the measured spectrum is quite smooth, with the exception of a small dip in the vicinity of the oxygen resonance at 432 keV. Part of this dip is due to the mylar vacuum windows in the flight path, and part is due to the $Al_2O_3$ end window of the counter. The end window transmission was corrected for in determining the neutron spectrum.

Considerable effort was expended in developing detection devices exhibiting desirable response functions and a minimum of multiple scattering. We next briefly describe each of these devices and their implementation in the measurements.

The 478-keV gamma ray from the $^{10}B(n,\alpha_1)^{7}Li^*$ reaction was observed by locating an 80-cc high-resolution (4-keV) Ge(Li) spectrometer in the center of the 9-inch-diameter neutron beam. The Ge(Li) spectrometer and its cryostat were shielded from the incident neutron beam. The remaining portion of the beam struck a thin slab of $^{10}B$ powder contained between mylar sheets. The slab was evacuated to hold the powder in a uniform layer. Doppler broadening of the gamma ray required the use of a 10-keV-wide gamma-ray energy window. A small background correction was obtained by replacing the $^{10}B$

slab with a graphite slab having approximately the same macroscopic scattering cross section. This background agreed well with that obtained by moving the gamma-ray bias window just above the 478-keV position.

The $^{10}B(n,\alpha_0+\alpha_1)^7Li$ and $^6Li(n,\alpha)T$ reactions were observed in a large, gridded ion chamber. An identical background chamber was constructed, but backgrounds were too small to be observable, and no correction was necessary. All of the chamber elements, with the exception of the source plates, were formed by 10-inch x 10-inch grids composed of No. 36 aluminum wire spaced ∿1/8 inch apart. The chambers were long enough (54 inches) to contain several source plates of $^{10}B$ and $^6Li$ simultaneously. It was thus possible to accumulate simultaneously data on both $^{10}B$ and $^6Li$ cross sections under nearly identical conditions. The chambers were operated at atmospheric pressure with a gas flow of ≈15 liters per minute of 90% argon, 10% $CO_2$.

The large energy-loss rate and relatively low energy of the $^7Li$ reaction product results in a poor response function for a useful thickness of $^{10}B$ deposited on a thick substrate. This is a serious problem, since the range of neutron energies covered in these measurements is sufficient to produce large changes in the response function due to the incident neutron kinetic energy. For this reason, a technique was developed for producing thin, self-supporting $^{10}B$ films for the 10-inch x 10-inch ion chamber source plates. These self-supporting plates allow observation of the sum of the α and $^7Li$ energies, thus greatly improving the response function and reducing bias efficiency corrections.

The films were formed from a liquid plastic solution containing a $^{10}B$ dispersion. The plastic was coated on a large glass plate, and then an ion chamber frame was cemented to the dried film. The film was made conductive by rubbing with graphite powder, and then stripped from the glass plate under water. The completed films contained ≈30% $^{10}B$ by weight. The sum response function is illustrated in Figure 1. Since the films contained hydrogen, it was necessary to use a neutron-energy-dependent bias in sorting the data. The bias efficiency corrections were obtained via calculated response functions (example given in Figure 1), which included detailed treatment of energy loss, particle ranges, branching ratio, angular distributions, etc. The energy dependence of the bias efficiency corrections, along with those of other detectors used in these measurements, is illustrated in Figure 2.

Because of the reactive nature of lithium and its compounds, it was not possible to produce self-supporting films containing this material. For this reason, $^6Li$ metal was evaporated on 1-mil aluminum foil. Two deposit thicknesses of ≈50 and ≈250 μg/cm$^2$ were used. The thinner deposit yielded the response function illustrated in Figure 3, and several plates of this thickness were used to obtain cross-section data of moderate statistical precision. The data from several of the thick deposits were then divided by the thin deposit data to obtain the ratio of the bias efficiencies. This ratio was grouped and smoothed to obtain the relative thick deposit biasing efficiency as a function of neutron energy. The thin deposit bias efficiency was calculated using a computer code similar to that used for the $^{10}B$ efficiency calculations. A comparison of calculated versus measured distributions is illustrated in Figure 3.

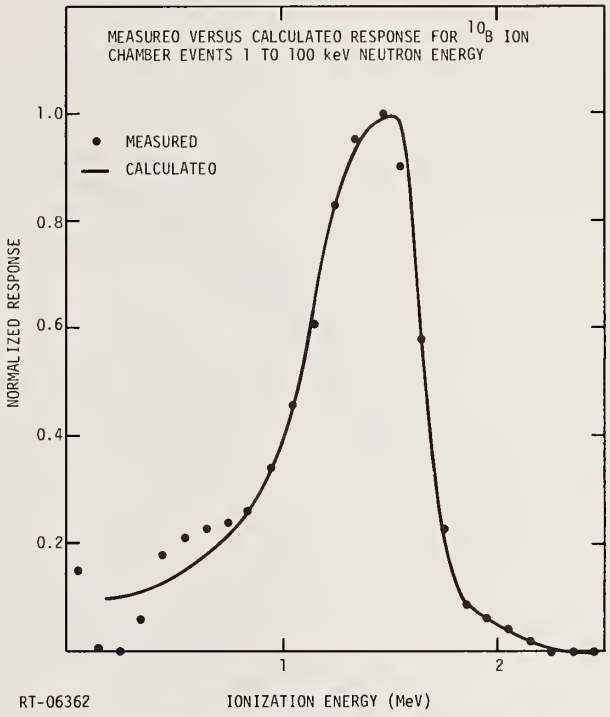


Figure 1. Measured versus calculated response for $^{10}B$ ion chamber events 1 to 100 keV neutron energy

The cross-section data were normalized to 1/V extrapolations of thermal values near 4 keV. This normalization energy was dictated by the large statistical fluctuations in the ion pairs produced in methane below 1 keV, which limited the flux bias efficiency calculations to energies above ≈3 keV.

Since it is desirable to obtain an independent check on the normalization, a $BF_3$ counter was fabricated which contained an admixture of methane. This allowed the observation of proton recoils in the same environment as the $^{10}B(n,\alpha)$ reactions. The two reactions are well separated on the basis of pulse height. After completion of the measurements, the counter was tapped and a chemical analysis of the gas composition performed. This allowed a determination of the $^{10}B(n,\alpha_0+\alpha_1)^7Li$ cross section, which is based only on the results of the gas analysis. When the inferior time resolution of these data relative to those obtained with the ion chamber is taken into account, the agreement of the two determinations of the cross section is satisfactory

## Results and Conclusions

Comparison of the present cross-section results with those of other workers is illustrated in Figures 4, 5, and 6. The present $^{10}B(n,\alpha)$ data, shown in Figure 4, are in good agreement with all previous measurements below 100 keV. In general, the present $^{10}B(n,\alpha)$ cross sections are in good agreement with

ENDF/B-Version III values, with the exception of the 450-keV resonance, which is seen more distinctly, and the sharpness of the decrease in the cross section above the resonance. The absolute $^{10}B(n,\alpha)$ cross-section measurement obtained using the $BF_3/CH_4$ proportional counter confirmed the ion chamber results from 200 to 1000 keV. The $^{10}B(n,\alpha_1)^7Li^*/^{10}B(n,\alpha_{0+}\alpha_1)^7Li^*$ branching ratio is compared to the Irving[1] evaluation in Figure 4. The agreement is quite good, except above 600 keV where the present results tend to be slightly lower. The $^6Li$ data illustrated in Figure 5 exhibit a higher and sharper peak at the 250-keV resonance than observed in previous measurements. This may be due in part to the good time resolution and small multiple scattering effects in the present data. $^{10}B(n,\alpha)/^6Li(n,\alpha)$ cross-section ratios, relatively free of systematic uncertainties, were also determined over the neutron energy range 1 to 1500 keV from the ion chamber results.

## References


1. D. C. Irving, "Evaluation of Neutron Cross Sections for Boron 10," ORNL-TM-1872 (1967).


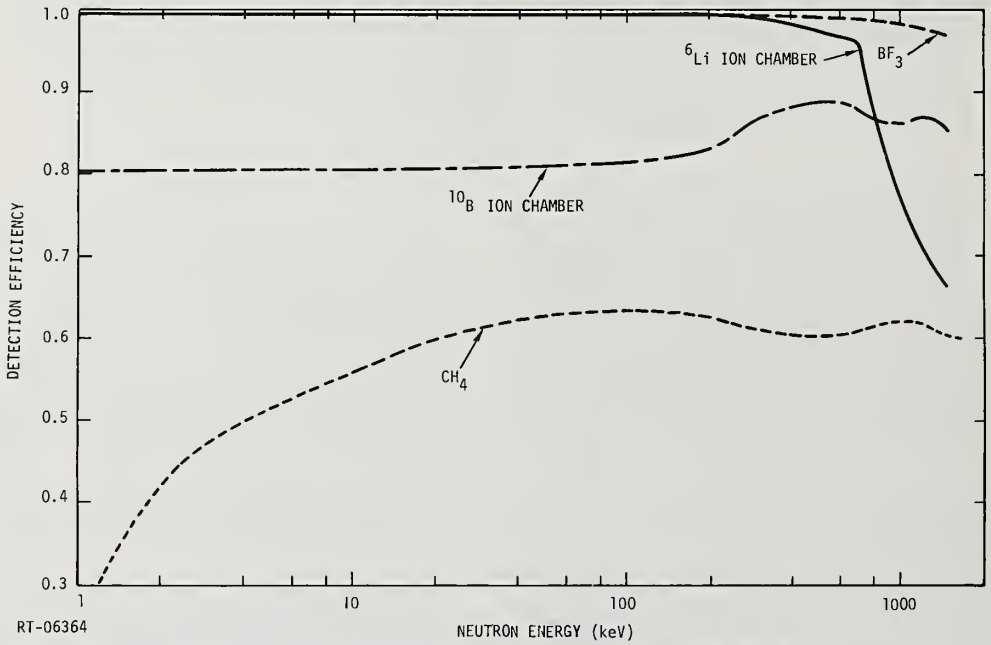


Figure 2. Detection efficiencies versus neutron energy

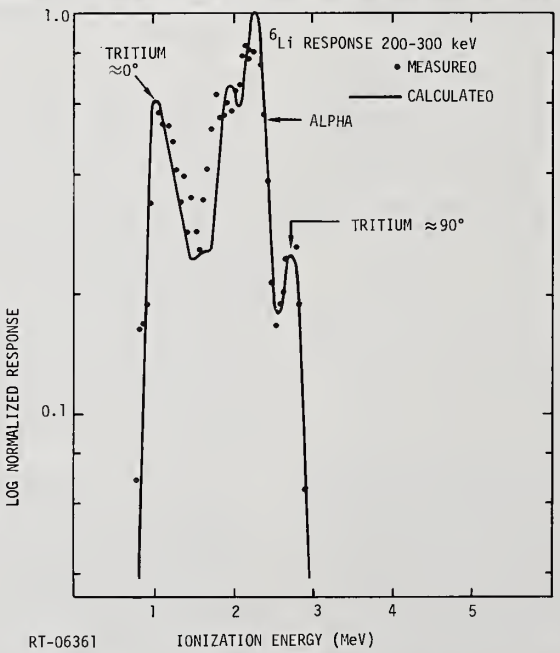


Figure 3. Calculated versus measured $^6Li$ ion chamber response

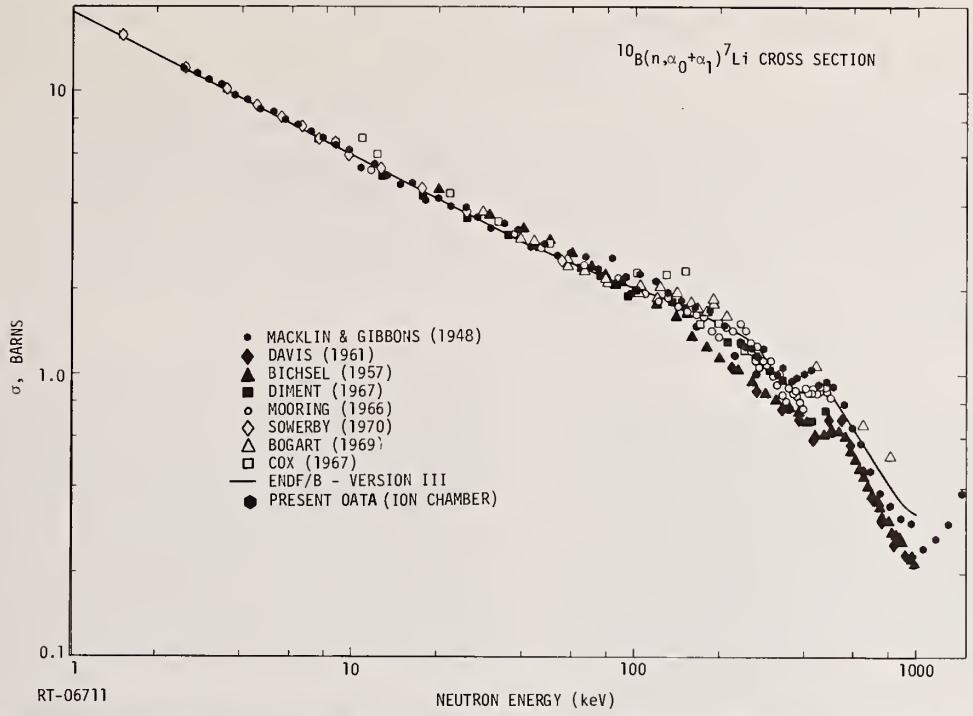


Figure 4. Comparison of present ion chamber measurements of $^{10}B(n,\alpha_0+\alpha_1)^7Li$ cross section to those of other workers

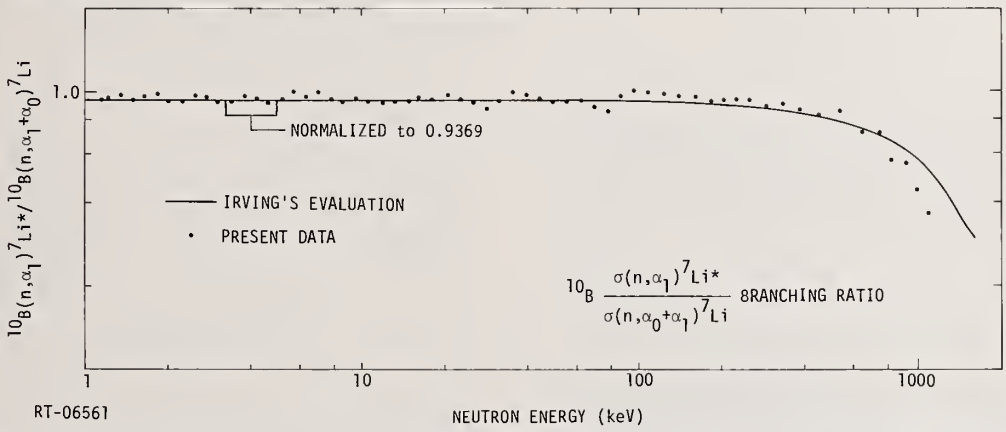


Figure 5. $^{10}B(n,\alpha_1)^7Li^*/^{10}B(n,\alpha_0+\alpha_1)^7Li$ branching ratio obtained from Ge(Li) versus $BF_3$ measurements

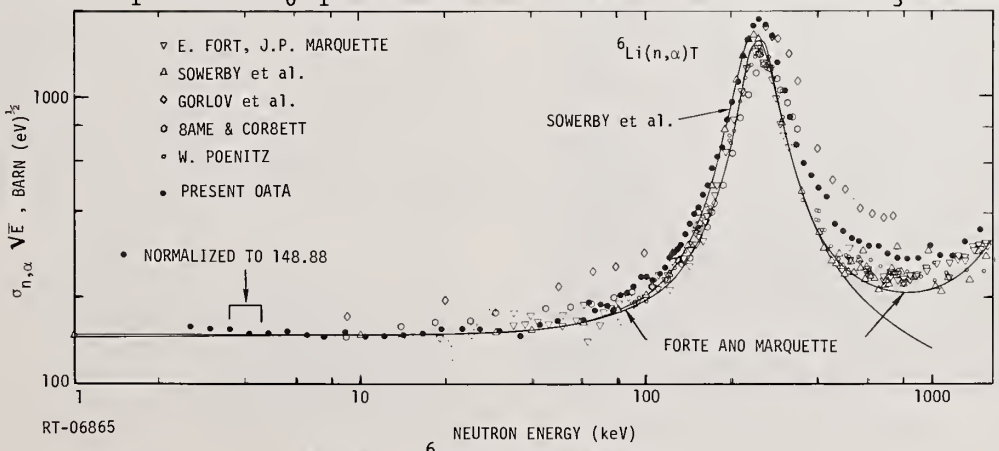


Figure 6. $^6Li(n,\alpha)T$ cross section

# AN ABSOLUTE MEASUREMENT OF THE $^{6}Li(n,\alpha)$ CROSS SECTION AT 964 keV

W. P. Stephany and G. F. Knoll
The University of Michigan
Ann Arbor, Michigan 48104

A value of 356 mb ± 12% was obtained for the $^{6}Li(n,\alpha)$ cross section at 964 keV. Neutrons were produced using a spherical Na-Be photoneutron source, calibrated relative to NBS-II using The University of Michigan manganese bath. Thin $^{6}LiF$ targets enriched to 95 atom percent $^{6}Li$ were vapor deposited onto the electrode surfaces of a 42 micron thick, fully depleted Si surface barrier detector. A summary of the data, corrections, and error analysis is presented.

(Neutron cross sections; $^{6}Li(n,\alpha)$; absolute cross section measurements; photoneutron sources; manganese bath; surface barrier detectors)

## Introduction

The measurement was undertaken as an attempt to resolve the substantial discrepancies reported during the last few years for the $^{6}Li(n,\alpha)$ cross section in the energy range near 1 MeV. Accurate knowledge of the cross section would enhance the usefulness of $^{6}Li$ for neutron flux measurements in this energy range. The use of thin targets, having mass thickness of about 175 μgms/cm$^2$, as well as accurate data on the isotopic composition of the Li, eliminated two of the well known systematic error sources encountered in previous measurements. The limits of the present measurement were determined by the effects of the intense gamma activity of the photoneutron source (about 35 Ci of $^{24}Na$) on the detector response and by the uncertainties in the correction to the neutron flux due to local inscattering.

## Experimental Procedure

### Facilities

The experimental facilities for performing the cross section measurements are described elsewhere in these proceedings.[1] In particular, the experimental aspects and primary data reduction for determination of the neutron activity of the Na-Be source are credited to D. Gilliam.[2]

### Procedure

The detector, rigidly supported in the low scatter stainless steel tubular frame, is shown in Figure 1.

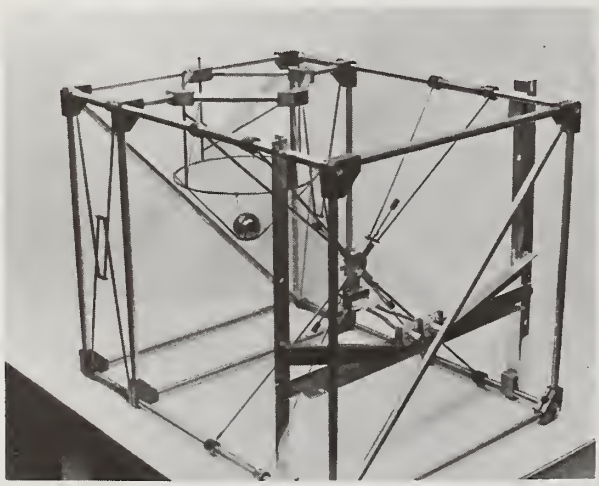

Figure 1. Source-Detector Support Frame

This frame allowed accurate positioning of the photoneutron source relative to the detector, using a positioning jig to obtain approximate alignment, followed by measurement of the exact source-detector separation distance using calibrated micrometers. Experiments were done at two source-detector spacings to allow direct elimination of the room return flux contribution. Each experiment consisted of two measurements. First a $^{24}Na$-aluminum clad photon source of equivalent gamma activity to the Na-Be photoneutron source was run, duplicating the system response to all background characteristics encountered during the photoneutron source run; then the photoneutron source was run. Data was accumulated in counting periods of short duration, usually 8000 seconds, to allow monitoring of the stability of the system and subsequent statistical evaluation. After each experiment, the photoneutron source was calibrated by direct comparison with NBS-II. The source-detector arrangement is schematically shown in Figure 2.

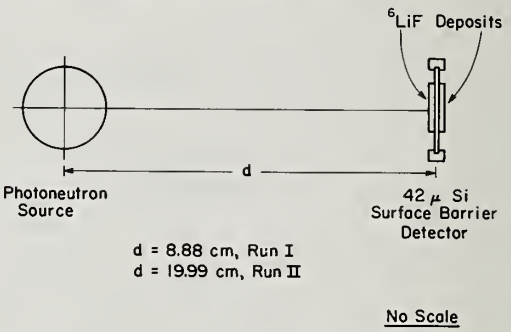


Figure 2. Source-Detector Arrangement

### Detector-Target Composite

A 42 μ thick Si surface barrier, with the $^{6}LiF$ targets directly vapor deposited on the electrode surfaces was used to record the events, which in turn were processed by a fast electronic system to minimize pulse pile-up caused by the high gamma event rate. Energy discrimination was used to suppress the gamma background. The target deposits had an area of approximately 1 cm$^2$ whereas the active area of the detector was 2 cm$^2$.

## Summary of the Data

To determine the cross section three primary factors or their equivalents must be known:

1. the number of target nuclei
2. the neutron flux
3. the reaction rate

The results will be presented in this order.

# NEUTRON TOTAL CROSS SECTION OF $^{6}$Li FROM 10 eV TO 10 MeV

J. A. Harvey and N. W. Hill
Oak Ridge National Laboratory*
Oak Ridge, Tennessee 37830

Transmission measurements have been made at ORELA upon two metal samples of $^{6}$Li(98.72%) with inverse sample thicknesses of $^{6}$Li of 11.99 and 2.987 b/atom. The measurements at low energies (from 10 eV to 300 keV) were made using a $^{6}$Li glass scintillation detector at 17.878 m and 78.203 m and at high energies (from 50 keV to ∿10 MeV) using an NE-110 scintillation detector at 78.203 m. The total cross section data from both samples and detectors are in good agreement and are believed to be accurate to 1 to 2% below 1 MeV. Total cross section data obtained from both samples at ∿25 discrete energies up to 1 MeV using an iron-filtered beam are in good agreement with the continuous spectra data.

(Nuclear Reactions: $^{6}$Li, $\sigma_{nT}$, En = 10 eV to 10 MeV)

## Introduction

One of the more useful neutron standards in the energy region below 1 MeV is the $^{6}$Li(n,α) reaction since fast, efficient, stable neutron detectors utilizing this reaction can be readily constructed. Below ∿10 keV the $^{6}$Li(n,α) cross section follows a 1/v law and is known to ∿1% accuracy.[1] However, at high energies the accuracy varies from 5 to 15%. Values from recent measurements[2,3] differ by ∿10% at the peak of the resonance at 246 keV. It is well known[1,4] that total cross section data are valuable in establishing the (n,α) cross section particularly in the region of the 246-keV resonance. Many total cross section measurements have been made upon $^{6}$Li in the past 20 years; these data were reviewed in 1970 by Uttley *et al.*[1] The two most recent measurements[5,6] agree in cross section but show an 8-keV energy discrepancy in the region of the 246-keV resonance. One of the recommendations made by Uttley *et al.*[1] was that the total cross section should be remeasured from a few eV to a few MeV.

## Experimental Measurements

Transmission measurements have been made upon two metal samples of $^{6}$Li (98.72%) with inverse sample thickness of $^{6}$Li of 11.99 and 2.987 b/atom. The samples were contained in stainless steel cylinders 3.0 cm diameter and sealed to prevent the formation of nitrides and oxides. Data were taken at the higher neutron energies (> 30 keV) using an NE-110 scintillation detector located 78.203 m from the standard neutron target[7] at ORELA. For these higher energy measurements, 5 nsec bursts 1000 pps were used resulting in an energy resolution $\Delta E/E$ of $0.001\sqrt{1+4\ E(\text{in MeV})}$. A 1.1-cm-thick uranium filter was used to reduce the gamma flash and a $^{10}$B filter (0.6 gm/cm$^2$) to eliminate overlap neutrons. For the lower energy measurements, a $^{6}$Li glass scintillator (1.27 cm thick, 11 cm dia) was used at both the 78.203 m and 17.878 m flight paths. At the longer flight path 22-nsec bursts 800 pps were used with a 7-mm Pb filter and a $^{10}$B filter (0.6 gm/cm$^2$) to reduce overlap neutrons. At the shorter flight path 7.5-nsec bursts 180 pps were used with a 7-mm Pb filter and a 1-mm Cd filter to prevent overlap. In addition to these continuous energy measurements, measurements at ∿25 discrete energies (with energy spreads of from ∿0.7 to 5 keV) have been made using iron window neutrons produced by a 29-cm iron filter in the beam and the NE-110 detector located at the 78.203 m flight path.

## Experimental Results

The time-of-flight spectra measured with the NE-110 detector must be corrected for 3 backgrounds, each < 1%: first, the presence of 2.23-MeV gamma rays from neutron capture by the water moderator which decays with a ∿17.6-μsec decay time; second, the 478-keV gamma rays produced by capture in the boron in the pyrex of the phototube which has a 1-2 μsec decay time for the 2-cm-thick NE-110 scintillator; finally, a constant room background which is mainly due to gamma rays. Figure 1 shows the total cross section of $^{6}$Li from 50 to 550 keV obtained with the NE-110 detector. The data below 5.5 barns was obtained from the thick sample and above 5.5 barns from the thin sample. Comparison of the thin and thick sample data (excluding the thick sample data above ∿8 barns) showed a difference of ∿0.1 barns which was explained by assuming that there was a slight amount of nitrogen in the thin sample. The data obtained using the iron-filtered neutrons also showed this ∿0.1-barn difference between the thick and thin samples. Hence, the thin data are only used in the energy region where the cross section is > 5.5 barns and, hence, any error in applying the ∿0.1-barn correction is very small. The values for the cross section in Fig. 1 are actually 0.987 $\sigma(^{6}\text{Li})$ + 0.013 $\sigma(^{7}\text{Li})$ rather than $\sigma(^{6}\text{Li})$. However, since the cross section of $^{7}$Li is nearly the same as that of $^{6}$Li the difference is small (< 1%) over the entire energy range. Nevertheless we plan to measure the $^{7}$Li total cross section in order to make this small correction accurately. The peak cross section at 246 keV was 10.95 ± 0.10 barns. Data obtained using the $^{6}$Li glass detector and the thin sample in the region of this

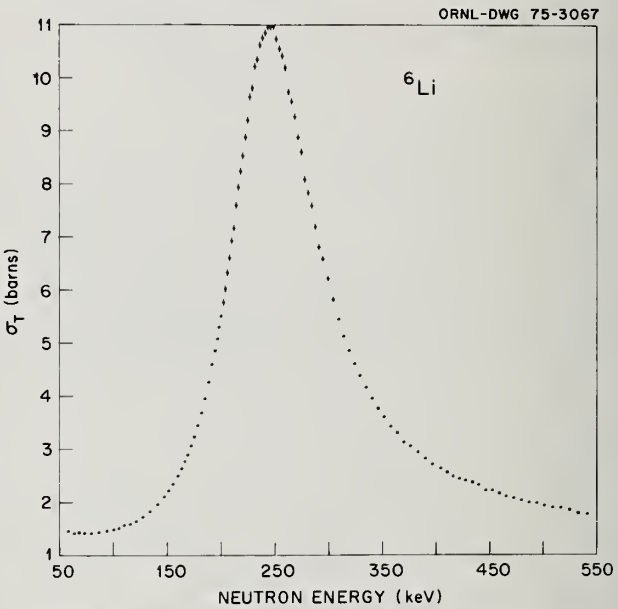


Fig. 1. Neutron Total Cross Section of $^{6}$Li.

246-keV resonance are in good agreement within ∿1%. The peak cross section at 246 keV was 10.97 ± 0.10 barns.

Figure 2 shows the total cross section of $^6$Li from 0.5 to 10.5 MeV obtained from the thick sample using the NE-110 detector. Above ∿3 MeV the statistical accuracy is relatively poor since the intensity of high energy neutrons is quite low from the water-moderated Ta(γ,n) target. We have shown recently that a greatly increased intensity of these higher energy neutrons can be realized by looking directly at the ORELA Ta target through a thick uranium filter, especially when only a small amount of sample is available. We plan to make new measurements up to ∿20 MeV using these unmoderated Ta(γ,n) neutrons.

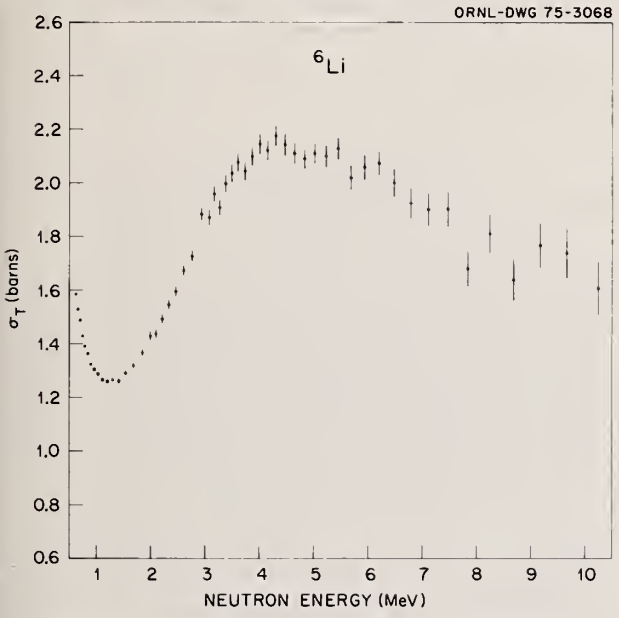


Fig. 2. Neutron Total Cross Section of $^6$Li.

The total cross section data obtained using iron-filtered neutrons are listed in Table 1. These data agree with the data shown in Figure 1 to an accuracy of ∿1%.

The low-energy total cross section data obtained with the $^6$Li glass scintillator are in excellent agreement up to several keV with the formula proposed by Uttley,[1] namely $\sigma_T$ = constant × $149.5/\sqrt{E\ (\text{in eV})}$. Data from 10 eV to 10 keV were obtained using the 17.878-m flight path and from ∿100 eV to 300 keV using the 78.203-m flight path. Since the $^6$Li(n,α) thermal cross section is known accurately (∿0.5%), it follows that the 1/v part of the total cross section in the eV energy region has an uncertainty of only ±0.5%. Thus the excellent agreement (∿1%) between the total cross section data and the equation confirms the accuracy of the thicknesses of the samples.

## Conclusions

The total cross section of $^6$Li has been measured to an accuracy of 1 to 2% below 1 MeV. The data are in good agreement with the data reported in references 5 and 6 except that the energy values in the region of the 246-keV resonance from reference 6 are ∿8 keV higher than from the present measurement or from reference 5. The energy scale in the present measurement is accurate to ∿0.1%. From 0.5 to 3 MeV the total cross sections have been measured to an accuracy of from 2% to 3% but the uncertainty increases to ∿10% at 10 MeV.

Table 1. Neutron Total Cross Section of $^6$Li Determined from Iron Window Measurements

| Energy (keV) | Energy Spread (keV) | $\sigma_T$ (barns) |
|---|---|---|
| 24.6 | 1.1 | 1.79 ± 0.02 |
| 81.6 | 0.7 | 1.45 ± 0.02 |
| 128.6 | 0.7 | 1.74 ± 0.02 |
| 137.2 | 1.4 | 1.90 ± 0.02 |
| 167.7 | 1.0 | 2.86 ± 0.03 |
| 183.7 | 1.4 | 3.91 ± 0.04 |
| 219.1 | 1.1 | 8.46 ± 0.08 |
| 244.1 | 0.9 | 10.85 ± 0.10 |
| 273.6 | 1.5 | 8.68 ± 0.08 |
| 312.5 | 1.3 | 5.29 ± 0.05 |
| 352.0 | 2.2 | 3.64 ± 0.03 |
| 375.7 | 1.6 | 3.09 ± 0.03 |
| 404.1 | 1.8 | 2.66 ± 0.05 |
| 436.9 | 2.1 | 2.34 ± 0.03 |
| 468.1 | 2.3 | 2.11 ± 0.02 |
| 497.8 | 2.5 | 1.94 ± 0.02 |
| 556.0 | 2.9 | 1.77 ± 0.03 |
| 610.0 | 5.0 | 1.61 ± 0.02 |
| 645.0 | 10.0 | 1.56 ± 0.02 |
| 703.0 | 4.0 | 1.48 ± 0.02 |
| 836.0 | 5.0 | 1.35 ± 0.03 |
| 954.0 | 3.0 | 1.30 ± 0.03 |

*Operated by Union Carbide Corporation for the Energy Research and Development Administration.


[1] C. A. Uttley, M. G. Sowerby, B. H. Patrick, and E. R. Rae, *Proceedings of Conf on Neutron Standards and Flux Normalization*, AEC Symposium Series 23 (1971), p. 80.

[2] W. P. Poenitz, Z. Physik 268, 359 (1974).

[3] S. J. Friesenhahn, V. J. Orphan, A. D. Carlson, M. P. Fricke, and W. M. Lopez, Bull. Am. Phys. Soc. 20, 144 (1975).

[4] G. M. Hale, Bull. Am. Phys. Soc. 20, 148 (1975).

[5] C. A. Uttley and K. M. Diment, British Reports AERE-PR/NP-14, 1968; AERE-PR/NP-15, 1969; AERE-PR/NP-16, 1969.

[6] J. W. Meadows and J. F. Whalen, Nucl. Sci. and Eng. 48, 221 (1972).

[7] R. L. Macklin, NIM 91, 79-84 (1971).